



1-1-2013

Vascular Endothelial Growth Factor In Cortical Development

Jacob Thomas Cain

Follow this and additional works at: <https://commons.und.edu/theses>

Recommended Citation

Cain, Jacob Thomas, "Vascular Endothelial Growth Factor In Cortical Development" (2013). *Theses and Dissertations*. 1406.
<https://commons.und.edu/theses/1406>

This Dissertation is brought to you for free and open access by the Theses, Dissertations, and Senior Projects at UND Scholarly Commons. It has been accepted for inclusion in Theses and Dissertations by an authorized administrator of UND Scholarly Commons. For more information, please contact zeinebyousif@library.und.edu.

VASCULAR ENDOTHELIAL GROWTH FACTOR IN CORTICAL
DEVELOPMENT

By

Jacob Thomas Cain
Bachelor of Arts, University of North Dakota, 2004
Bachelor of Science, University of North Dakota, 2005

A Dissertation
Submitted to the Graduate Faculty

of the

University of North Dakota

In partial fulfillment of the requirements


for the degree of

Doctor of Philosophy

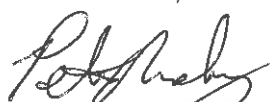
Grand Forks, North Dakota

May
2013


This dissertation, submitted by Jacob Thomas Cain in partial fulfillment of the requirements for the Degree of Doctor of Philosophy from the University of North Dakota, has been read by the Faculty Advisory Committee under whom the work has been done, and is hereby approved.




Diane Darland, Ph.D



Peter Meberg, Ph.D



Turk Rhen, Ph.D




Steven Kelsch, Ph.D



Van Doze, Ph.D

This Dissertation is being submitted by the appointed advisory committee as having met all of the requirements of the Graduate School at the University of North Dakota and is hereby approved.



Wayne Swisher
Dean of the Graduate School

May 2, 2013

Title Vascular Endothelial Growth Factor in Cortical Development
Department Biology
Degree Doctor of Philosophy

In presenting this dissertation in partial fulfillment of the requirements for a graduate degree from the University of North Dakota, I agree that the library of this University shall make it freely available for inspection. I further agree that permission for extensive copying for scholarly purposes may be granted by the professor who supervised my dissertation work, or in her absence, by the Chairperson of the department or the dean of the Graduate School. It is understood that any copying or publication or other use of this dissertation or part thereof for financial gain shall not be allowed without my written permission. It is also understood that due recognition shall be given to me and to the University of North Dakota in any scholarly use which may be made of any material in my dissertation.

Jacob Thomas Cain
May 2013

TABLE OF CONTENTS

LIST OF FIGURES.....	v
LIST OF TABLES.....	vii
ACKNOWLEDGEMENTS.....	viii
ABSTRACT.....	ix
CHAPTER	
I. INTRODUCTION.....	1
II. METHODS.....	24
III. RESULTS.....	37
IV. DISCUSSION.....	107
APPENDICES.....	120
REFERENCES.....	160

LIST OF FIGURES

Figure		Page
1.	Alignment of Vegf A homologues among vertebrate organisms.	2
2.	Vegf splice variants form isoforms with differential diffusion potential. .	3
3.	Vegf isoform distribution in the developing neuroepithelial microenvironment.	10
4.	Neural stem cell differentiation and early cortical layer formation.	15
5.	Vegf isoform expression in early forebrain.	21
6.	Early brain vesicle formation.	38
7.	Anatomical areas in the developing telencephalon.	39
8.	E9.5 Vegf isoform mice display unique transcriptome profiles.	42
9.	E9.5 Vegf120/188 forebrain transcriptome is unique from wild-type. . .	45
10.	Meta-analysis of transcriptome shifts of embryonic forebrain in Vegf isoform mice compared against an E9.5 wild type background.	48
11.	Separate technical batches of E9.5 wild type forebrain microarrays display no statistically different genes in a meta-analysis.	51
12.	Cross-comparisons of transcriptional shifts between Vegf isoform forebrains and embryonic time points.	53
13.	qPCR heatmap comparing fold change for target gene expression in the Vegf isoform mice versus wild type.	60
14.	qPCR confirmation of the meta-array analysis.	63
15.	Enriched Gene Ontology Categories in Vegf isoform mice.	65

16.	Proportion of differentially expressed genes contributed by the Vegf Isoform mice in each GO category.	66
17.	Changes in Vegf isoform profile affects deposition and quantities of ECM and ECM-interacting proteins at E11.5.	69
18.	Vegf isoform profile affects Laminin proteins levels.	72
19.	Altered Vegf bioavailability alters early neural stem cell fate and basement membrane organization.	75
20.	Vegf regulation of NSC proliferation and differentiation.	78
21.	Vegf isoform profile affects the distribution of Calbindin positive cells.	81
22.	Vegf isoform misexpression affects radial glia morphology and periventricular blood vessels.	86
23.	Vascular compromise and migration defects in the Vegf isoform mice.	88
24.	Vegf isoform bioavailability affects Calbindin-positive cell morphology in the LGE.	91
25.	Radial distribution of intermediate progenitors is modulated by the available Vegf isoform profile.	94
26.	The available Vegf isoform profile does not affect early post-mitotic neuronal differentiation.	97
27.	Vegf affects neocortical layering at postnatal day 0.	100
28.	Vegf is required for the differentiation and stratification of Tbr1+ cells.	102
29.	Vegf affects formation of neocortical layer V at PO.	104
30.	Vegf isoform profile affects the distribution of Ctip2+ cells of neocortical layer V.	106
31.	Predicted protein interactions network with a subset of differentially expressed genes identified in the Vegf isoform mice.	112

LIST OF TABLES

Table		Page
I.	PCR primers used to genotype Vegf isoform mice.	121
II.	Primer pairs used in qPCR analysis.	122
III.	Differentially-expressed genes in E9.5 forebrain of Vegf isoform mice compared to wild type (WT).	123
IV.	Genes identified as differentially expressed in E9.5 Vegf isoform mice and E11.5 wild types relative to a E9.5 wild type background.	138
V.	Covariate analysis of qPCR quantitation for key growth factor signaling genes (Shh, Notch3, Cxcl12, Cxcr7, Nrp1, Nrp2) and reference genes (18S and Gapdh).	139
VI.	Covariate analysis of qPCR quantitation for key transcription modulators (Suz12, Dnmt3a, Id1, Pax6, Hey 2, Fezf2, Pax3, FoxM1, and Zfhxb1) and reference genes (18S and Gapdh).	147
VII.	Covariate analysis of qPCR quantitation for key extracellular matrix proteins (Lama4, Lama5, Lamc3, FN) and reference genes (18S and Gapdh).	156

ACKNOWLEDGEMENTS

I wish to express my sincere appreciation to the members of my advisory committee for their guidance and support during my time in the doctoral program at the University of North Dakota. I would like to thank Diane Darland, my primary mentor, without whom this project would not have been possible, as well as all of the members of the Darland lab with whom I collaborated and made the work much more enjoyable. This work was supported by University of North Dakota faculty start up funds and North Dakota EPSCoR (DD), as well as the National Institute of Health (NIH-NINDS R15 NS057807-01/-02 and 3R15NS057807-01S1, DD). Additional support was provided by the Red River Valley Neuroscience Initiative (JC), as well as the American Heart Association (AHA0715542Z, JTC).

For
Bill, Teri, Justin, Elizabeth,
Tom, Jan, Mayrinda, Philippe,
And Kari

ABSTRACT

One of the characteristics unique to mammalian evolution is the development of the neocortex. The neocortex is a highly ordered six-layered structure, the development of which is tightly regulated. The formation of the cortex is concomitantly dependent upon an outward expansion of the neuroepithelium, a tissue from which all of the neuronal subtypes and glia are born and differentiated, and the investment of blood vessels from the outer pial surface. Orchestration of neurogenesis and blood vessel investment, or angiogenesis, in the cortex is critical for development; however, these processes are often studied independent of one another. While independent investigation of neurogenesis can simplify a study, by removing the potentially confounding variable of angiogenesis, this reductionist approach ignores the fact that the two processes, neurogenesis and angiogenesis, are dependent upon each other and intimately linked.

Many growth factors and transcription factors have roles in both angiogenesis and neurogenesis. Members of both the Notch and Inhibitor of DNA binding (Id) family of proteins have been shown to guide differentiation in neural stem cells, as well as to direct the migration of newly sprouting vessels. Another growth factor that has been linked to both angiogenesis and neurogenesis is Vascular endothelial growth factor A (Vegf). Vegf is a

pleiotrophic factor linked to a broad range of effects in neurovascular systems including proliferation, migration and differentiation. Vegf and its receptors (VegfR1, VegfR2, Nrp1, and Nrp2) are expressed in many of the cell types critical for neurogenesis and angiogenesis.

The Vegf gene is expressed as three main isoforms in the mouse brain, and these isoforms have distinct biochemical properties based on the presence or absence of a heparin sulfate proteoglycan (HSPG) binding domain. Vegf isoforms with the full HSPG-binding domain are not diffusible in the microenvironment (Vegf188) without proteolytic cleavage, those with a partial HSPG-binding domain are partially diffusible (Vegf164), and those lacking the domain entirely are freely diffusible (Vegf120). The different biochemical properties of the Vegf isoforms allow gradients of Vegf to form in the microenvironment. We hypothesize that it is through these differing gradients of Vegf isoforms, that Vegf can orchestrate neurogenesis and angiogenesis in the cortex. To investigate this, we took advantage of a transgenic mouse model in which mice express single Vegf isoforms (Vegf120 or Vegf188), or combinations of Vegf isoforms (Vegf120/188), and lack the Vegf164 isoform. These mice represent a loss of function model (no Vegf164) as well as misexpression models through which we can test the role of Vegf in cortical neurogenesis and angiogenesis.

The role of Vegf in angiogenesis has been extensively studied, and changes in the available isoform profile have been linked to altered blood vessel morphology, specifically vessel integrity (Vegf120) and capillary branching

(Vegf188). Since angiogenesis is tightly coupled with neurogenesis, the dysmorphic vessels in the Vegf isoform mice may indirectly affect neurogenesis independent of the effect of altered Vegf isoform signaling and localization. To minimize these indirect effects, we investigated the earliest stages of cortical development, beginning at stages where blood vessels have yet to invest the neuroepithelium. At E9.5, a stage where there is no blood vessel investment within the dorsal-anterior neuroepithelium, we looked at the neuroepithelial transcriptome across the wild type and Vegf isoform mice. We found that the Vegf isoform mice had unique patterns of expression when compared to wild type and to each other. Identified amongst these differentially expressed genes were cohorts of genes with functional annotations linked to neurogenesis and neural stem cell differentiation.

Based on the differentially expressed genes identified in the transcriptome profiles of the Vegf isoform mice we predicted that early neural stem cell proliferation, migration, and differentiation may be affected at later stages. At E11.5, a critical period in neuroepithelial expansion, design-based stereology was used to quantify cells immunolabeled for markers of proliferation (Phospho-histone H3, Phh3), differentiation (T-box related proteins 2, Tbr2), and migration (Calbindin, Calb1). The Vegf isoform mice had shifts in total cell number, neuroepithelial Phh3-positive cells, Tbr2-positive cells, and calbindin1-positive cells with patterns of expression varying across the Vegf isoform genotypes relative to the wild type.

In order to link disruption of normal Vegf isoform expression to changes in

early neural stem cell differentiation and the subsequent establishment of the neocortical layers, we used immunolabeling of cortical layer-specific markers to identify regionality in the developing cortical layers at P0. At this time point only the deepest layers of the six-layered cortex are established, specifically layers V and VI. Immunolabeling of markers specific to layer VI (Tbr1) and layer V (Ctip2) revealed extensive migration and lamination defects resulting in expanded regions of Tbr1-positive cells in layer VI of the Vegf isoform mice as well Ctip2-positive cells in presumptive layer V relative to wild type.

Taken together our evidence points to a role for Vegf in neocortical development. To our knowledge, these data constitute the first comprehensive transcriptome assessment of the Vegf isoform mouse forebrain at a point in development that precedes major cortical lamination. Our data support a key role for the different Vegf isoforms in modulating neural stem cell proliferation, differentiation, and migration with dramatic effects on early layer (VI and V) formation in the cortex. Moreover, we have identified a role for Vegf188, particularly, in modulating normal tangential migration of the calbindin-positive neural precursor population that eventually gives rise to a major portion of the GABA-ergic interneurons of the cortex. These results beg the question, “what is the long-term consequence for cortical function given the abnormal lamination observed with disrupted Vegf isoform profile? Future studies will likely attempt to link early establishment of neural populations and their appropriate connections/positions with sensory processing abnormalities in a mature cortical system. It is clear, however, that a full complement of Vegf isoforms is

necessary not only for normal blood vessel investment of the cortical neuroepithelium, but also for the proliferation, differentiation, and migration of neural stem cells that constitute the major functioning unit of the mouse cortex.

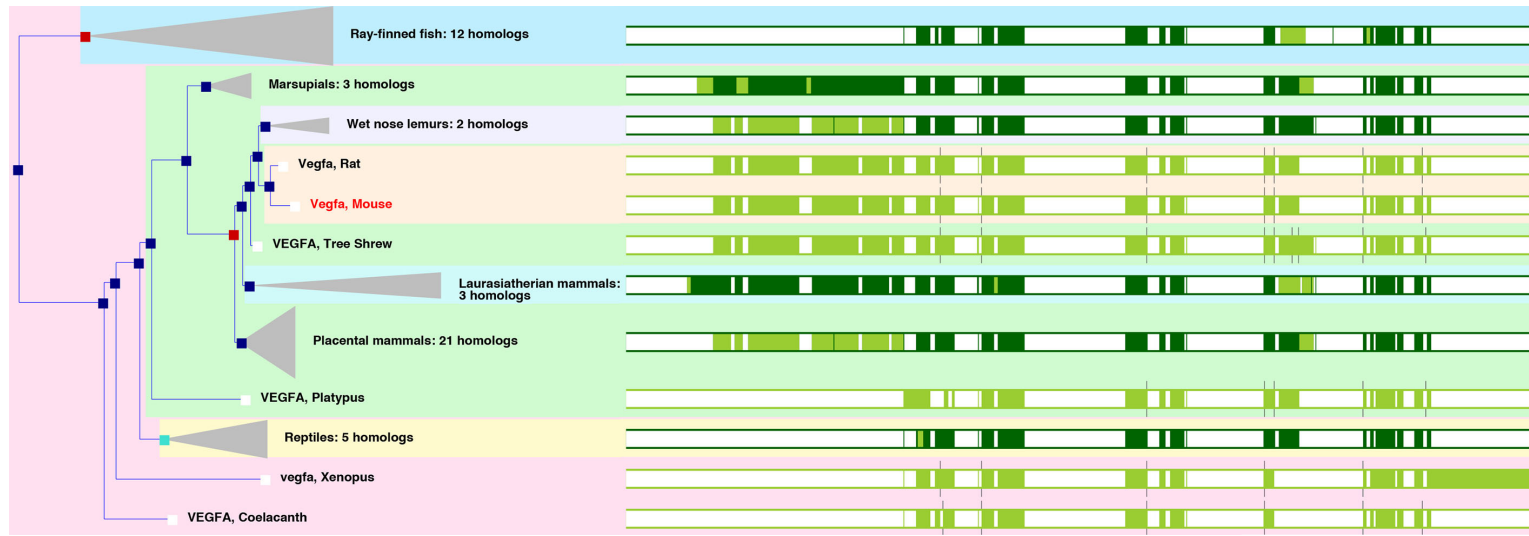
CHAPTER I

INTRODUCTION

Vascular endothelial growth factor A

Vascular endothelial growth factor (Vegf) A is a secreted protein important in the regulation and development of both the vascular and nervous systems. Vegf A is a member of the Vascular endothelial growth factor/Platelet-derived growth factor family of proteins. The major members of this family include Vegf A, Vegf B, Vegf C, and Vegf D all of which belong to a cysteine-knot superfamily of signaling biomolecules. Evolution of Vegf is thought to have occurred early in animal development as the Vegf family of proteins is highly conserved between teleosts, reptiles, and mammals (Figure 1), and Vegf-like homologs, Vascular permeability factor (VPF), are found in *Drosophila melanogaster* and *Caenorhabditis elegans* (reviewed in [1], [2]).

The Vegf A, henceforth referred to as Vegf, gene contains 8 exons that are alternatively spliced to generate several isoform variants in mouse: Vegf120, Vegf145, Vegf164, Vegf188, and Vegf208. The predominant isoforms in the mouse brain are 120, 164, and 188 [3-6] (Figure 2A). These isoforms differ in amino acid number and composition resulting in different biomolecular properties, including differential ability to bind heparin and heparan sulfate proteoglycans (HSPG), as well as the various Vegf receptors (Figure 2B).



2

Figure 1. Alignment of Vegf A homologues among vertebrate organisms.

Using the Taxonomy browser and the Tree-building platform in the National Center for Biotechnology Information (<http://www.ncbi.nlm.nih.gov>), a dendrogram was constructed that highlighted the major taxonomic branch points and sequence relatedness among several vertebrate classes compared to the mouse Vegf A gene. Genomic sequence alignments are indicated as 0-33% (white blocks/gaps), 33-66% (light green), or 66-100% (dark green). Speciation nodes are indicated with blue squares and duplication or gene split events are indicated with red nodes. The number of homologues described to date are indicated for major subdivisions.

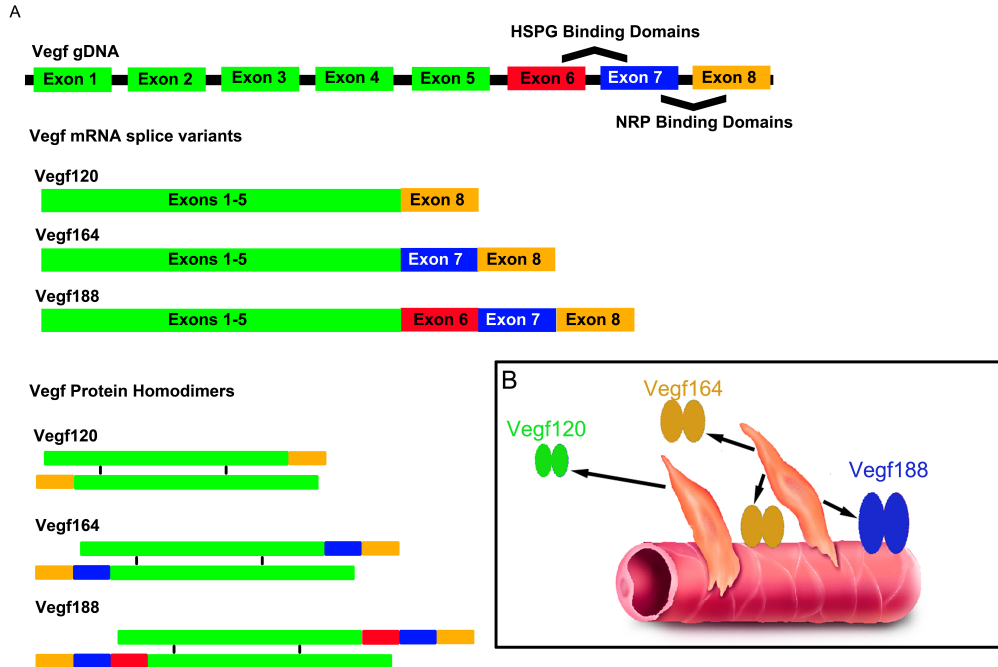


Figure 2. Vegf splice variants form isoforms with differential diffusion potential. (A) Genomic Vegf consists of eight exons, which after transcription can be spliced to form isoforms, with unique exon 5 borders. The three main Vegf isoforms, Vegf120, Vegf188, and Vegf164, all share exons 1-5 (green) and 8 (gold). Vegf120 lacks the HSPG-binding domain coded by exons 6 (red) and 7 (blue) and is freely diffusible. Vegf188 contains all eight exons, including the full HSPG-binding domain, and is non-diffusible. Vegf164 lacks exon 6, but includes exon 7, leaving it with a partial HSPG-binding domain and is locally-retained and diffusible. The Vegf isoforms dimerize in a head-to-tail fashion to bind to transmembrane receptors. (B) This differential diffusion capacity allows for Vegf to act as an autocrine, juxtacrine, and paracrine signaling factor as depicted in this cartoon of a forming vessel lumen with perivascular cells producing Vegf isoforms that either diffuse (Vegf120 or Vegf164) or are retained in the local microenvironment (Vegf164 or Vegf188).

All of the Vegf isoforms share exons 1 through 5 and 8, however they differ at their exon 5 borders (Figure 2A). The Vegf120 isoform lacks the HSPG binding domain normally coded for by exons 6 and 7, and is thus freely diffusible throughout the extracellular microenvironment [4, 7]. In contrast, the Vegf188 isoform contains all 8 exons, including the full HSPG binding domain making it locally retained within the microenvironment, unless released by proteolytic cleavage. Vegf164, the primary Vegf isoform in the mouse brain, lacks exon 6 resulting in a partial HSPG binding domain allowing it to be both locally retained and diffusible [8-10]. These differences not only result in the isoforms having differential behaviors in the extracellular environment but also the capacity for differentially activating the Vegf receptors [11, 12].

Vegf mediates its actions through a range of autocrine, juxtacrine, and paracrine effects via its interaction with integral membrane receptors. Vegf signals through the receptor-tyrosine kinases (RTK), Vegfr1 and Vegfr2, as well as non-tyrosine kinase receptors Neuropilins 1 and 2, (Nrp1 and Nrp2)[12-16]. Vegfr2 is well described for its role in promoting angiogenesis, the formation of new vessels from pre-existing vessels; and, more specifically, for its positive regulation of endothelial cell (EC) proliferation and migration. The role of Vegfr1 in mediating Vegf signaling is less well understood. Vegfr1 activation does not induce angiogenesis to the degree that Vegfr2 does; however, Vegfr1 has been suggested to function as a Vegf trap, or sink [17, 18]. If the “sink” hypothesis is valid, then Vegfr1 indirectly controls Vegf signaling by preventing binding to

Vegfr2 or other Vegf receptors. Signaling through these receptors is mediated through the formation of various heterodimers and homodimers, including combinations of the Vegfr2 receptor with Nrp1 or Nrp2 [19].

Not only do the different combinations of receptors elicit differential downstream signaling when bound to a Vegf ligand, but the Vegf isoforms also may have differential abilities as ligands to bind those receptors, particularly to the Nrps [12-14, 20-22]. The ability of Vegf to bind to and activate the Nrps is thought to be coded by exons 7 and 8, which are alternatively spliced in the Vegf isoforms. For example, the Vegf120 isoform lacks the Nrp-binding domain coded by exon 7, and therefore has a lower affinity to bind to homodimers of either Nrp1 or Nrp2 with, but might be able to bind more strongly to heterodimers of Vegfr2 and Nrp1 or 2 [1]. Nrps are expressed on neural populations and are well described for their ability to bind semaphorins, which act as migratory cues during neurogenesis [23-25]. Because Vegf can signal via Vegfr2-Nrps heterodimers, signaling within both neural and vascular systems is possible.

Vegf expression begins in the mouse as early as embryonic day (E) 7, and increases in expression throughout embryonic development, with prominent mRNA expression in the myocardium and neuroectoderm [26, 27]. Vegf expression decreases during adulthood; however, expression remains elevated in the vascular bed of the choroid plexus, lung alveoli, kidney glomeruli, and heart [1]. Vegf gene expression has been linked directly to oxygen levels in the microenvironment. Moreover, hypoxic conditions during development or after injury have been shown to increase Vegf expression [28]. Hypoxia responsive

enhancers surround the Vegf gene and bind Hypoxia-inducible transcription factors that mediate Vegf expression in response to hypoxia [28].

Initially described as Vascular permeability factor (VPF), Vegf was first identified for its ability to induce permeability in vessels of tumor ascites, in mice [29]. Since then Vegf and its receptors have been well described for their roles in vasculogenesis and angiogenesis [30]. Vasculogenesis is the formation of new blood vessels, de novo, versus angiogenesis, which is the sprouting of new vessels from existing vasculature. In the mouse, vasculogenesis is largely restricted to the yolk sac, in which Vegfr1 expression has been detected as early as E6.5 by in situ hybridization [31]. Mice lacking Vegfr1 are embryonic lethal by day E9.0 as the cardiovascular system fails to form properly and development cannot proceed past this point [32]. Absence of a single allele of Vegf or Vegfr2 also results in embryonic lethality indicating the importance of tightly regulating Vegf protein levels in a developing organism. Decreased Vegf signaling impairs hematopoiesis and endothelial cell differentiation in the yolk sac [32]. Mice lacking Vegfr2 fail to form blood islands in the yolk sac, resulting in abnormal migration of the hematopoietic cells that arise in the yolk sac and migrate to the embryo proper. In addition, the Vegfr2 heterozygous knockout mice display impaired vasculogenesis [33, 34] further supporting a critical role for Vegf and its receptors during early embryonic development.

Vegf is crucial to angiogenesis as it drives endothelial cell proliferation and guides vessel migration, key cellular processes required for establishment, expansion, and elaboration of the vascular system. Gradients of Vegf in the

microenvironment may direct angiogenesis and guide vessels to their targets. Ruhrberg and coworkers have proposed the gradient hypothesis for Vegf action with microenvironmental location established based on the different biochemical properties of the Vegf isoforms [4]. Specifically, they have proposed that Vegf120 has the potential to diffuse away from the Vegf producing cell since it lacks the HSPG binding domains. In contrast, any Vegf188 would likely remain in close proximity to the cell producing it, as the protein would bind tightly to HSPG on the cell surface or embedded within the extracellular matrix. The Vegf164 protein, possessing only part of the heparin sulfate proteoglycan binding domain would display intermediate properties, being bound locally as well as able to diffuse short distances (Figure 2B, 3) [4]. In keeping with the gradient hypothesis, the Vegf isoforms are differentially expressed in different organ systems during development and in the adult [3]. In addition, mice have been generated that express single or combinations of single Vegf isoforms in lieu of the normal complete profile of Vegf isoform expression [3, 5, 6, 35-37]. The altered Vegf gradient in mice expressing only the diffusible Vegf120 isoform leads to early postnatal embryonic lethality due to abnormal development of the cardiopulmonary system [3, 35]. In these mice, lung alveoli did not form and the normal capillary investment of the lung buds was incomplete. Interestingly, it was later shown that Vegf188 is the predominant isoform in the mouse lung [3] and its absence in the Vegf120 mice completely prohibited normal lung development. The Vegf120 mice also showed abnormal blood vessel formation in the retina and hindbrain leading to vessels with broad lumens and reduced

vessel branching. Mice expressing only the locally-retained Vegf188 isoform were fully viable and exhibited highly ramified blood vessels with decreased luminal diameter [5, 36, 37]. Altering the local Vegf gradient with locally-retained Vegf protein isoforms (Vegf188 or Vegf164) results in supernumerary blood vessels in the developing neural tube [38]. Therefore, the bioavailability of Vegf and its localization in the microenvironment are critical for directing angiogenesis.

Crucial to the distribution of growth factors, such as Vegf, throughout the microenvironment are interactions with extracellular matrix (ECM) and HSPGs on the cell surface. Growth factors with HSPGs-binding domains have reduced diffusion through the microenvironment. In vitro, only Vegf120 and Vegf164 are detected in media conditioned with cells producing a normal contingent of Vegf isoforms. Vegf188 protein, with its strong HSPG-binding domain, is not detected unless heparinase is added to the media, thereby releasing the Vegf188 from the HSPGs [8, 39].

The ECM not only acts as a binding scaffold directing migrating cells, but components of the ECM can also sequester growth factors thereby establishing signaling gradients and working as co-receptors for growth factors. The distribution of ECM components, like laminin (LN), fibronectin (FN), and HSPGs, in the microenvironment are critical to guiding the vasculature and disruption of ECM deposition or HSPG synthesis impairs normal developmental patterning [40-42]. Interactions between Vegf and the ECM regulate cell behavior and modulate Vegf receptor signaling. Vegf binding to ECM is required for activation of some of Vegf's signaling pathways [43]. For example, cells grown on

fibronectin-coated surfaces in culture and treated with Vegf display increased cell proliferation and cell migration relative to cells grown in the presence of either Vegf or FN alone [44]. Vegf binding to FN regulates endothelial cell proliferation via subsequent downstream signaling through integrin receptors and Vegfr2 [45]. The differential adhesion of Vegf isoforms to ECM and HSPG allows the isoforms to act as juxtacrine, autocrine, and paracrine factors depending on the isoform being expressed and its localization in the microenvironment. Differential Vegf isoform profiles can modify downstream Vegf signaling pathways based on differential isoform-dependent receptor activation.

Development of the Nervous system in concert with the investment of the circulatory system

Development of the circulatory system is concomitantly coordinated with the development of the nervous system [46, 47]. From an anatomical perspective, the layout of the peripheral nervous system closely parallels the patterning of the vessels of the circulatory system, suggesting the possibility for molecular and physical crosstalk between the two systems as they develop [46, 48]. In the central nervous system (CNS), the early stages of forebrain formation are characterized by proliferation of an initially avascular neuroepithelium (NE) followed by blood vessel investment from the pial surface. Angiogenesis always accompanies the expansion of the NE and is tightly coordinated, spatially and temporally, with neurogenesis in the NE [49-51] (Figure 3).

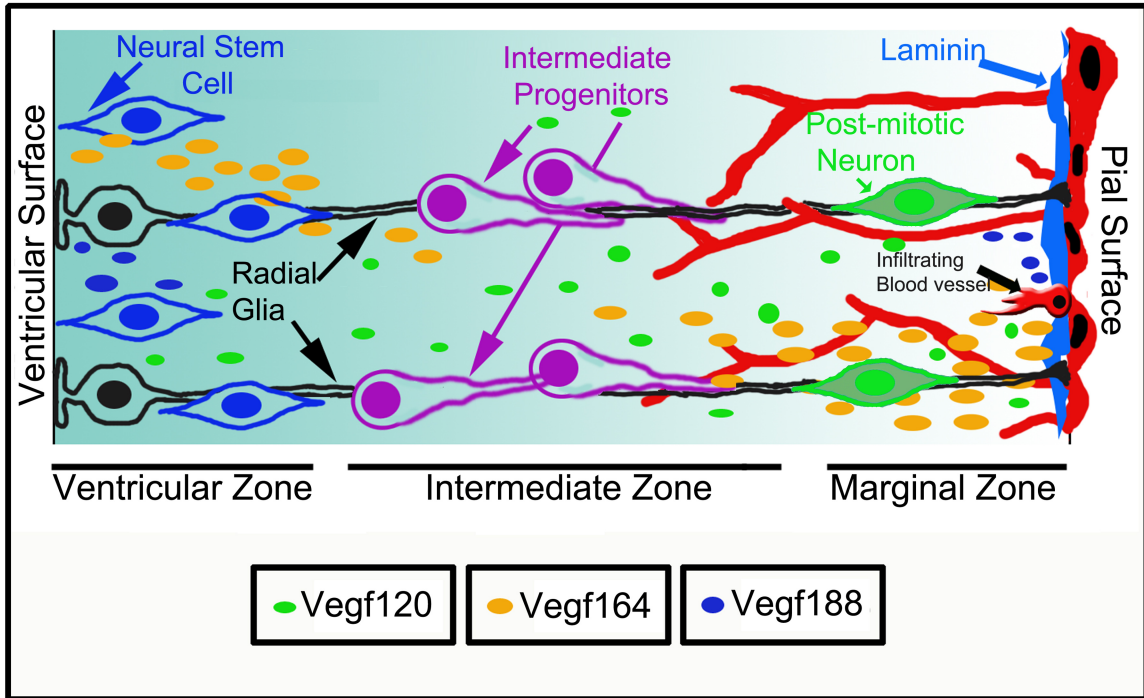


Figure 3. Vegf isoform distribution in the developing neuroepithelial microenvironment. The differential ability of the Vegf isoforms to bind HSPG can establish gradients of Vegf within the cellular microenvironment. The cartoon depicts the early stage of forebrain development with the pial surface shown to the right. Here, vessels are established in the epidermal-derived surface tissue of the embryo and begin sending sprouts into the neuroepithelial tissue during angiogenesis (red cells). Laminin in the basement membrane is shown as a blue deposit along the pial surface. New capillary growth initially invests the tissue in a radial fashion with subsequent formation of lateral plexi later in development. On the ventricular surface of the neuroepithelium is the zone of proliferating cells (blue cells) and the soma of radial glia (black cells). Intermediate progenitors (purple cells) and post-mitotic committed neural precursors (green cells) are closely associated with the radial glia processes and the ingressing blood vessels. The Vegf120 (green circles), Vegf164 (gold

circles), and Vegf188 (blue circles) are produced by cells within the neuroepithelium, although the specific sources are unclear. Vegf production is depicted to occur at both the ventricular and pial surfaces to include both major potential sources of this potent neural and angiogenic factor. Gradients of Vegf are critical to serve as molecular guides for the migration and differentiation of neural stem cells from the ventricular surface in parallel with vessel investment from the pial surface into the expanding neuroepithelium.

Neurogenesis is the process that drives neural stem cell (NSC) populations to differentiate into the neural and glial derivatives of which the CNS is comprised. The formation of the CNS begins as a thin avascular neural tube that grows exponentially as neurogenesis proceeds. Early stem cells expand in number through a rapid series of cell divisions, which in turn, thicken the neural tube. This expansion of the neural tube results in a specific neuroepithelial arrangement of cells, with some of those cells possessing processes contacting both the inner and outer surfaces of the tube. These particular cells are radial glia. Radial glia are a source of neural progenitors, they function to guide the differentiation of NSCs, the migration of post mitotic neurons, and the investment of blood vessels. Radial glia are neural progenitors that divide and undergo mitoses along the inner surface of the neuroepithelium, known as the ventricular zone (VZ) [52, 53] (Figure 4A). These cells also undergo an interkinetic nuclear migration between divisions, whereby the nuclei of these cells will cyclically migrate towards the outer surface of the neural tube, the pial surface (PS), and back during the S-phase of the cellular cycle [54]. Radial glia maintain contact with both the ventricular and pial surfaces throughout the life of the individual, although radial glial numbers are severely reduced in adulthood and the population is often referred to as tanicytes [52, 53]. Their role as a progenitor population in the adult has been hotly debated over the last several years [52, 54].

Besides being a primary source of neural progenitors, radial glia serve as “guides” for post-mitotic neurons migrating to their appropriate destination within

the laminar neuroepithelium and as contact points for infiltrating blood vessels investing the neuroepithelium. As the metabolic demands of thickening neuroepithelium increase, blood vessels from the PS invest the tissues. Radial glia, a source of Vegf, may serve to coordinate these processes by providing a gradient of Vegf for invading ECs and differentiating NSCs to follow [55] (Figure 3). Vegf binding of Nrp1 is required for invading ECs to properly migrate along the RG following the Vegf gradient as they invest the neuroepithelium [56], while Vegfr2 on migrating neurons guide them as they migrate along the radial glia. There is little known about the direct role that Vegf may play in regulation of radial gliogenesis, differentiation, or function; however, Vegf and Vegfr2 protein immunolabeling have been associated with radial glia, neurons, and the vascular cells of developing human fetal telencephalon [56, 57]. Vegf signaling promotes neuronal survival and axon outgrowth in cultured peripheral neurons [58, 59], in cortical neurons in culture, and *in vivo* [60, 61]. Vegf has been shown to be critical for coordinating sensory neuron migration and arteriole branching in both the peripheral nervous system and the neocortex, although the sources of Vegf were not clarified in these studies [56, 62]. Taken together, these results suggest a possible role for Vegf in coordinating neurogenesis and angiogenesis in the forebrain.

Critical to the coordination of neurogenesis and angiogenesis is the collection of ECM molecules secreted by the radial glia and surrounding tissue. ECM provides pathway and migration cues, mediates cell survival via adhesion, and acts as a reservoir for growth factors, such as Vegf [63, 64]. Differential

binding of Vegf isoforms to ECM may establish Vegf gradients in the NE microenvironment that are dependent upon both diffusible and ECM-associated Vegf isoforms. Proper function of radial glia is not only dependent upon these growth factor signals associated with the surrounding ECM, but also upon direct interactions with ECM proteins, themselves. For example, radial glia bind to laminin in the ECM via the $\alpha 6$ and $\beta 1$ integrin receptor complex [65-67]. Both $\alpha 6$ and $\beta 1$ integrin subunits have been shown to be necessary for proper radial glia end-feet attachment at the cortical surface. The loss of these subunits resulted in bundled end-feet that failed to correctly attach to the basal lamina at the cortical pial surface [68]. Apical and basal lamina contact with the basement membrane (via LN), as well as adherens junctions, are critical for proper radial glia differentiation and migration, as they help to anchor the cell and maintain a basal-apical polarity within the cell [52]. The polarity of radial glia, established by its apical and basal contacts with ECM, allows these cells to divide both symmetrically and asymmetrically. The type of division radial glia undergo has been linked to unequal distribution of integrins along the cell surface, as well as other cytoplasmic components, and results in differential cell fates [52, 69] (Figure 4A). When the NSC divides symmetrically and the two daughter cells maintain contact with the ventricular surface, both progeny maintain NSC status. When the daughter cells undergo asymmetric division and one of the progeny loses contact with the ventricular surface, that daughter progresses down the neural lineage.

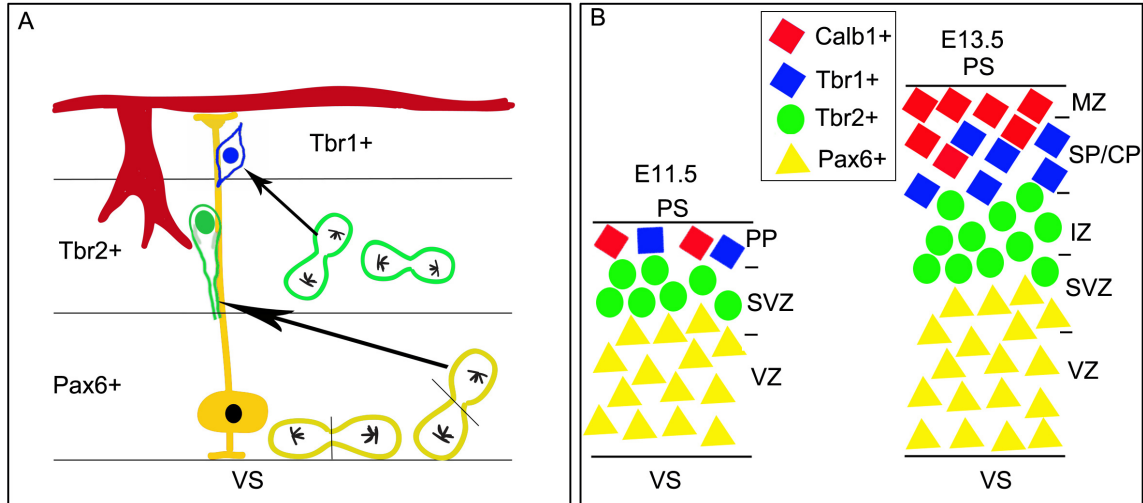


Figure 4. Neural stem cell differentiation and early cortical layer formation.

Early neural stem cells are Pax6+ cells found in the Ventricular zone (VZ). These cells divide along the Ventricular surface (VS), where they can undergo either a symmetric, proliferative, division to increase their numbers, or an asymmetric, differentiative division whereby one cell remains Pax6+ and the other becomes Tbr2+ and migrates from the VZ. These Tbr2+ cells are known as intermediate progenitors, and they also can undergo both proliferative symmetric divisions, or differentiate into Tbr1+ positive cells with an asymmetric division. These Tbr1+ cells are post-mitotic neurons, which migrate along the radial glia into the six-layered neocortex (a). The pallium of the adult neocortex forms six layers, and is populated by two major neuronal cell types, the pyramidal cell and the interneuron. The six layers are formed from the inside-out migration and differentiation of pyramidal cells born in the VZ and subventricular zone (SVZ) of the pallium, as well as a tangential migration of Calb1+ interneurons born in the GE. At E11.5, the pallium consists of two germinal zones, the VZ,

consisting of Pax6+ cells, and the Subventricular Zone (SVZ), where the Pax6+ cells transition to Tbr2+. At this stage the early post-mitotic neurons form a layer known as the Pre-Plate (PP). At E13.5, the three initial zones stratify even more adding the intermediate zone (IZ), sub-plate (SP), and cortical plate (CP). As Tbr2+ intermediate progenitors transition to Tbr1+ post-mitotic neurons they migrate from the IZ to the SP and CP. The six-layers of the neocortex form between the CP and MZ, starting with the deepest cortical layer, VI. Concomitant with the stratification of the neocortex and radial migration of the pyramidal cells is the investment of Calb1+ interneurons arriving via a tangential migration along the pial surface from the GE.

Neural stem cell differentiation

The thickening neural epithelium of the primitive forebrain becomes stratified early on as NSC populations give rise to additional radial glia, proliferating intermediate progenitor populations, or dedicated neuronal or glial lineages [70-74]. As NSCs shift from a proliferative stem cell state, they proceed along a stepwise differentiation pathway, reflected by a sequential shift in the expression of several transcription factors, paralleled by an outward migration (Figure 4A). Most of the early proliferative cells are radial glia with Pax6-positive nuclei found in the ventricular zone. These Pax6-positive cells can either expand their number with a symmetrical division, or they may undergo an asymmetrical division, with one daughter cell maintaining its Pax6 identity and the other daughter cell transitioning into a Tbr2-positive intermediate progenitor cell¹ which begins to migrate into the subventricular zones. The Tbr2-positive cells can take one of two potential paths, they may shift to a Tbr1-positive, post-mitotic, cell dedicated to a neuronal lineage, which then migrates into the intermediate zone (IZ) or subplate (SP) [70, 75]. A Tbr2-positive intermediate progenitor can also divide and form two more Tbr2-Positive cells, thus expanding the intermediate progenitor cell pool (Reviewed in [76]). Tbr2-positive cells and Tbr1-positive cell populations contribute directly to formation of the upper neocortical layers [55,

¹ The term intermediate progenitor refers to a neural progenitor cell that divides outside of the ventricular zone, away from the ventricular surface. In the literature, these cells are also known as basal progenitors.

75, 77, 78]. Due to the obvious need for a balance in the number, timing, and control of cell fate decisions, these sequential shifts in lineage determination are tightly regulated [74, 79, 80]. The key molecular regulators of these developmental transitions are an ongoing area of research, particularly in the multi-layered cortex [81, 82].

Neocortical Development

One of the distinctive features of the mammalian brain is its six-layered neocortex, consisting of two major neuronal cell types, the pyramidal cell and the interneuron. The unique laminar structure of the neocortex is formed through the coordinated radial migration and differentiation of cortical pyramidal cells and the tangential migration of interneurons from the ganglionic eminence [83]. The neocortical layers are formed from the inside out, and are specified in an orderly fashion early in cortex development.

Early NE (E9.5-12.5) of the developing cortex can be divided into three distinct germinal layers, starting at the inner VS is the ventricular zone (VZ), followed by the subventricular zone (SVZ), and finally an outer marginal zone (MZ) (Figure 4B). Neural progenitors are born in the VZ, and as they differentiate they migrate out and form additional layers. After E13.5, two additional germinal layers form between the SVZ and MZ, the intermediate zone and subplate. It is from these germinal layers that the six-layered mammalian neocortex arises (Figure 4B). Most of the pyramidal neurons that compose the six layers of the neocortex are born in and then migrate radially away from cells in the ventricular and subventricular zones. The neurons of each layer are formed sequentially,

starting with those in the deepest layer, VI, and proceeding in an “inside-out” fashion forming layer I last.

Coordinated with the outward laminar neocortical formation is the tangential migration of interneurons born in the ganglionic eminence (GE). These interneurons are Calbindin-positive (Calb1) and follow gradients of signaling molecules as they move from the Ganglionic Eminence (GE) into the developing pallium of the neocortex. One such signaling molecule is the chemokine, Cxcl12, which is expressed in the pallium and the cerebellum. The cortical interneurons use the receptor Cxcr4 to follow gradients of Cxcl12 as they migrate through the pallium [84]. Absence of Cxcl12 and Cxcr4 lead to major angiogenesis defects as well as lamination and migration defects in the developing cortex [85, 86]. Vegf has been shown to increase expression of Cxcr4 in endothelial cells [87, 88] and the converse is true as well with Cxcl12 increasing expression of Vegf in a variety of cell types [88, 89]. The role of Cxcl12/Cxcr4 in mediating cellular migration has been revisited recently with the observation that Cxcl12 can signal through RDC1, now named Cxcr7 [90-92]. Exciting new data on the impact of Cxcl12 signaling through Cxcr4 (pro-migratory) or Cxcr7 (anti-migratory) [93, 94] in the zebrafish nervous system has led to the idea that the impact of Cxcl12 signaling may be due to a balance between opposing signals through Cxcr4 or Cxcr7 with the outcome of the struggle determining whether or not cells migrate. To date, no direct link has been shown between Vegf and Cxcl12 signaling through Cxcr7. Microvascular ECs show altered expression of Cxcr4 and Cxcr7 in response to hypoxia, but not to direct application of Vegf [95]. How these various signaling pathways integrate

to regulate NSC fate choice and migration are unclear, but Vegf may be a central player based on its ability to impact both the vascular and neural systems directly.

Experimental Model

Given the contextual overlap amongst neural stem cell differentiation, neurogenesis, and vascular development, Vegf emerges as a central player, a factor potentially impacting all the cell types involved. Using Vegf120/120 mice, Vegf188/188 mice, and Vegf120/188 mice (mice which express individual or combinations of Vegf isoforms) the role of Vegf and its isoform variants in these processes can be elucidated. Taking advantage of these mice, henceforth referred to as Vegf120, Vegf188, and Vegf120/188, neural stem cell differentiation can be examined in the presence of altered Vegf isoform profiles in mice expressing only Vegf120, only Vegf188, or both Vegf120 and 188 (Vegf120/188). Since the Vegf164 isoform is the predominant form in the early forebrain [6], these former mice represent both loss of function (in the form of the Vegf164) as well as altered localization based on the differential distribution of the Vegf isoforms in the microenvironment. The Vegf120/188 mice represented a putative functional rescue as the combination of isoforms provides both a local source of Vegf, the non-diffusible Vegf188, and a diffusible source in the non-HSPG binding Vegf120. These different lines alter the microenvironmental localization of Vegf, without affecting total levels of available Vegf (Figure 5A and B).

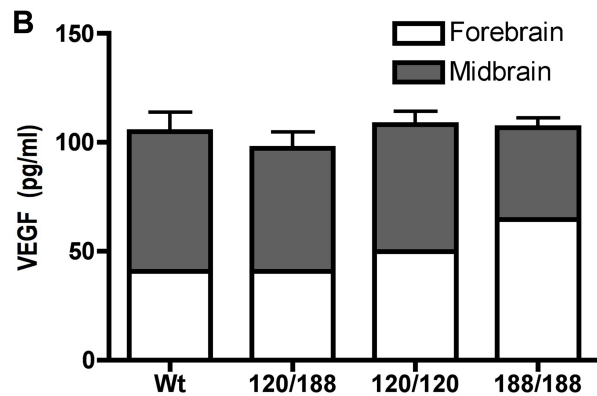
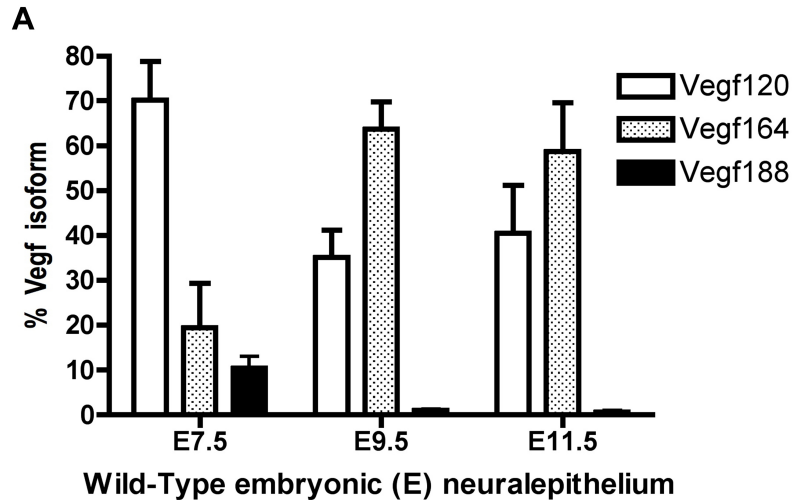


Figure 5. Vegf isoform expression in early forebrain. Expression of individual Vegf isoform mRNA was quantified by qPCR in wild-type neuroepithelium at E7.5, E9.5, and E11.5 (n = 11). Levels of each Vegf isoform are presented as a percent of total values for cDNA (DNA/ng RNA in original cDNA reaction) based on standard curves for each isoform. The proportion of Vegf isoform mRNA shifts as development proceeds, with the highest highest levels of Vegf120 and Vegf188 detected at E7.5. After E9.5, the proportion of Vegf188 mRNA was reduced to basal levels, while the proportions of Vegf120

and Vegf164 switched with Vegf164 becoming the highest expressed Vegf isoform in the forebrain (A). Vegf protein levels at E11.5 were quantified using an ELISA which detected total Vegf levels in the forebrain and midbrain based on a Vegf protein standard curve (B, N=7; ANOVA, no statistical difference among populations).

The effects of altered Vegf localization on NSC fate choice and subsequent cortical lamination can be investigated with these Vegf isoform mice. Our hypothesis is that Vegf signaling plays a key role in regulating the coordinated investment of vasculature in the CNS and the differentiation, survival, and migration of NSCs in the forebrain, processes which ultimately lead to proper cortical layer formation. We predict that altering Vegf isoform availability by changing the profile of expressed isoforms would alter cell fate choice at these critical junctures impacting proliferation, differentiation, and migration resulting in profound consequences for later neocortical layering specification.

It is important to note that the Vegf isoform mice display abnormalities in a range of developing organ systems, and that altering the Vegf isoform profile results in a variety of vascular abnormalities [3, 5, 6, 35-37]. Potential indirect effects of altered angiogenesis in the Vegf isoform mice must be taken into account when interpreting any results wherein the vascular system is compromised. These indirect effects can be avoided to some extent, in the forebrain, by using time points before which the vasculature is established in the neuroepithelium (E9.5). However, since NSC differentiation, migration, and subsequent cortical lamination occurs concomitantly with angiogenesis, we can not avoid these indirect effects entirely as later time points must be used to determine consequences of altering the Vegf isoform profile in these processes.

Chapter II

METHODS

Animal Husbandry

The mice used in these studies are derived from the C57 Black 6 (C57Bl6) line of mice. The mice are housed in Techniplast™ air filter flow chambers designed to cycle air and remove ammonia. The mice are provided with nestlets, cardboard houses, and wood chips for bedding and allowed free access to water and standard mouse chow. Mouse pups are weaned after three weeks, whereupon they are tail-cut for genotyping and ear-tagged. Individuals are identified using an ear punch designating a number 0-4 on the right ear. Females are housed together with 2-3 mice per cages, where as males are caged separately unless paired for breeding or timed pregnancy.

The viability of Vegf120 mice relative to wild type littermates was determined by analyzing genotype yields for E9.5 and E11.5 embryonic time points. A total of 53 E9.5 embryos from 9 litters derived from Vegf120 heterozygous crosses yielded a roughly normal distribution of genotypes with 9 wild-type (18%), 28 heterozygous (54%), and 14 homozygous (27%) embryos. A similar genotypic yield was obtained at E11.5 during neural epithelial expansion. A total of 42 E11.5 embryos from 13 litters derived from heterozygous crosses yielded 11 wild type (26%), 21 heterozygous (50%), and 10 homozygous (24%) embryos. Crosses between Vegf188 homozygotes (188/188) and Vegf188 (188/+) heterozygotes yielded 60% homozygotes and 40% heterozygote at E9.5, and 36.8% Vegf188 homozygotes at E11.5.

Generation Of Mouse Embryos And Genotyping

Vegf188, Vegf120, and Vegf120/188 transgenic mouse lines have been described [3, 36, 96]. In brief, the Vegf120 mouse line was established by homologous recombination to remove exons 6 and 7. The Vegf120 line is maintained using heterozygous Vegf120 mice, as the Vegf120 homozygous mice are early postnatal lethal, due to cardiopulmonary abnormalities [96]. The Vegf188 mice were generated by allelic recombination cloning in a cDNA for the Vegf188 construct to prevent alternative splicing of the transcript [3]. Vegf120/188 embryos were generated by crossing Vegf188 heterozygotes or homozygotes with Vegf120 heterozygous mice. Timed-pregnant mice (plug date, day 0.5) were used to generate embryos at embryonic day (E) 9.5, E11.5, and E13.5. Postnatal day (P) 0 collections were made within 6-8 hours of birth, although few Vegf120 mice survived to this stage. Genotype was determined using purified genomic DNA obtained from tail cuts and standard PCR protocols described in [6, 33, 35]. Genomic DNA was purified from tail cuts (adult and embryonic) and digested overnight in lysis buffer containing 0.1 M Tris (pH 8.5), 5 mM ethylenediaminetetraacetic acid (EDTA), 0.2% sodium dodecylsulfate (SDS), and 200 mM sodium chloride with constant rotation at 55°C. Genomic DNA was precipitated with an equal volume of isopropanol and then spun at 14,000 g for 8 minutes at 4°C. The DNA was washed with 70% ethanol to remove residual salts and lysate solution then air dried overnight. Genomic DNA was resuspended in 100 µl TE (50 µl for embryonic samples) for long-term

storage at -20°C. The genotype for each animal was determined using common forward primers and differential reverse primers that distinguished among the different alleles with cycling profiles optimized in the D'Amore Laboratory, Harvard Medical School (Appendix, Table I). The cycling profile for the Vegf120 reaction was a preheating at 94°C (3.75 minutes), followed by 3 cycles of 94°C (3 minutes), 56°C (2.5 minutes), 72°C (3.75 minutes), followed by 25 cycles of 94°C (3 minutes), 60°C (2.5 minutes), 72°C (3.75 minutes), followed by a final extension at 72°C (50 minutes). The cycling profile for Vegf188 was a preheating step at 95°C (3.75 minutes) followed by 27 cycles of 95°C (2.5 minutes), 62°C (2 minutes), 72°C (3.75 minutes), followed by a final extension at 72°C (20 minutes). The handling of animals and euthanasia methods used in this study followed the NIH recommended guidelines for the care and use of animals in research and was approved by the University of North Dakota Institutional Animal Care and Use Committee (#0807-1c, 0511-01, 1204-3c).

Forebrain microdissection, RNA purification, and cDNA synthesis

Embryonic heads (E7.5, 9.5, and 11.5) were collected and stored in RNALater (Life Technologies) prior to dissection. For the E7.5 samples, the anterior neural ectoderm of three E7.5 embryos was pooled to obtain sufficient RNA for cDNA synthesis. For the E9.5 embryos, the two dorsal anterior bulges of the telencephalon were dissected away from the forebrain with the top of the presumptive nasal process as the most anterior anatomical marker and the forward process of the diencephalon as the most posterior anatomical marker.

The optic cup was not included in the dissected material and pial vessel were peeled away where possible. The E11.5 embryo heads were dissected at the anterior divide between the forebrain and midbrain using the bifurcation of the cerebral artery as the dividing line. Total RNA was purified with guanidinium isothiocyanate lysis and column purification using PicoPure™ RNA Isolation (Applied Biosystems) and the resulting RNA quantified with a Nanodrop spectrophotometer. Optimal quality range for the RNA was based on a ratio of 1.8-2.0 for the absorbance at 260λ relative to 280λ. Two hundred ng of total RNA was converted to cDNA in a 40μl reaction volume (GeneAmp kit, Applied Biosystems). All cDNA samples were quality control checked with standard PCR amplification of glyceraldehyde phosphate dehydrogenase (Gapdh) prior to being used in the qPCR assay.

Amplicon sub-cloning and Quantitative Real-Time PCR.

Quantitative real time PCR was performed with SybrGreen detection on an ABI7300 Thermocycler (Applied Biosystems). Primer pairs were designed for each target and optimized for GC content (45-50%), base pair length (20-26 oligonucleotides), melting temperature (54-60°C), and amplicon size (75-450bp). Primer pairs were designed for each target gene and optimized using Primer Express Software (Applied Biosystems) and were selected based on minimal hairpin and dimerization secondary structures using Oligo Analyzer (Integrated DNA Technologies, Coralville, IA). The mRNA FASTA sequences were taken from the Entrez Gene website (<http://www.ncbi.nlm.nih.gov/sites/entrez>) and

compared against those found on Ensembl Mouse Gene Viewer (http://www.ensembl.org/Mus_musculus/index.html). (Appendix, Table II for Primers). Target product was amplified from E9.5 and E11.5 wild-type neuroepithelium cDNA and subcloned into TOPO-TA-Sequencing (Invitrogen). Cloned products were sequence confirmed using BigDye Terminator v3.1 Cycle Sequencing Kit (Applied Biosystems) on an ABI Prism 3100 Genetic Analyzer. Validated products were amplified off the plasmid, gel purified (Qiagen) and quantified with a Nanodrop spectrophotometer. The analysis approach was based on the previously published protocol [97] with modifications as described. Purified DNA product for each primer pair was used to generate 7-step standard curves plus a no-template control (only correlation coefficients of 0.98-0.99 were used) and the amplification efficiency was determined from the slope of the standard curve using the formula: $\log_{10}[-1/\text{slope}] - 1$. The efficiencies for the primers used ranged from 85-100%. The C_T of the product was corrected using the efficiency value determined for each primer pair and a melting curve was included in the run to check for uniform product formation based on the sequence-confirmed amplicon. This approach was used to calculate the amount of target cDNA, relative to the standard curve, transcribed from the mRNA for a target gene and expressed in attograms of DNA per 2.5 ng total RNA loaded into the original cDNA synthesis reaction. Amplification of 18S rRNA and Gapdh or 18S rRNA alone were run for each cDNA sample in parallel and run as a covariate in the analyses to control for variation in transcription efficiency and sample-to-sample variation.

Transcriptional analysis with microarray

Purified total RNA from forebrains of six wild-type, four Vegf120, four Vegf188, and three Vegf120/188 were submitted to Genome Explorations Inc. (Memphis, TN) for processing and preliminary analysis. The RNA concentration was determined from the OD260/280 ratio and quality determined by capillary electrophoresis on an RNA 6000 Nano Lab-on-a-Chip kit and the Bioanalyzer 2100 (Agilent Technologies, Santa Clara, CA). 15 ug of biotinylated cRNA were hybridized for 16 hr at 45°C on the GeneChip 430.2 mouse array (Affymetrix; GPL1261). GeneChips were washed and stained with streptavidin-phycoerythrin using the Affymetrix Fluidics Station 450, according to the manufacturer's protocol. Hierarchical clustering analysis was conducted using the Probe Logarithmic Intensity Error Estimation (PLIER) [98] values for genes that were differentially changed at least 0.5 fold with t-test values ≤ 0.05 . The log₂-transformed values were mean centered prior to clustering analysis by the farthest neighbor method with Euclidean distance and Pearson Correlation as the similarity metrics.

Microarray Meta-Analysis

Data from six E9.5 and four E11.5 wild-types microarrays of neuroepithelium, from Hartl and coworkers [99], were downloaded from the Gene Expression Omnibus (GEO record GSE8091) and were compared against our microarrays (6 E9.5 wild types, 4 E9.5 Vegf120, 4 E9.5 Vegf188, and 3 E9.5 Vegf120/188 mice). Although this is a public database, permission to use the

.CEL files was requested and obtained. The E9.5 microdissection described by Hartl and coworkers [99] was comparable to our method and the resulting transcriptomic analysis showed similar arrays of genes expressed in the two batches of E9.5 samples. Principal Components Analysis revealed a batch variation effect, so raw expression values from all arrays were PLIER normalized and Log2 transformed. A MAS5 algorithm [100] was used to generate Presence/Absence calls for each gene, and probes with two or less “presence” hits were removed from further analysis. Samples were batch normalized using a non-parametric Empirical Bayes approach with a multivariate model (Batch, Age, and Genotype) using the R-script ComBat.R [101]. The BAMarray freeware [102] was used to run a Bayesian-modeled ANOVA to test for significance using the E9.5 wild types as a baseline for comparison. Genes detected as significantly different from wild type were based on an adaptive test statistic that compared the increasing distance of the Z-cut from zero as well as the posterior variance as it approached one.

The Affymetrix annotation numbers for genes that were differentially expressed among the Vegf isoform samples relative to wild type were uploaded onto the Database for Annotation, Visualization, and Integrated Discovery (DAVID) platform and the enriched functional clusters identified with the mouse genome as the population background [103, 104]. The geometric mean of all the enrichment values for each gene per cluster is expressed as the enrichment score. The Expression Analysis Systematic Explorer (EASE) score is expressed as a p value (determined from a modified Fisher’s exact test) [105] and reflects

the significance of the enrichment score as a representation of a functional gene group relative to the expected representation based on the population background. Gene functional categories and individual networks of interest were identified based on high stringency settings and the EASE score [105]. Differentially expressed genes from key clusters were run through the Search Tool for the Retrieval of Interacting Genes/Proteins (STRING) platform [106] to build interaction networks linking functional groups as well as individual genes. Based on literature reports of coexpression, binding data, and convergent or interacting pathways.

Immunolabeling

Embryos were fixed in buffered 3.7% paraformaldehyde and equilibrated to 30% sucrose. Cryosectioning of Neg₅₀ (Fisher Scientific/Thermo Scientific, Pittsburgh, PA) embedded tissue was cut with a Leica HM550 cryostat and slides were stored at -20° C. Sections to be immunolabeled were blocked and permeabilized in 3% donkey serum, 2% goat serum (Vector Laboratories, Burlingame, CA), 0.1% Triton X-100, and 1% bovine serum albumin (BSA) in phosphate-buffered saline (PBS) overnight at 4°C. The primary antibody incubation was 2 hours at room temperature or overnight at 4°C. The absence of primary antibody or use of species-matched immunoglobulins were used as negative controls. Rabbit polyclonal antibodies were phosphohistone H3 (PHH3, 1:200, Upstate Biotechnology, Lake Placid, NY), Tbr1, Tbr2, Ctip2 (1:400, Abcam, Cambridge, MA), and *G. simplicifolia* lectin B4 conjugated to fluorescein

isothiocyanate (FITC; 1:200, Vector Laboratories, Burlington, CA). For immunofluorescent detection of primary antibodies, a series of fluorochrome-coupled secondary antibodies were incubated in block solution for one hour at room temperature (cy3, and FITC used at 1:200; Jackson ImmunoResearch Laboratories, West Grove, PA). Nuclei were labeled with DAPI (Vector Labs) for standard fluorescent microscopy. For immunolabeling at P0, the paraformaldehyde-fixed brains were equilibrated through a 30% sucrose gradient. The head was placed nose side up and 5 μ m coronal sections were cut through to the hippocampus. Immunolabeling was conducted as described above. Bound primary antibody was detected with species-matched fluorescent conjugated secondary antibodies (1:200, Jackson Immunologicals) and nuclei identified with DAPI (Vector Laboratories, Burlingame, CA).

Design-based Stereology

Design-based stereology was used to quantify PHH3-, Tbr2-, Tbr1-, Calb1-positive nuclei. At E11.5 whole embryos were serially sectioned in the parasagittal plane at 30 microns with a ten-section interval. Sections were immunolabeled with a PHH3, Tbr2, or Calb1 primary antibody, as described above, followed by a biotinylated secondary antibody (Goat anti-rabbit~biotin, 1:200; Jackson Laboratories) and Vectastain Elite ABC horseradish peroxidase staining kit (Vector Labs) and developed with a DAB substrate kit for Peroxidase (Vector Labs) as per the manufacturer's protocols. The immunolabeled sections were counterstained with methyl green. In brief, the DAB developed slides were

put in distilled water, and then a 0.5% methyl green in 0.1M sodium acetate buffer, pH 4.2 solution for five minutes. Slides were then dehydrated through an alcohol series, including 95% alcohol, and two changes of 100% alcohol, and finally cleared in xylene and mounted with Vectamount Permanent Mounting Medium(Vector Labs). (protocol from www.IHCworld.com) E13.5 heads were mounted nose up and 30 micron coronal sections were cut through the entire head using a ten section interval. The sections were immunolabeled with Tbr1 using the same protocol as the E11.5. Primary antibody positive nuclei and total nuclei were counted using an Olympus BX51WI microscope with a motorized XYZ stage. Quantification was done using the Optical Fractionator workflow in StereoInvestigator 9.0 (Microbrightfield, Inc., Wiliston, VT). For the PHH3 counting, the contour outlined the neuroepithelium within 100 μ m of the ventricular surface of the forebrain. For the Tbr2 counting, the contour outlined the pial and ventricular surface of the forebrain. Calb1 counting used a contour outlining the pial surface of the forebrain, with an internal boundary of 100 microns from the pial surface. The forebrain was also further subdivided into an area anterior to the Ganglionic Eminence (GE), the GE itself, and areas posterior to the GE. Tbr1 tracing of the E13.5 embryos included contours of only one of the lateral ventricle. The outer contour followed the pial surface while the interior countour followed the extent of Tbr1+ zone or 100 μ m from the pial surface, whichever was thicker. Tracing of sections began immediately before the emergence of the GE and stopped on the section after the re-joining of the medial and lateral GE. For all counts, positive nuclei and total nuclei were

counted in every 10th section in systematically-selected frames based on optical dissector frames and grid sizes empirically determined for each counting paradigm so that the coefficient of error was less than 0.1 (10%). The total numbers were estimated using the optical fractionator algorithms in Stereoinvestigator V9 (Microbrightfield). The formula $N = 1 / (ssf \cdot asf \cdot hsf) \cdot \sum Q^-$ is used for the estimation, where ssf = section sampling fraction(10), asf = area sampling fraction (area sampled/ total area), hsf = height sampling fraction (counting frame height/30 μ m, and $\sum Q^-$ (total particle count). Neuroepithelial volume was measured based on the total tracing area, the actual z-plane measured section thickness (to account for tissue shrinkage), and the section interval. The statistical analyses were performed using GraphPad Prism (GraphPad Software, Inc., LaJolla, CA) or JMP (SAS Institute Inc., Cary, NC). Comparisons between wild type, Vegf120, Vegf188, and Vegf120/188 mice were run using standard Analysis of Variance with Dunnett's post hoc test for comparisons of Vegf isoforms against a wild type baseline. Data shown are the mean +/- the standard error of the mean (SEM) with the number of replicates indicated in the figure legend. (Table of Sampling parameters, and Tracing).

Protein Quantification and ELISA Assays.

Forebrain tissue from E11.5 embryos was microdissected and triturated in modified RIPA lysis buffer (25 mM Tris-HCl pH 7.6, 150 mM NaCl, 1% NP-40, 1% sodium deoxycholate, 0.1% SDS) containing a cocktail of protease and phosphatase inhibitors (Sigma) and passed through 18 and 23 gauge needles to

disrupt cells and shred genomic DNA. Non-soluble material was separated from the lysed material with a 10-minute centrifugation at 20,000 rcf and samples were stored at -80°C. Total protein from E11.5 brain tissue was determined with a Bio-Rad R_CD_C Protein Assay and loaded at the appropriate concentration for each ELISA detection assay. For detection of Vegf protein, 50 µg of total protein was loaded in a Vegf ELISA kit (R & D Systems) with the assay conducted following manufacturer's instructions. The Vegf levels in E11.5 lysate samples were determined using a eight point Vegf standard curve starting at 500 pg and serially diluted 1:1 seven times. The r^2 for the standard curve was 0.9992 and the slope used to calculate the unknown concentrations within the linear range of the assay. Values are expressed as pg Vegf/µg total protein in the assay. For detection of fibronectin protein we used 2 µl of E11.5 lysate material loaded onto a precoated ELISA plate (Innovative Research, Novi, MI) and processed according to manufacturer's instructions. The fibronectin levels were determined using a fibronectin standard curve run in parallel and ranging from 500 pg to .005 pg with an r^2 of 0.998. Values are expressed as pg fibronectin/µg total protein. For detection of laminin, we developed our own standard ELISA assay approach by coating a 96-well assay plate coated overnight at 4°C with either a 10-fold dilution curve of species laminin protein, 5000 to 5 pg/ml (Sigma) or with E11.5 lysate solution diluted 1:30 in sodium carbonate coating buffer (pH 9.5). After 3 washes with 1X PBS with 0.05% Tween-20, the plate was blocked with 0.1% bovine serum albumin in PBS followed by incubation with 5 µg/ml of rabbit polyclonal antibody to laminin (L9393; Sigma). The laminin assay was optimized

for coating conditions, lysate coating concentration, detection antibody concentration, and specificity to laminin using Bovine Serum Albumin and fibronectin as negative controls. The concentration of laminin in the lysates was calculated based on a standard curve with an r^2 of 0.99.

Chapter III

Results

Angiogenesis and Neural Development in the early forebrain

The early mouse brain starts as a neural tube and is specified at a region of the developing embryo known as the neural plate. Early on in neural development, the neural tube differentiates into three distinct vesicles, the prosencephalon (forebrain), mesencephalon (midbrain), and rhombencephalon (hindbrain). The prosencephalon then gets further subdivided into the telencephalon, which gives rise to the cortex, and the diencephalon (Figure 6). At E9.5 the mouse telencephalon is little more than a hollow neural tube, surrounded by pial vessels and lined on the inside with NE. The telencephalon can be divided dorsally and ventrally. The dorsal telencephalon gives rise to the pallium, from which the majority of the glutamatergic pyramidal neurons are born, with the anterior-lateral portion of the dorsal pallium giving rise to the neocortex. The ventral half of the telencephalon forms the medial, lateral, and caudal ganglionic eminences (MGE, LGE, and CGE respectively). It is from the MGE that the majority of the gamma-Aminobutyric acid (GABA)-positive interneurons are born and which eventually migrate into the pallium of the neocortex. (Figure 7) GABA is the major inhibitory neurotransmitter in the cortex, allowing for tight signaling conduction control through the network via GABAergic interneurons.

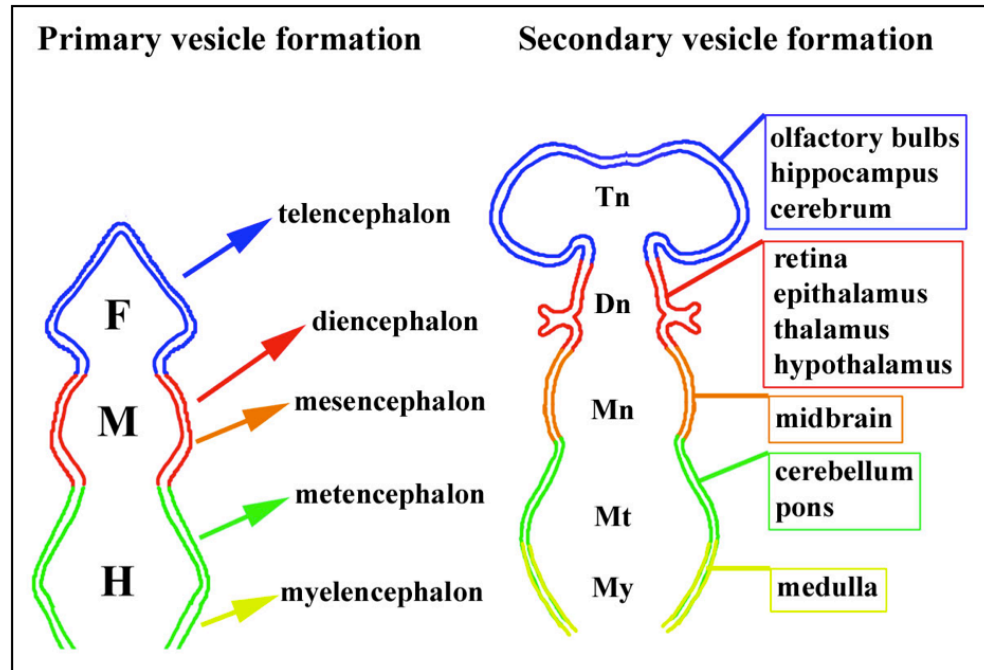


Figure 6. Early brain vesicle formation. The early neural tube of the developing brain gets specified into several compartments, or vesicles. The earliest vesicles specified are the forebrain (F, prosencephalon), midbrain (M, mesencephalon, and hindbrain (H, rhombencephalon). From these three vesicles, five more arise; from the forebrain comes the telencephalon (Tn), from the midbrain comes the diencephalon (Dn) and mesencephalon (Mn), and from the hindbrain comes the metencephalon (Mt) and myelencephalon (My). It is from the telencephalon that the neocortex forms.

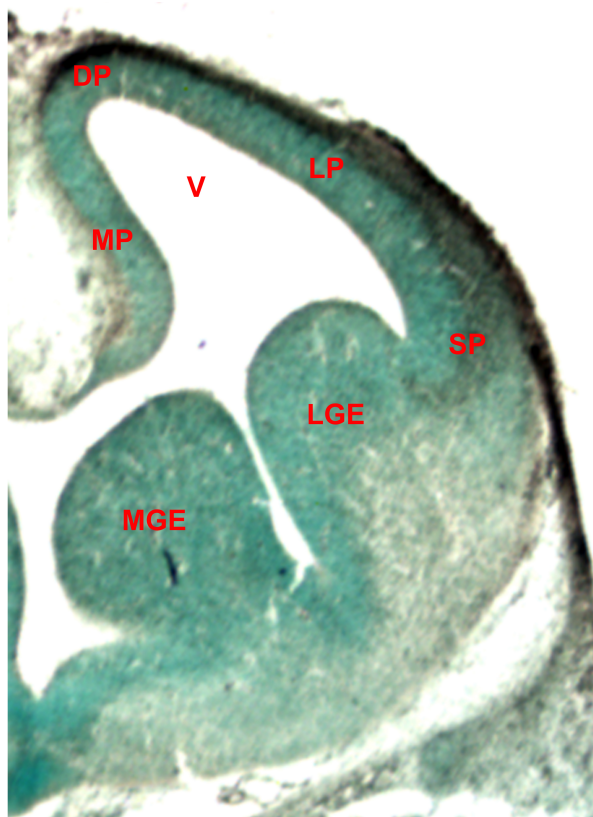


Figure 7. Anatomical areas in the developing telencephalon. The early telencephalon can be divided into several basic anatomical areas. In this coronal section in the E13.5 mouse are the Medial Ganglionic Eminence (MGE), Lateral Ganglionic Eminence (LGE), Subpallium (SP), Lateral Pallium (LP), Dorsal Pallium (DP), Medial Pallium (MP), and Ventricle (V).

In parallel with the differentiation of the telencephalon into the primitive cortex, angiogenesis begins in the mouse cranial region by E7.5. By E9.5 the early telencephalon is enveloped by a series of pial vessels; however, at this stage the pial vessels cover but do not invest the NE. Periventricular vessels invest the developing brain in a dorsal to ventral, caudal to rostral pattern and the major plexi are established in the NE by E11.5 with capillary expansion continuing throughout development [49]. Vascular investment of the murine brain is guided primarily by Vegf and its receptors Vegfr2 and Nrp1 [107]. Vegf is expressed in the ventricular zone, while migrating endothelial cells of investing vessels express Vegfr2 [108, 109]. Endothelial cells in mice lacking Nrp1 fail to invest the NE in the forebrain and hindbrain [56]. In the absence of Nrp1, the endothelial tip cells that initiate new vessel formation and migration follow normally along the radial glia guides, but fail to turn or sprout in the locations where lateral plexus formation should occur. These results further emphasize the importance of microenvironmental signaling with regard to fine-tuning the cerebral vasculature [56].

Altered Vegf isoform profile affects the NE transcriptome at E9.5

In order to clarify the role of Vegf and its predominant isoforms in early cortical development, we took the approach of analyzing transcriptome-level changes associated with altered Vegf isoform expression at E9.5. This allowed us first to determine which genes were being expressed at E9.5 in the neuroepithelium and to identify possible regulatory networks developmentally linked downstream of altered Vegf isoform expression. To this end, we isolated

early neuroepithelium from E9.5 wild type mice (N=4) as well as mice expressing either the Vegf120 isoform (N=4) only, or the Vegf188 isoform (N=4). Using these mice we were able to look at the effects of Vegf in the absence of the diffusible isoforms, and in the absence of the locally-retained isoforms. We chose the E9.5 time point in order to look at shifts in gene expression attributable to the changes in available Vegf isoform profile and localization independent of periventricular vascular investment in the forebrain. At E9.5, the pial vessels have elaborated on the surface of the developing forebrain, but significant sprouting into the primitive telencephalon does not occur until E11.5 [48, 49, 110]. This early time point also represents a period during which the NSCs within the neuroepithelium are relatively homogenous, as they have yet to begin the rapid differentiation that occurs at later time points.

Using the transcriptome-wide profiles in gene expression we compared overall patterns of expression across wild type and Vegf isoform mice, identifying key gene clusters shifted up or down with an altered profile of Vegf isoform expression. We conducted ANOVA analysis on PLIER normalized array data from wild type and Vegf isoform mice to generate a heat map quantifying differentially-expressed genes among replicate animals from 2-3 different litters (Figure 8). With this analysis approach, genes were identified based on a fold change greater than 1.5 and a p-value of 0.05, or less. This approach identified 257 genes differentially expressed in the Vegf188 NE, 330 genes in the Vegf120 NE, and 24 genes that were shifted in both groups, relative to wild type (Figure 8).

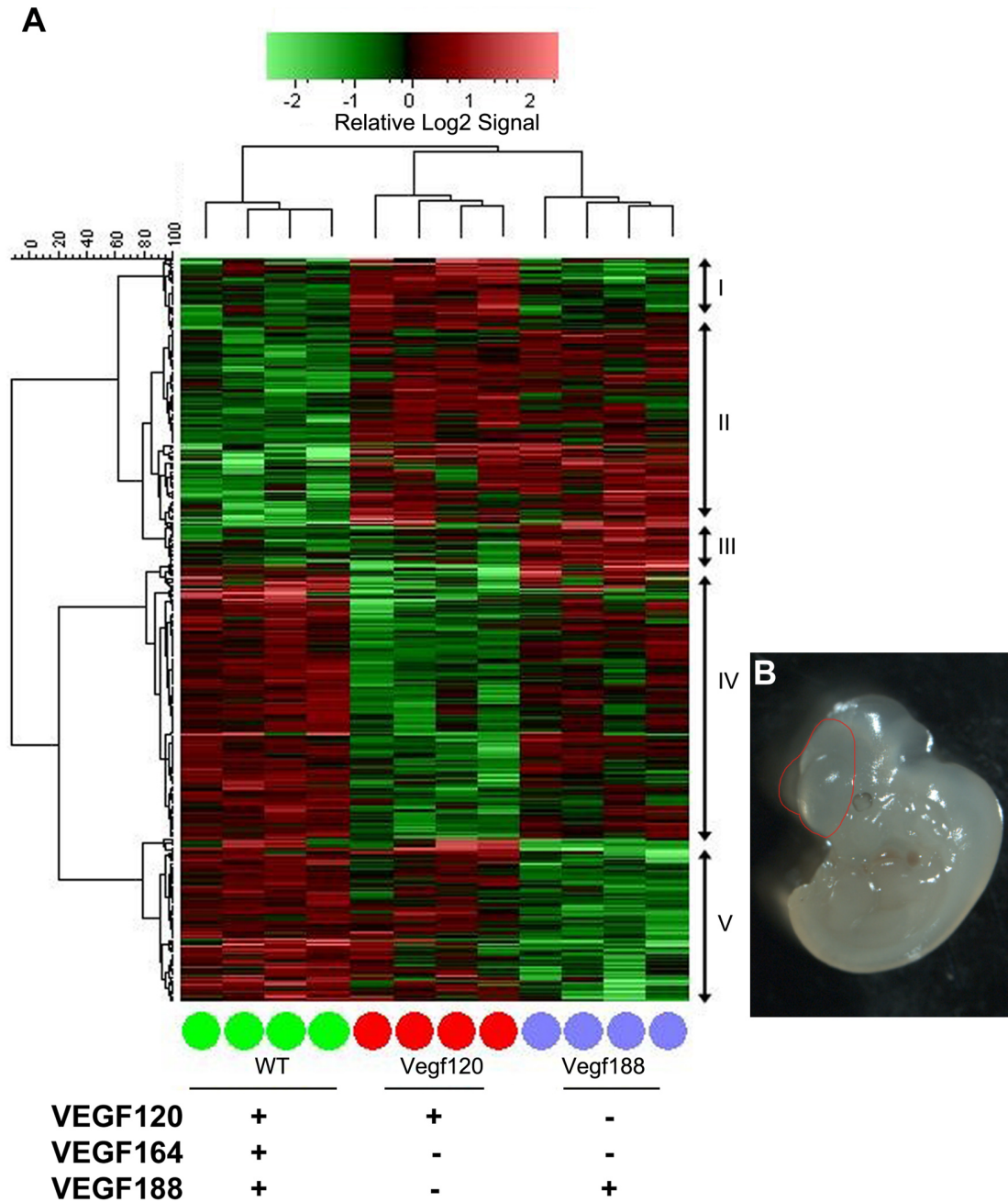


Figure 8. E9.5 Vegf isoform mice display unique transcriptome profiles.

Total RNA was purified from E9.5 mouse forebrains (4 WT, 4 Vegf120, and 4 Vegf188) and mRNA was quantified on an Affymetrix 430.2 array. PLEIR normalized signal values for the differentially expressed genes were log₂

transformed and mean centered before undergoing unsupervised hierarchical clustering using the Complete Linkage algorithm based on a Euclidean Distance similarity metric. The individual genotype samples were clustered based on a Pearson Correlation. Genes were considered differentially expressed based on an ANOVA p-value ≤ 0.05 , an absolute fold change ≥ 1.5 , and an independent t-test p-value ≤ 0.05 . Cluster I contained 49 probe sets which were generally up in the Vegf120. Cluster II contained 137 probe sets which were generally up in wild-type relative to the Vegf isoform mice. Cluster III contained 26 probe sets that were up in the Vegf188 mice. Cluster IV contained genes down in the Vegf120 mice (189 probe sets) and Cluster V contained genes down in the Vegf188 mice (114 probe sets). Vegf isoforms present in each array set are represented by either "+" if present, or a "-" if not. Total RNA was collected from forebrain neuroepithelium dissected based on the red line (B).

Based on our analysis, it was clear that misexpression of the Vegf isoforms, shifting the profile to either diffusible (Vegf120) or locally-retained (Vegf188) altered the transcript profile significantly. Moreover, the pattern of gene expression was distinct in the Vegf120 mice relative to the Vegf188 indicating that not just the shift in isoform expression, but the type of isoform expression was a distinct factor in the transcriptome profile (Figure 8).

In order to further clarify the role of diffusible versus locally-retained Vegf, we look at the transcriptome profile of the E9.5 Vegf120/188 neuroepithelium. The Vegf120/188 mouse represents a potential rescue phenotype as it has both diffusible and locally retained isoforms. It also represents a loss of function, in that it still lacks the primary Vegf164 isoform. We ran this second set of arrays with three Vegf120/188 samples and two wild type samples, the latter used as baseline controls for comparison with the initial microarray. We combined our previous microarrays with these five additional arrays and identified genes that were differentially expressed using the same analytical method as described above with one exception. The PLEIR normalized values were also mean-centered to correct for batch effects between technical replicates. Using this method with wild types as a baseline, we identified differentially expressed genes in the Vegf isoform mice: Vegf120 (112 genes), Vegf188 (140 genes), and Vegf120/188 (152 genes). The annotated gene lists and their fold change relative to wild type in the array are provided in Table III. The pattern of gene expression was quite distinct among the Vegf isoform mice, with different gene clusters down-regulated in the Vegf120 and Vegf188 mice, relative to the wild type mice.

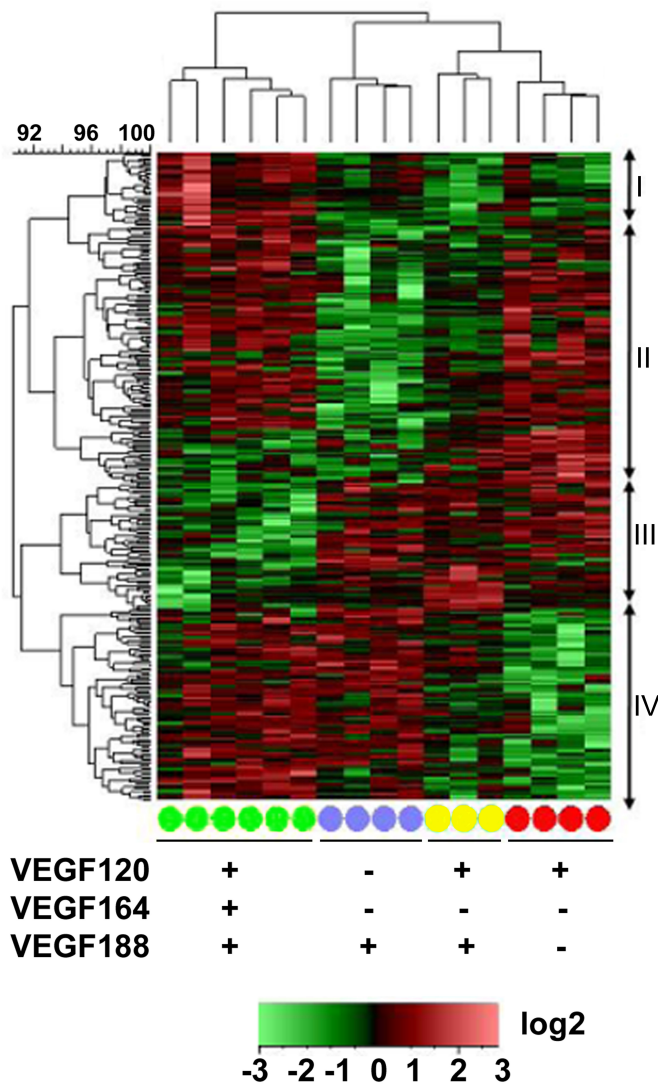


Figure 9. E9.5 Vegf120/188 forebrain transcriptome is unique from wild-type. Vegf120/188 (yellow, n=3) forebrain transcriptome differs significantly from wild-type (green, n=6), implying that the presence of both a diffusible and non-diffusible isoform is not sufficient to rescue the wild-type phenotype and the absence of the primary Vegf 164 isoform. The Vegf120/188 transcriptome phenotype appears to be a combination of the Vegf120 (red, n=4) and the Vegf188 (purple, n=4) transcriptomes. Cluster I shows increased expression in

the wild-type mice compared to the three isoform mice (32 probe sets). Cluster II showed a general decrease in expression in the Vegf188 and Vegf120/188 mice (111 probe sets). Cluster III showed a decrease in gene expression among the wild-type mice (55 probe sets). Cluster IV showed a decrease in expression amongst the Vegf120 and Vegf120/188 mice (83 Probe sets) Presence (+) or absence (-) of a Vegf isoform in a particular group is indicated below the heat map. Analysis was performed as described in Figure 8, with the addition of a batch normalization. Cluster information can be found in Appendix Table III.

The pattern for the Vegf120/188 mice appeared intermediate between the Vegf120 and Vegf188 mice rather than a recapitulation of the wild type expression pattern as would have been expected from a “rescue” phenotype (Figure 9). It is important to emphasize that while the Vegf120 mice are early postnatal lethal, both the Vegf188 and Vegf120/188 mice are viable and breed normally.

In a separate, more in-depth approach to analyzing the microarray data set, we conducted a Bayesian analysis on batch- and PLIER-normalized data sets to potentially elicit additional differential gene expression patterns and enriched gene functional clusters. We chose the Bayesian approach based on its ability to reduce the false discovery rate while maintaining acceptable statistical power in a highly dimensional data set, with multiple batches [111]. In order to further increase the statistical power of our study, we compared our E9.5 wild type samples to each of the E9.5 Vegf isoform samples, as well as to E9.5 and E11.5 wild types that had been previously published for a comprehensive early forebrain transcriptomic analysis by Hartl and coworkers [99]. Our rationale for including the E11.5 time point from the Hartl et al. study was based on our observation that many of the upregulated genes in the Vegf120 mice were associated with later stage differentiation of cortical neuron populations. Therefore, we speculated that the comparison with the later timepoint (E11.5) would provide a developmental backdrop if we were observing precocious differentiation in any of the Vegf isoform mice.

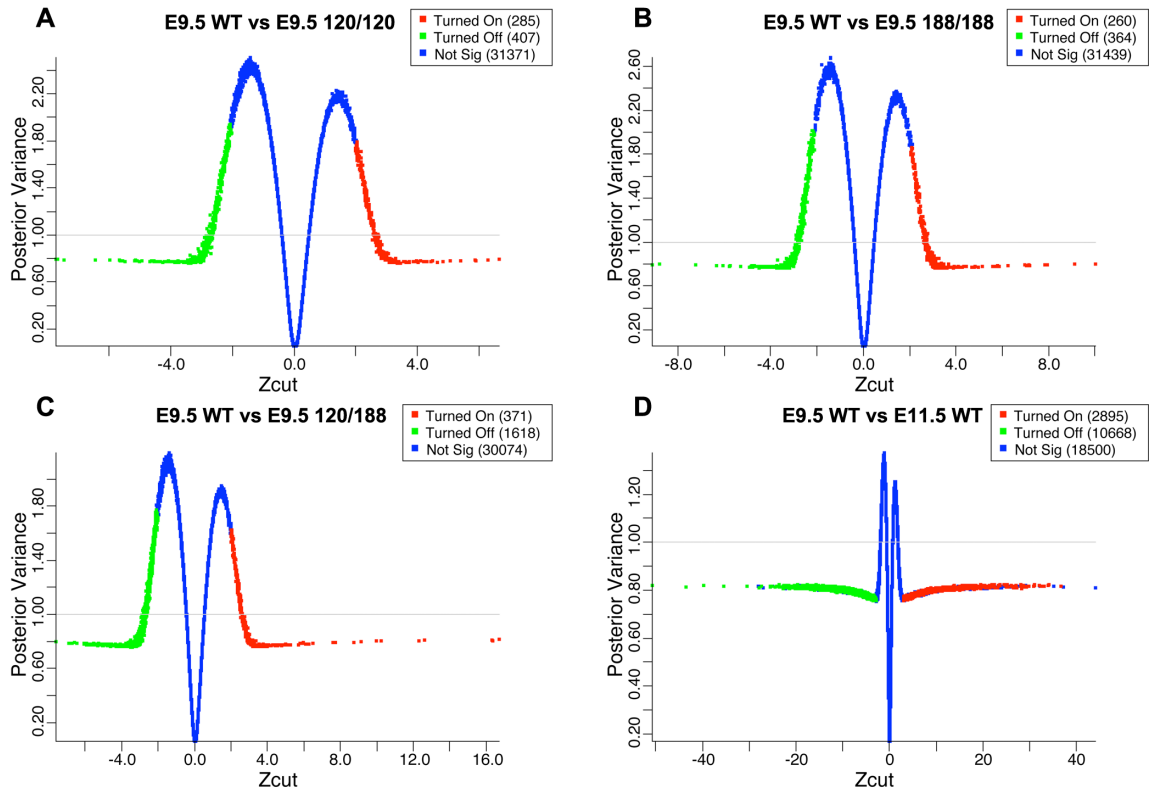


Figure 10. Meta-analysis of transcriptome shifts of embryonic forebrain in Vegf isoform mice compared against an E9.5 wild type background.

Microarray data from two previously published articles were downloaded from the Gene Expression Omnibus and incorporated into our analysis [34,56]. Unprocessed .CEL files were downloaded from GEO (6 E9.5 wild types, 4 E11.5 wild types) and analyzed with our microarray runs (6 E9.5 wild types, 4 E9.5 Vegf120, 4 E9.5 Vegf188, and 4 E9.5 Vegf120/188). All runs were PLIER and batched normalized, Presence/Absence filtered with MAS5, Log2 transformed, and tested for significance using a Bayesian modeled ANOVA run with BAMarray software and expressed as Zcuts relative to the E9.5 wild types. The genes that were significantly up-regulated (red) or down-regulated (green) were selected based on an adaptive test statistic that used the increasing distance of the Zcut from zero and the approach of the posterior variance as it neared one. The

shrinkage plots shown are the Zcut values graphed relative to the posterior variance. Significance is a reflection of distance from the 0 point for E9.5 wild type versus Vegf120 (A), Vegf188 (B), Vegf120/188 (C), and E11.5 wild type (D). Genes that were not significantly changed (Blue, Not Sig) center around a Zcut of zero and an increasing posterior variance away from one. Appendix Table IV contains the specific information on the individual probes and their scores.

In total, this comparison included our E9.5 wild types, Vegf120, Vegf188 and Vegf120/188 samples (n=6, n=4, n=4 and n=3; respectively), and previously published E9.5 wild types (n=6), E11.5 wild types (n=4). Differentially expressed genes were identified using a Bayesian ANOVA performed by BAMArray. We developed shrinkage plots using the BAMArray analysis that express the confidence of differential gene expression as a Z-cut (modified z-score) relative to the posterior variance of the comparison (Figure 10). In the Vegf120 mice we observed 285 genes that were up-regulated and 407 genes that were down-regulated with respect to the E9.5 wild type samples. The Vegf188 mice showed the fewest genes statistically changed relative to wild type with 260 up-regulated and 364 down-regulated genes. The Vegf120/188 had the greatest number of genes shifted relative to wild type with 371 up-regulated and 1618 down-regulated genes. The E11.5 wild type mice had 2,895 genes up-regulated and 10,667 genes down-regulated, a reflection of the dramatic developmental changes occurring from E9.5 to E11.5 in the forebrain. As a control we compared the batch normalized E9.5 wild types from the three different technical batches, including our two batches (N=4, N=2) and that of Hartl and coworkers [99] (N=6) and found no differentially expressed probes (Figure 11), demonstrating proof of principal for our technical and analytical approaches.

In addition to identifying the differential gene expression patterns between each of the isoform mice and the wild type forebrain samples, we wanted to compare changes in gene expression profiles generated between the isoform mice relative to the shifts that occurred relative to E9.5 wild types.

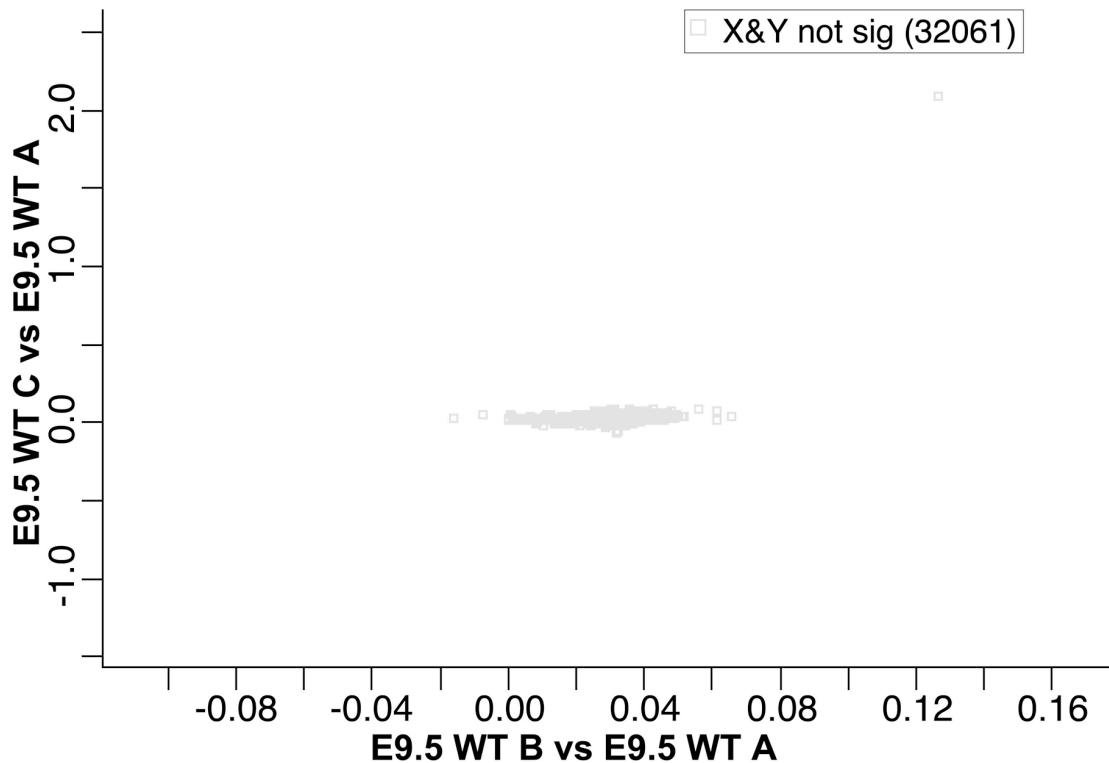


Figure 11. Separate technical batches of E9.5 wild type forebrain microarrays display no statistically different genes in a meta-analysis.

Zcuts were obtained from three separate wild type technical batches using a Bayesian-modeled run in BAMarray. E9.5 wild type forebrains from our two technical batches (WT A, n = 4, and WT B, n = 2) were compared to those from and Hartl et al., 2008 (WT C, n = 6) {Hartl, 2008 #805} and plotted on a scatter plot comparing WT A versus WT B on the y-axis and WT A versus WT C on the x-axis. No genes were detected as significantly changed in any of the technical runs, demonstrating a proof of principle for our meta-analysis approach.

To this end, we generated scatter plots of the Z-cut values generated by group for each of the Vegf isoform mice relative to wild type. We compared each group to each other (Figure 12 A, C, and E). The Vegf120 and Vegf188 mice had 71 genes that were either up or down-regulated together. The Vegf120 and Vegf120/188 shared 81 genes that shifted in the same direction while the Vegf188 and Vegf120/188 shared 68 genes. When the Vegf isoform mice were compared to the E11.5 mice a large proportion of genes were shifted in a similar direction (Figure 12 B, D, and F; Vegf120 = 219 genes, Vegf188 = 92 genes, and Vegf120/188 = 662). The differentially expressed genes identified by this approach are listed in Table IV along with their Z-cut score and the direction of change in the array.

To validate our microarray analysis we performed qPCR on a subset of genes. Genes were selected for qPCR analysis based on the criteria that they were either detected as significantly changed in the microarray analysis, or have a well-established role in neurogenesis based on evidence in the literature. We collected total RNA from the neuroepithelial forebrains of wild type, Vegf120, Vegf188, and Vegf120/188 mice using the same dissection as described for the microarray collections. 200 nanograms of the total RNA was converted to cDNA for use in the reactions. We looked at 21 different genes, including two reference genes, Gapdh and 18s rRNA. ANOVAs using the reference genes as covariates followed by a Tukey's post test were used to test for significance. The ANOVA tables, group signal means, p-values, and fold changes versus wild type are consolidated in Tables V-VII. In brief, the results of the individual runs will be described below.

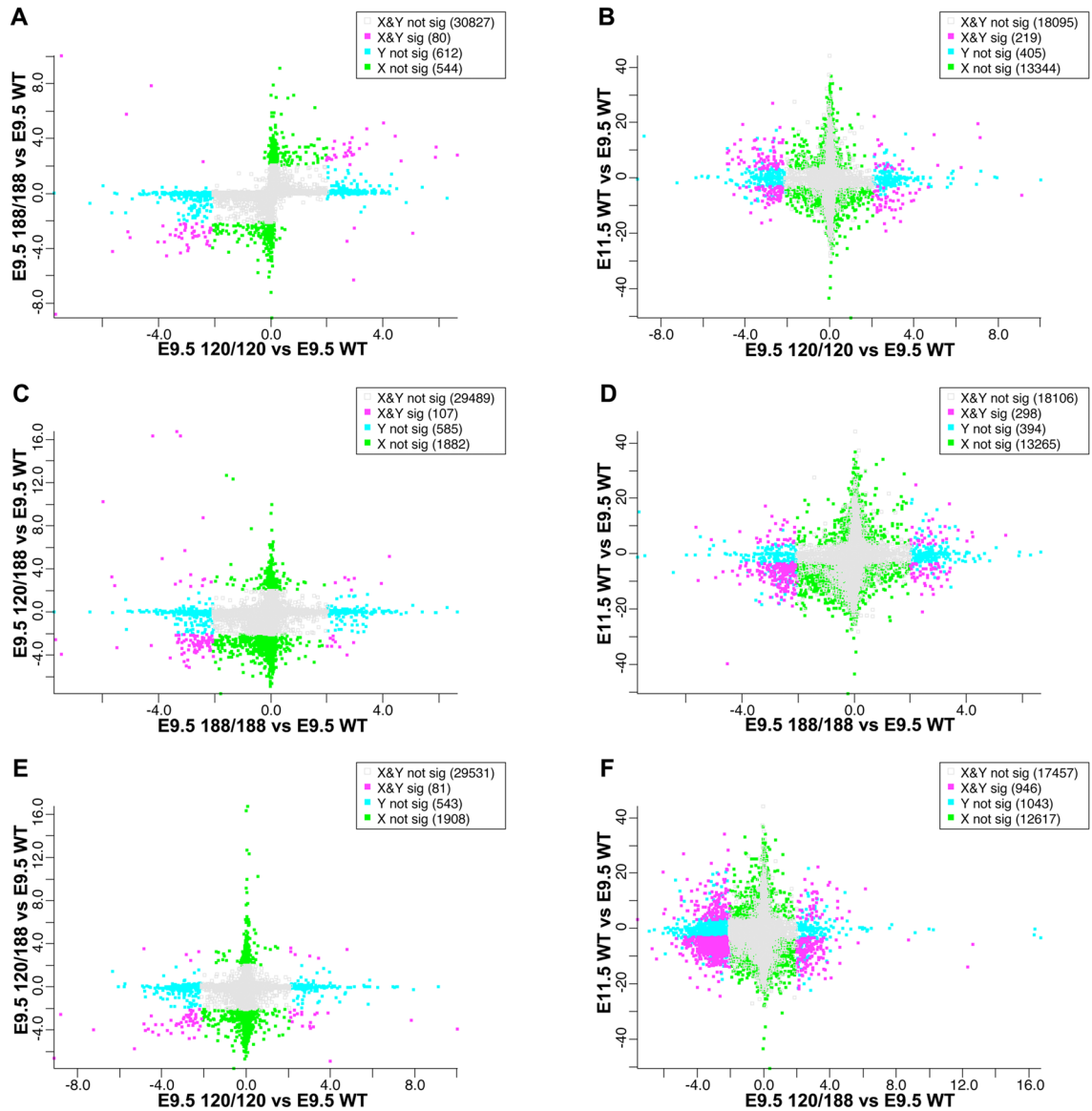


Figure 12. Cross-comparisons of transcriptional shifts between Vegf isoform forebrains and embryonic time points. Zcuts from two different group comparisons versus wild type were plotted on the X and Y axis. Scatter plots on the left side compare how pairs of Vegf isoform forebrains shift relative to E9.5 wild type. Scatter plots on the right side compare shifts in gene expression of the individual E9.5 Vegf isoforms versus E11.5 wild types all relative to an E9.5 wild type baseline. Genes are sorted based on being significant in any one group but

not the other (Blue and Green boxes), significant in both groups (Red boxes), or not significant in either (Grey boxes). Genes found in the upper-right and lower-left quadrants are shifted in the same direction relative to the E9.5 wild type base line.

Gapdh and 18s rRNA were selected as reference genes to use as a basis for comparison in covariate analyses of selected genes of interest. One-way ANOVAs of 18s rRNA and Gapdh demonstrated that there were no significant shifts in expression between any group (Table V, g,h).

Shh is a growth factor critical to the dorsal-ventral patterning of the telencephalon. Shh serves as a morphogen, whose effects are dependent upon its concentration. Shh is a ventralizing factor in the forebrain and its actions are mediated by the Gli family of transcription factors and Smoothed (Smo) (reviewed in[112]). Our qPCR analysis demonstrated that the Vegf188 mice had a roughly fifty percent decrease in expression levels versus wild type and the Vegf120 mice ($p < 0.1$). No other groups were statistically different (Table V, a).

We also quantified Notch3, which is a member of the large Notch family of proteins that are important regulators of both vascular development and neural stem cell proliferation and differentiation (reviewed in [113, 114]). In particular Notch3 has been shown to regulate differentiation of neural stem cells and push them towards an astroglial fate at later stages of development [115]. qPCR analysis of Notch3 at E9.5 showed a fifty percent decrease in expression in the Vegf188 mice compared to all other groups ($P < 0.05$; Table V, b).

Cxcr7 and Cxcl12 are key regulators of migration in both the angiogenic and neural migration pathways[93, 94]. Both the Vegf120 and Vegf188 mice had decreased expression of Cxcl12 compared to wild type and Vegf120/188 ($p < 0.1$). Cxcr7 was also down in the Vegf120 and Vegf188 mice relative wild type;

however, the difference versus Vegf120/188 was not significant (Table V c,d). Changes in these chemokines imply that altered Vegf isoform profile may have repercussions in later neural migration pathways and angiogenesis.

The Vegf receptor Nrp1 showed increased expression in the Vegf120/188 mice relative to the other groups ($p < 0.1$), while Nrp2 expression was down in both Vegf188 and Vegf120/188 mice relative to the wild type ($p < 0.05$). Since these Vegf receptors are found in both the nervous and vascular systems, changes in their expression has the potential to affect both systems (Table V e, f).

Suz12 is a member of the Polycomb group proteins, and serves to regulate histone methylation[116]. Suz12 is expressed in the neocortex during development, and heterozygous knockout results in neural tube defects and brain malformations[117]. The Vegf120 and Vegf120/188 mean values demonstrated a trend of increased expression versus wild type and Vegf188; however, the differences were not statistically significant (Table VI, a).

DNA methyl-transferase 3a, Dnmt3a, is a modulator of gene expression. Transition from Dnmt3b to Dnmt3a is an indicator of neuronal differentiation, and marks the transition of an intermediate progenitor becoming an early post mitotic neuron[118]. qPCR quantification demonstrated that the Vegf188 mice had a three-fold lower expression compared to wild type, and a ~2.5 (Log2) fold lower expression the Vegf120 and Vegf120/188 ($p < 0.05$; Table VI, b).

Id1 is key regulator of neurogenesis and angiogenesis. Disruption of Id1 expression results in precocious differentiation of neural stem cells, and the

failure of angiogenic investment of the CNS [119]. Changes in the Vegf isoform profile resulted in isoform specific shifts in Id1 mRNA expression. Expression was down in the Vegf188 mice and up in both the Vegf120 and Vegf120/188 mice versus wild type, however only shift in the Vegf120/188 mice were significant ($p < 0.05$). Id1 was significantly down in Vegf188 versus Vegf120 and Vegf120/188 ($p < 0.05$; Table VI, c). These isoform dependent shifts indicate that Vegf isoform profile may modulate early neural stem cell differentiation.

Pax6 is a well established marker of neural stem cells in the ventricular zone of the developing cortex as expression of this key transcription factor is linked to maintenance of the neural stem cell phenotype. Compared to wild type, expression of Pax6 was reduced roughly 60% in the Vegf isoform mice ($p < 0.05$, Table VI, d). Reduction in Pax6 may be indicative of a reduction in the early neural stem cell population, or a premature transition from a proliferative to a differentiative state.

Hey2 is an essential downstream effector of Notch signaling. As an effector of Notch, changes in its expression could have consequences for both neurogenesis and angiogenesis. Hey2 knockout mice have a clear phenotype that results in early neonatal death with characteristic vascular defects with abnormal heart formation and incomplete capillary formation in the pups, particularly notable in the CNS [120]. In *Drosophila*, there is only one homologue, Hey, that mediates Notch-induced directional control of symmetric (proliferative) versus asymmetric (differentiative) neural stem cell divisions [121].

The Vegf isoform mice all showed a statistically significant increase in Hey2 expression versus wild type ($p < 0.05$ Table VI, e).

Fezf2 is a well described regulator of differentiation, and is part of the network which can direct the differentiation of intermediate progenitors and early post-mitotic neurons in the neocortex [122]. Fezf2 was not statistically significant in any of our groups, however expression levels in the Vegf120 mice were one-fold (Log2) change lower than wild type ($p = 0.18$) and Vegf120/188 ($p = 0.11$).

Pax3 is another regulator of stem cell maintenance and neurogenesis [123]. Pax3 expression was slightly up in Vegf120 mice versus wild type and slightly down in Vegf188; however, these shifts were not significant. The expression in the Vegf120 mice was significantly higher than that detected in the Vegf188 ($p < 0.05$; Table VI, g).

Foxm1 is a cell cycle regulator and its expression is dependent upon Pax6 regulation[124]. Pax6-induced changes in Foxm1 expression can result in alterations of cell cycle duration. Foxm1 expression is significantly down in all of the Vegf isoform mice relative to wild type ($p < 0.1$; Table VI, h).

Zfhx1b specifies neural fate early in development [125]. In our qPCR analysis, Zfhx1b expression was down seven-fold (Log2) in the Vegf188 mice relative to wild type and Vegf120/188 mice. The Vegf120 mice were also reduced relative to wild type; however, the difference was not significant ($p = 0.13$; Table VI, i).

Laminin is a heterotrimeric ECM protein often found in basement membranes and around angiogenic vessels. We looked at laminin expression in

three different genes, Lam α 4, Lam α 5, and Lamc3. Overall, there was no statistical difference in laminin expression, except in the Vegf188 mice, where Lam α 4 had significantly lower expression than wild type, Vegf120, and Vegf120/188 mice ($p < 0.1$; Table VII, a-c).

Fibronectin expression, as determined by qPCR, was not significantly changed in the Vegf isoform mice relative to wild type at E9.5. The individual isoforms showed distinct trends of shifted expression, where the Vegf188 mice had significantly lower expression than the Vegf120 mice ($p < 0.05$; Table VII, d).

In order to do a comprehensive comparison with this subset of genes analyzed by qPCR, we conducted a hierarchical cluster analysis to generate a relatedness dendrogram. We visualized the changes in expression patterns of the log₂ values for the wild type mice minus the individual Vegf isoform mice using a heatmap. Expression values that are lower in the wild type relative to the Vegf isoform mice are shown in green, while an increase in expression in the wild type relative to the Vegf isoform mice is shown in red with the color intensity reflecting magnitude of change (Figure 13). We confirmed that with this subset of genes, the Vegf isoform mice show distinct gene expression patterns relative to one another. This pattern recapitulates what we observed in the initial microarray analysis (wild type to Vegf120 and Vegf188) as well as the larger meta-analysis (wild type to Vegf120, Vegf188, and Vegf120/188).

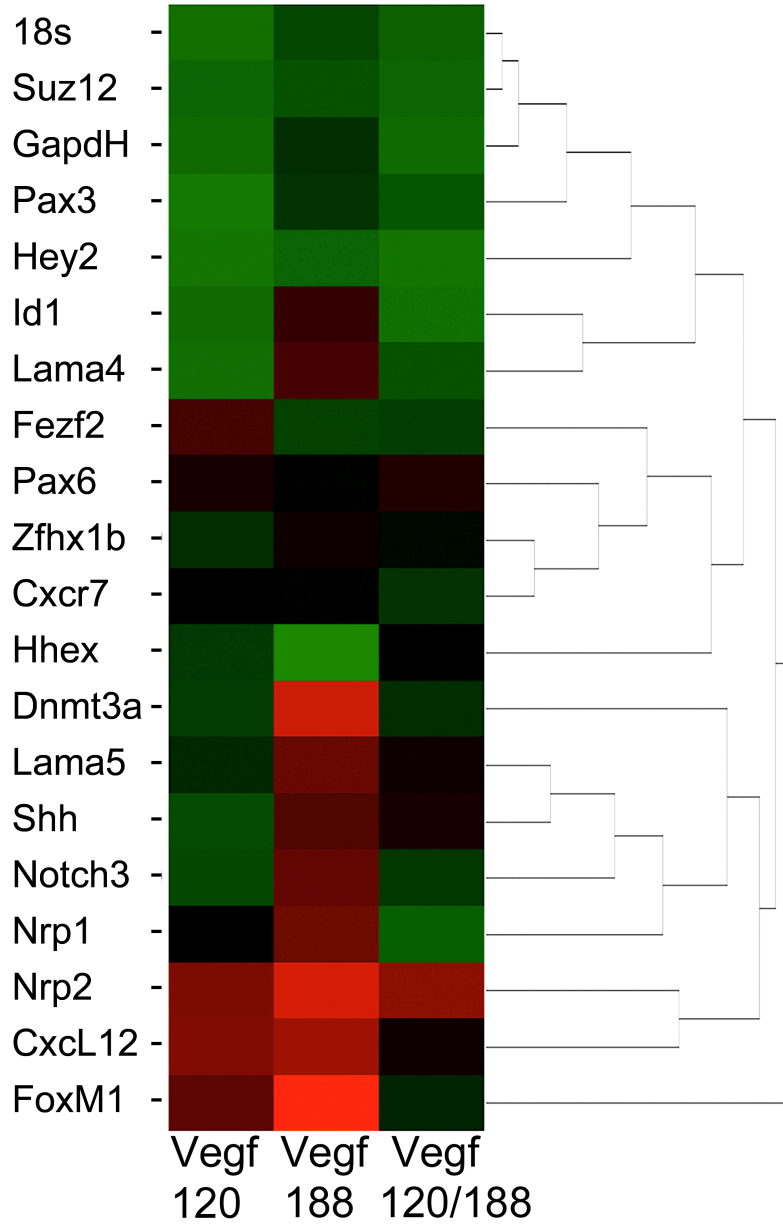


Figure 13. qPCR heatmap comparing fold change for target gene expression in the Vegf isoform mice versus wild type. Quantitative real-time PCR was run on twenty genes using total RNA isolated from E9.5 forebrain neuroepithelium collected from wild type, Vegf120, Vegf188, and Vegf120/188 mice. The expression values were converted to Log2 and the respective fold changes (wild type minus Vegf Isoform) were calculated. These values were loaded into the JMP statistical package and Hierarchical Clustering was run to

generate a dendrogram relating gene expression changes relative to wild type across the three Vegf isoform mice. Log₂ fold change is reflected in the color scheme where an increase relative to wild type (negative values) are shown in green and decreases relative to wild type (positive values) are shown in red with magnitude reflected in color intensity. qPCR values for each run are located in Appendix Table V-VII.

To determine whether our qPCR validation overall was comparable to the changes observed in the microarray meta-analysis, we conducted a correlation analysis using a subset of 16 genes for each of the three fold change comparisons. We compared the fold changes of qPCR expression values (wild type versus each of the Vegf isoform mice) to their corresponding fold changes of the microarray expression values. We ran a Spearman correlation, and determined that the shift in relative expression as detected in our microarray positively correlated with the values determined by qPCR (Spearman's $r = 0.6501$, $p < 0.0001$, $m = 1.069$) (Figure 14).

In order to characterize the genes differentially expressed in the meta-array analysis among the Vegf isoform mice, we utilized the functional annotation clustering platform on the Database for Annotation, Visualization, and Integrated Discovery (DAVID) platform to identify gene groups. DAVID identifies Gene Ontology categories that over-represented amongst a list of genes. Affymetrix Probe Ids of differentially expressed genes detected in the E9.5 mice were uploaded into DAVID. Genes were identified in the top eleven Gene Ontology (GO) categories using an enrichment score filter of 2.0 (Figures 15 and 16, Table VIII). The first functional annotation cluster identified had the GO category *transcription* (134 probe ids). Within this cluster there were several probes identified for their potential roles in cell fate choice, for example Notch3, and neural development for example, Dachshund 1(Dach1) and Dachshund 2 (Dach2). The second annotation cluster, GO Category *positive regulation of transcription* (46 genes), included Meis homeobox 2 (Meis2), Distal-less homeobox2 (Dlx2), Sonic hedge hog (Shh), Sry-box 4 (Sox4), Bone morphogenetic protein 4 (Bmp4), and Neurogenin 2 (Neurog2).

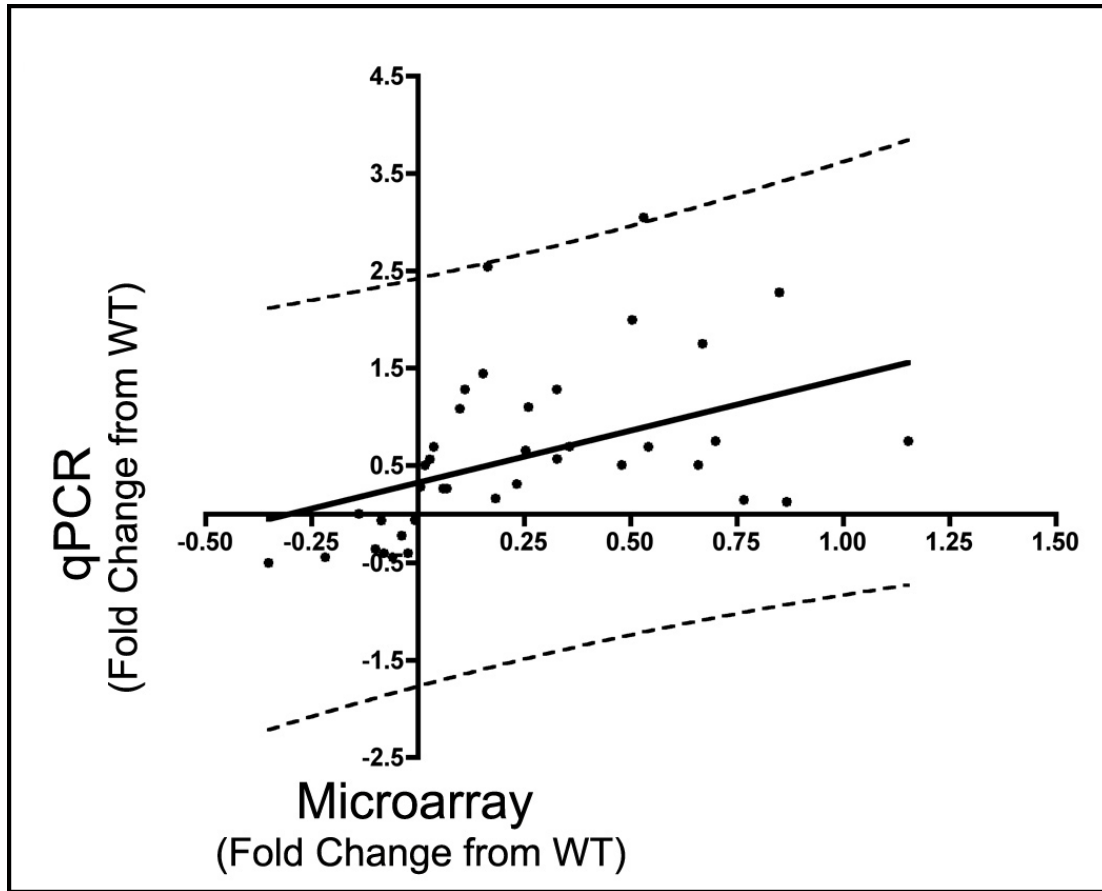


Figure 14. qPCR confirmation of meta-array analysis. qPCRs were run on 16 genes and the fold change between WT and individual Vegf isoforms (Y-Axis) was plotted against the fold changes of the corresponding microarray probe expression values (X-Axis). The scale on both axis is Log2. The solid black line represents the regression line ($m = 1.07$) and the dashed lines indicate the 95% confidence intervals. These latter values were used to remove outliers. We ran a Spearman correlation analysis on 37 (black circles) of the 48 pairs and obtained a positive r-value of 0.6501 ($p < 0.0001$).

GO category *regulation of neurogenesis* (19 probes) identified many of the genes listed above, but in addition included Inhibitor of differentiation 4 (Id4), Distal-less homeobox 1 (Dlx1) and Neuropilin 1 (Nrp1). The two functional annotation clusters with the highest numbers of identified probes were *zinc ion binding* (143 probe ids) and *cation binding* (238 probe ids). Within these categories were many transcription factors, cell signaling ligands, matrix interacting proteins, and epigenetic regulators, including members of the Notch signaling pathway, Jagged 1 and Jagged 2. Several ECM and ECM-interacting proteins were identified within these clusters including Versican, and Integrin-alpha 6. The GO category *neuron development* (26 probe ids) contained several genes involved in neuronal migration and axon path finding, including chemokine receptor 4 (CXCR4), Eph receptor9 A7 (Epha7), Microtubule-associate protein 1B (Mtap1b), and Doublecortin-like kinase 1 (Dclk1). Another interesting functional annotation cluster had the GO category *chromatin organization* (30 probe ids). Genes in this category included histone deacetylase (Hdac9) as well as the methyltransferases, Set domain 8 (Setd8) and DNA-methyltransferase 3 alpha (Dmnt3a).

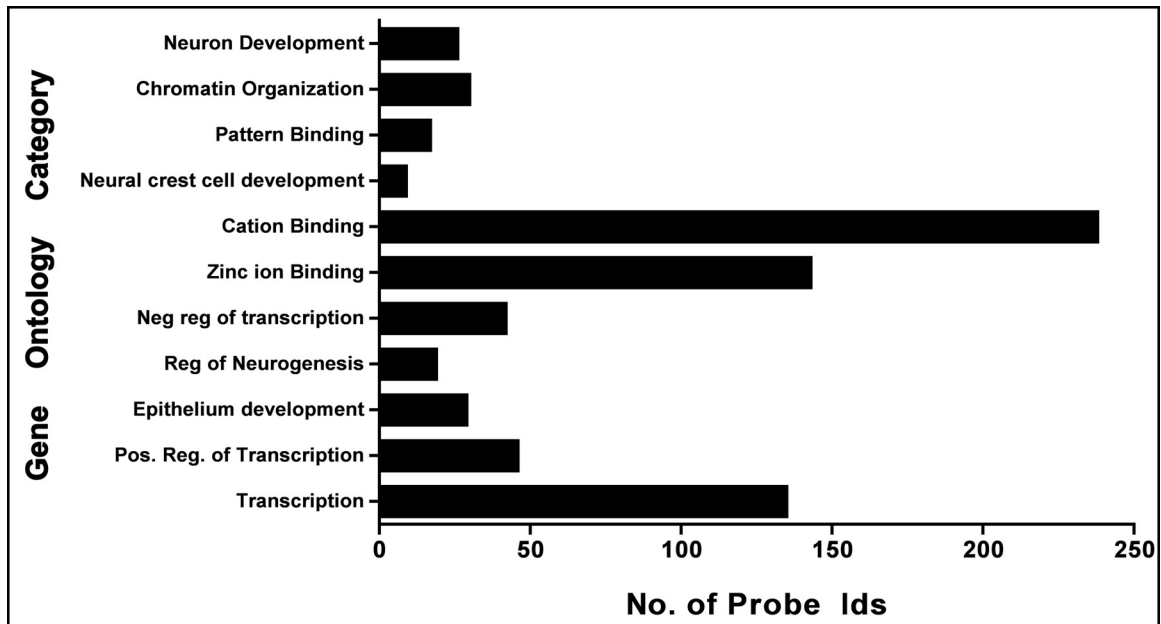


Figure 15. Enriched Gene Ontology Categories in Vegf isoform mice. Affymetrix probe identification numbers (Ids) of differentially expressed genes that were detected as significantly changed by BAMarray in the Vegf120, Vegf188, and Vegf120/188 microarray meta-analyses were uploaded as a single list into DAVID. Functional Annotation Clustering was run on the high setting with the Bonferroni adjustment and GO Terms with an Enrichment Scores within a range of 2 to 6 and and p -values less then 0.01 were reported. The DAVID analysis identified GO categories that were overly represented amongst the differentially expressed genes. The bar graphs represent the number of probe Ids for each functional category. Specific probe Ids, as well as, the DAVID statistics are located in Table VIII.

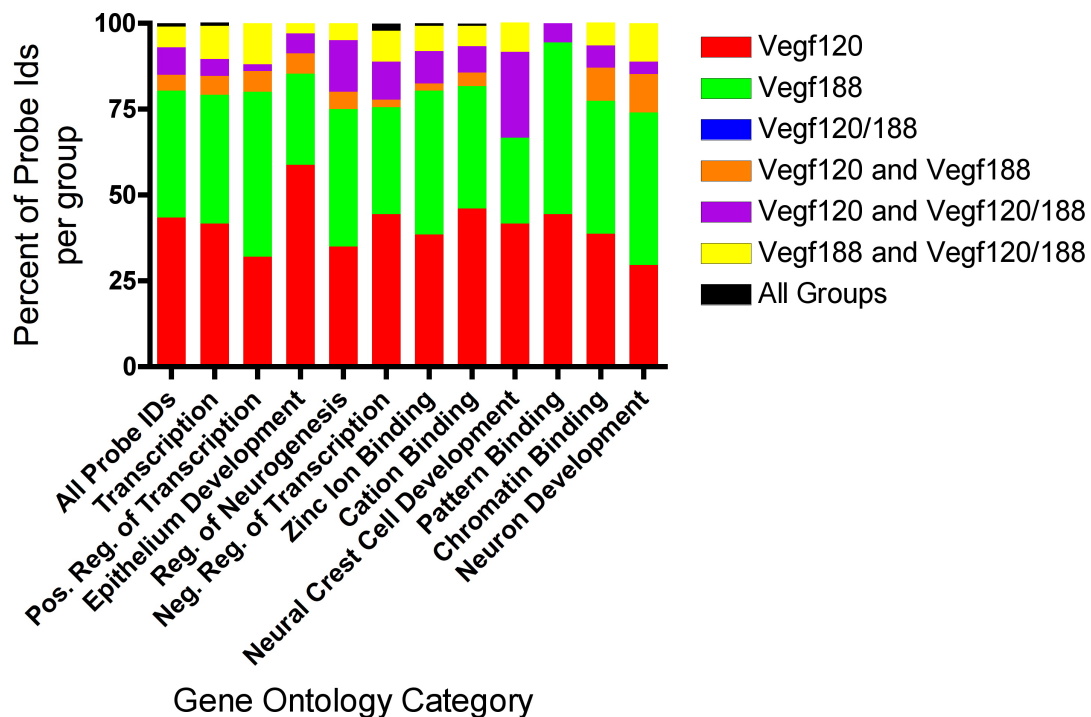


Figure 16. Proportion of differentially expressed genes contributed by the Vegf isoform mice in each GO category. 417 unique differently expressed genes were identified by DAVID with GO categories that were statistically over-represented. The gene contribution from each group of Vegf isoform mice into the various GO categories were broken down into their relative proportions. Of these genes roughly 40% were found changed in either the Vegf188 mice only, or Vegf120 mice only. No genes were identified by DAVID as being unique to the Vegf120/188 mice.

Vegf isoform regulation of early neural stem cell differentiation and migration

By E11.5, the periventricular vessels have invested the neuroepithelium of the telencephalon and neural progenitors have begun proliferating and differentiating. The increase in proliferation thickens the neuroepithelium forcing the radial glia to span an even further distance as they remain in contact with the both the ventricular and pial surfaces. Both angiogenic investment and radial glia polarity are dependent upon the ECM in the microenvironment. Fibronectin (FN) has been shown to guide the differentiation and proliferation of angiogenic endothelial cells, even serving as a track guiding their migration towards sources of Vegf [126, 127]. The ECM protein Laminin (LN) is also required for angiogenesis and serves to regulate vessel diameter. LN is deposited into the basement membrane by the endothelial cells of sprouting vessels, and surrounds the stalk of the growing blood vessel tube. Disruption of the various LN subunits, that form LN trimer, causes vessels of increased diameter (Lamc3), embryonic lethality (Lama5), and early postnatal bleeding (Lama4)[128-131]. The radial glia endfeet embed into the basement membrane and the pial surface, having direct connections with the LN via the cell surface integrin receptors. Disruption of LN in the pial basement membrane alters radial glia orientation and results in bundled end feet of the radial glia processes. While this does not disrupt radial glia proliferation, neuronal migration into the upper layers of the neocortex is affected [132].

Because bioavailability of Vegf is linked to extracellular matrix in the microenvironment and Vegf signaling is modified by ECM binding [11], we wanted to investigate the impact of disrupted Vegf isoform expression on matrix deposition itself. To this end, we examined FN production in the forebrain of Vegf isoform mice using immunolabeling to assess FN localization as well as Enzyme linked immunosorbent assay (ELISA) to quantify total levels of FN protein (Figure 17). Immunohistochemical labeling demonstrated that the wild type mice had low levels of FN with some punctate staining surrounding cells at the pial surface. Qualitatively, the Vegf mice with just the diffusible form of Vegf (Vegf120) had a broader deposition pattern of fibronectin labeling, dispersed at the ventricular surface with some punctate labeling away from the surface. The expression pattern of FN in the presence of the locally-retained Vegf isoform (Vegf188) was dramatically different from wild type with nearly all cells within a three-four cell width of the ventricular surface having positive immunolabeling for FN in punctate clusters on and around the cells. This latter localization is based on z-stack analysis from confocal images (data not shown). This distribution of FN in the Vegf120 and Vegf188 mice was consistent around the developing telencephalon, but most prominent in the anterior loop (Figure 17A). In addition, co-labeling for the FN interacting protein, integrin $\alpha 6$, was expressed in a similar punctate pattern in regions from the ventricular outward, although not directly co-localized with FN protein. This is in agreement with the cell surface localization of integrin $\alpha 6$ relative to FN which can be secreted and deposited in surrounding matrix, bound to the surface of the cell, or proteolytically cleaved and released into the microenvironment [126,127].

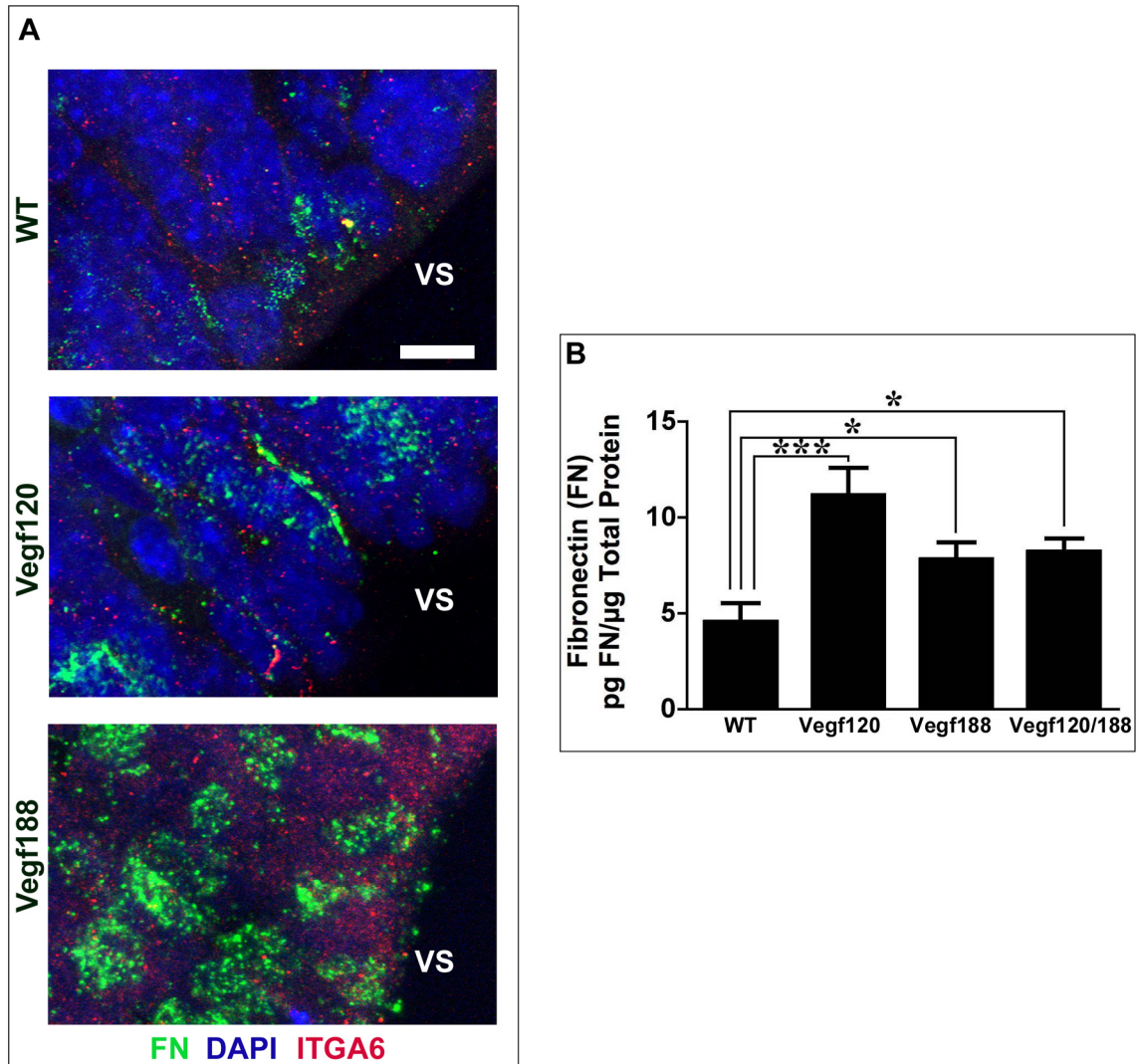


Figure 17. Changes in Vegf isoform profile affects deposition and quantities of ECM and ECM-interacting proteins at E11.5. Fibronectin (Green), Integrin- α 6 (ITGA6, Red), and Nuclei (Blue) were immunolabeled at the ventricular surface (VS) in the anterior loop of the telencephalon at 100x (Scalebar = 100 μ m, A). Wild-type (top, A) samples had qualitatively less fibronectin and integrin then Vegf120 (middle, A) or Vegf188 (bottom, A). The qualitative shifts in FN deposition were confirmed with an ELISA quantifying total FN protein levels in the E11.5 forebrain. Total neuroepithelial forebrain protein

was isolated from wild-type (n = 6), Vegf120 (n = 6), Vegf188 (n =6), and Vegf120/188 (n = 6). Loss of the primary Vegf isoform, Vegf164, in the all of the Vegf isoform mice resulted in a significant increase in total FN, with the greatest increase in the Vegf120 mouse. A 1-way ANOVA followed by Tukey's post-hoc test were used to test for significant differences between the Vegf genotypes (*p < 0.05, ***p < 0.001, B).

The Vegf188 mouse had the most pronounced immunolabeling for both FN and integrin $\alpha 6$. We confirmed these qualitative shifts in FN by measuring total protein levels of FN in the E11.5 forebrain using an ELISA assay that detects both soluble and insoluble FN (Figure 17B). The FN ELISA demonstrated that mice lacking the Vegf164 isoform have increased levels of FN. The Vegf188 and Vegf120/188 mice showed roughly a fifty percent increase in total FN levels and were significantly changed versus wild type ($p < 0.05$). FN protein levels were almost double in the Vegf120 mice versus wild type ($p < 0.001$). As this assay detects both locally-retained and soluble fibronectin, the relative levels differ from the apparent distribution intensity of FN in the microenvironment as detected by immunolabeling. However, in all cases the FN is higher (ELISA) and has a broader distribution pattern (immunolabeling) relative to the wild type, confirming an increase in FN by two different methodological approaches.

Because FN has been historically associated with cell adhesion during migration, we wanted to also examine the expression of LN that has been more closely linked to basement membrane production during development, particularly in sites of cell-cell contact. Therefore, we conducted qualitative and quantitative analysis of LN in the E11.5 mouse forebrain. Laminin immunolabeling in the Vegf isoform mice was grossly similar to that of the wildtype mice and closely associated with the basement membrane barrier between the neuroepithelium and the pial vessel surface (Figure 18, A-D).

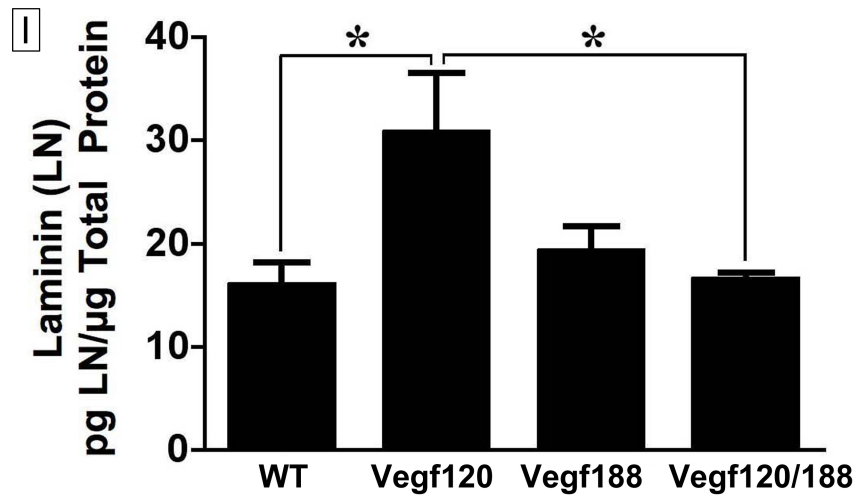
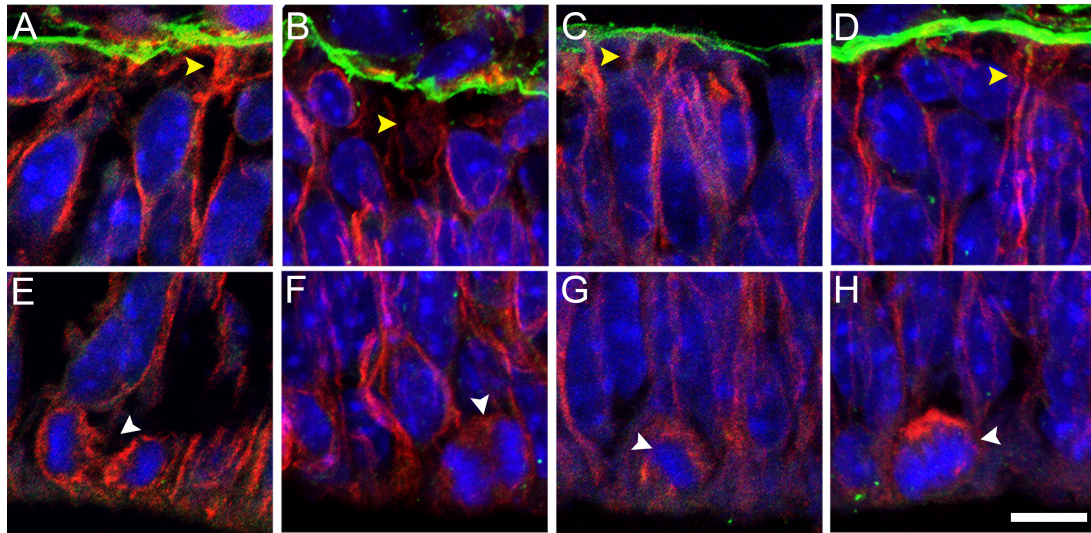


Figure 18. Vegf isoform profile affects Laminin proteins levels. The dorsal-anterior telencephalon loop in E11.5 WT (A,E), Vegf120 (B,F), Vegf188 (C,G), and Vegf120/188 (D,H) were immunolabeled with the ECM protein Laminin (LN, green), the radial glia marker nestin (red), and DAPI to label nuclei (Blue). At the pial surface (A-D) LN staining marks the basement membrane where radial glia end feet (yellow arrowheads) implant themselves. At the ventricular surface (E-H), the intermediate filament nestin surrounds dividing cells (white arrowheads). Images were taken at 100x with a scalebar equal to 10 μ m. ELISA quantification

of LN protein levels in the E11.5 mouse forebrain demonstrates a dramatic increase of LN in the Vegf120 mouse (I). Statistical significance was determined with a 1-way ANOVA followed by a Tukey's Post-Hoc test (Each group had a N = 6, *p < 0.0001).

No specific immunolabeling for LN was detected at the ventricular zone (Figure 18, E-H). Protein quantification of total LN revealed that the forebrains of Vegf120 mice had a significant increase in total LN relative to wildtype and Vegf120/188 ($p < 0.05$) forebrains. The Vegf188 forebrain lysates had reduced levels of LN protein relative to Vegf120; however, the results were not statistically significant. There was no significant difference in LN protein levels among wildtype, Vegf188, and Vegf120/188 (Figure 18, I).

To assess the morphology and distribution of radial glia and neural stem cells we looked at two proteins whose expression has been closely associated with stem cells, Nestin and Pax6 (Figure 18 and Figure 19 respectively). Nestin is an intermediate filament associated with radial glia. It appears early in neural development and persists until the radial glia differentiate into astrocytes whereupon nestin expression transitions to Glial fibrillar acid protein (GFAP) expression. At E11.5, immuno-positive nestin fibers span the length of the neuroepithelium, coalescing in the radial glia end feet at the pial surface (Figure 18A-D) with the somatic contacts at the ventricular surface. In the ventricular zone of the neuroepithelium, nestin filaments surround the nuclei of dividing cells, demonstrating that radial glia do serve as neural progenitors (Figure 18E-H). Pax6 is a transcription factor expressed in many stem cell populations, particularly neural stem cells. Loss of Pax6 expression correlates with specification to a neural or glial lineage, depending on developmental stage and cell fate choice (Reviewed in [76]). At E11.5 Pax6 is generally restricted to the ventricular zone of the neuroepithelium (Figure 19A-C).

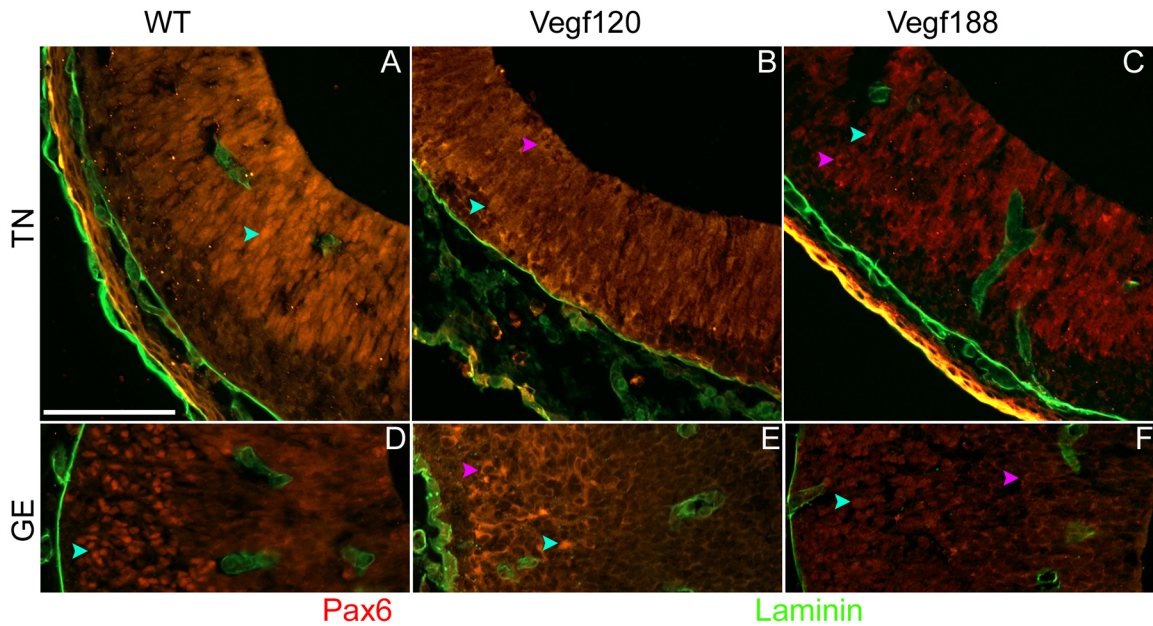


Figure 19. Altered Vegf bioavailability alters early neural stem cell fate and basement membrane organization. E11.5 mouse forebrains were immunolabeled with the radial glia stem cell marker Pax6 (red) and ECM protein laminin (green). In the telencephalon (TN) and ganglionic eminence (GE) Pax6 localization is altered in the Vegf isoform mice. The WT and Vegf188 have clear ventricular-subventricular zone borders, marked by the transition of Pax6-positive to Pax6-negative cells, while Pax6-positive cells run all the way to the pial surface in the Vegf120 mouse. Pax6 immunolabeling is strictly limited to the nuclei (blue arrowhead) of the WT (A,D) mice, while Vegf120 (B,E) and Vegf188 (D,F) mice also have Pax6 limited to the cytosol (purple arrowheads). Laminin labeling is present in the vessels along the pial surface (Left), along the basement membrane, and surrounding the periventricular vessels. (40x, scalebar = 50 μ m)

Pax6 expression transitions to Tbr2 expression as neural stem cell differentiation proceeds and the cells begin their final migration out of the ventricular zone. In the more caudal regions of the primitive forebrain at E11.5, Pax6-positive nuclei are present in the pallium and GE. In wild type mice Pax6 is entirely located in the nuclei, whereas the Vegf120 and Vegf188 mice display a distinct sub-localization with many cells having Pax6 restricted to the cytosol, leaving the nucleus immunonegative (Figure 19, compare D-F). The expression pattern of Pax6 is particularly unique in the GE of the Vegf120 mice. Where most of the nuclei are Pax6 positive in the WT and Vegf188 GEs, Pax6 seems to be mostly absent in comparable nuclei of the Vegf120 mice and is, instead, localized to the cytosol. The Vegf isoform-dependent changes in Pax6 cellular localization suggest a link between Vegf localization and neural stem cell differentiation.

In order to dissect the role of Vegf bioavailability in the regulation of neural stem cell differentiation and neocortical development, we had to survey the status of neural stem cell proliferation as well as early stages in the neural differentiation pathway. To this end we quantified proliferating cells by counting Phospho-Histone H3 (Phh3), a marker of mitotic cells, and Tbr2/Eomes, that is expressed by the intermediate progenitor population once they have been restricted to the neural lineage. We chose to begin looking at these stage markers early in neural development, at E11.5, so that we could rule out any secondary effects associated with any abnormal vasculature in the Vegf isoform mice. At this early stage, the periventricular vessels are only just beginning to establish themselves, and the neuroepithelium is still thin enough to facilitate gas

exchange via simple diffusion. The bulk of the proliferating cells are in the Pax6-positive ventricular zones. Phh3-positive proliferating cells line the ventricular surface. In a complementary distribution pattern, their differentiated, Tbr2-positive, counterparts have begun migrating and aligned in a cellular border subjacent to the pial surface (Figure 20A-L). We quantified the populations of the both the Phh3-positive and Tbr2-positive cells, as well as total neuroepithelial cells, in the E11.5 forebrains using unbiased, design-based stereology.

For the Phh3 and total neuroepithelial cell counts, we traced an area spanning 100 μ m from the ventricular surface along the entire forebrain. The Vegf120 and Vegf188 mice had less Phh3-positive cells compared to wild type and Vegf120/188. However, a one-way ANOVA followed by Dunnett's post-test showed that only Vegf120 was significantly different from wild type (wild type n = 6, Vegf120 = 4, Vegf188 = 3, and Vegf120/188 = 6, $p < 0.05$). Total neuroepithelial cells were counted in parallel and again the Vegf120 mice showed a decrease relative to wild type ($p < 0.05$). There was no significant difference in total cell numbers among the other genotypes (Figure 20M,O).

To assess the early stages of differentiation, we counted Tbr2-positive cells along the pial surface in animals matching those used in the previous counts. The counting region we traced differed from the one used for the Phh3 counts in that we traced from pial surface to 100 μ m in towards the ventricular surface. The Vegf188 and the Vegf120/188 mice had fewer Tbr2-positive cells when compared to wild type and Vegf120; however, only the difference between Vegf188 and wild type was significant ($p < 0.05$).

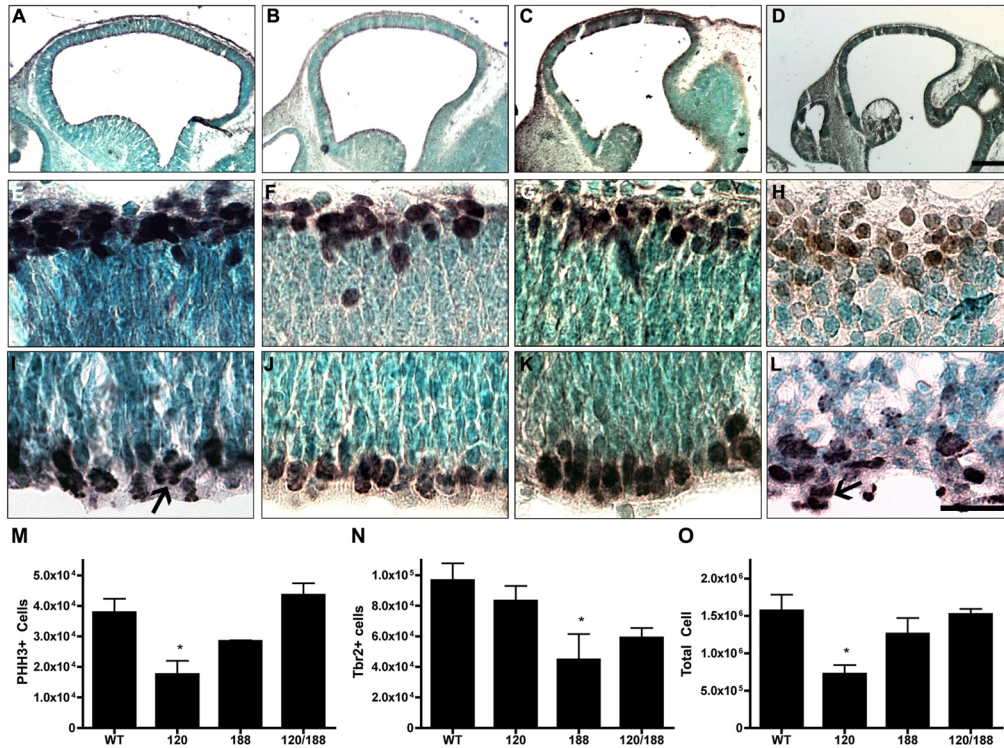


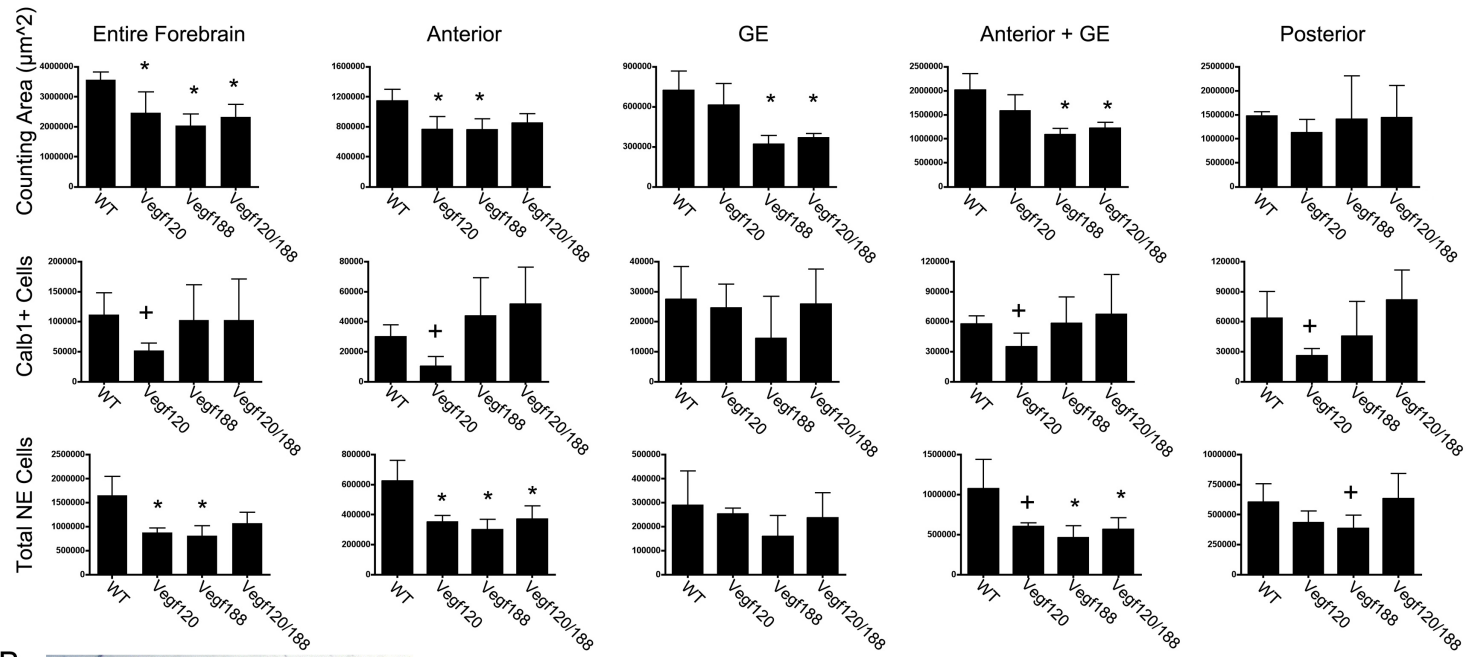
Figure 20. Vegf regulation of NSC proliferation and differentiation. E11.5 wild types (A, E, I), Vegf120 (B, F, J), Vegf188 (C, G, K), and Vegf120/188 (D, H, L) forebrains were sectioned in the parasagittal plane and immunolabeled with PHH3 (A-H) or Tbr2 (I-L) and counter-stained with methyl-green. The whole forebrain imaged at 2x showed no major differences between the Vegf isoform mice versus wild type (A-D, scalebar = 500 μ m). At 40x magnification Tbr2⁺ cells are labeled uniformly along the pial surface (E-H), and PHH3⁺ cells line the ventricular surface (I-L, scalebar = 50 μ m). Arrows indicate dividing cells along the ventricular surface. Counts of PHH3⁺, Tbr2⁺ cells, and total neuroepithelial cells were completed using Stereoinvestigator (M-O). Groups were tested for significant differences using a 1-way ANOVA followed by a Dunnett's post-test using wild types as the control. The Vegf120 mice showed a significant reduction in total neuroepithelial cells and PHH3⁺ cells versus wild type. ($P < 0.05$, wild type

n = 6, Vegf120 n = 4) The Vegf188 mice showed reduced numbers of Tbr2+ cells compared to wild type ($P < 0.05$, Vegf188 n = 3). The Vegf120/188 mice were not statistically significant from wild type ($P > 0.05$, n = 6). Errors bars represent standard error of the mean.

It was interesting that despite having decreased number of proliferating cells that corresponded with a decrease in the total cell number, the Vegf120 mice produced an equivalent number of intermediate progenitors relative to the wild type mice (Figure 19N).

Since the tangential migration of neurons into the pallium contribute a significant number of interneurons in the neocortex, we also immunolabeled sections matching those in the previous Tbr2 and Phh3 counts using Calbindin (Calb1). Calb1-positive cells are born in the GE and from there they migrate out, eventually taking positions in the cortical layers. Calb1-positive cells migrating into the anterior portion of the forebrain (pallium) and become the interneurons of the neocortex. We divided the E11.5 mouse forebrain into three sections based on anatomical markers and cortical derivatives: the GE, an area anterior to the GE, and the area posterior to the GE (Figure 21). We traced the entire neuroepithelial area for the GE and anterior portions; however, since some areas in the posterior section were substantially thicker we only traced around the Calb1-positive areas, or $100\ \mu\text{m}$ from the pial surface to avoid cut-angle bias. Using stereology we counted the Calb1-positive cells and total neuroepithelial cells for each anatomic region and compared these across wild type and Vegf isoform genotypes. We also quantified the neuroepithelial area traced in wild type ($n = 4$), Vegf120 ($n = 4$), Vegf188 ($n = 4$), and Vegf120/188 ($n = 4$). We looked at each of these parameters in the Anterior, Posterior and GE portions, as well as combinations of all three. All tests of significance were measured using a one-way ANOVA followed by Tukey's post test.

A



B

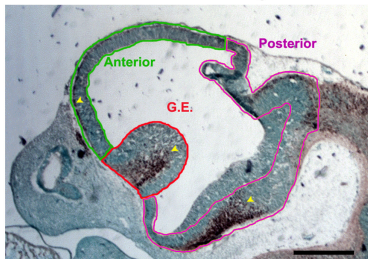


Figure 21. Vegf isoform profile affects the distribution of Calbindin positive cells.

Figure 21, Con't. Calbindin (Calb1) positive cells born in the ganglionic eminence (GE) migrate towards the anterior forebrain (green, B) to form inhibitory-interneurons in the pallium. Changes in the microenvironmental distribution of Vegf, in the isoform mice, resulted in dramatic changes in the localization of the Calb1+ cells in the forebrain. Calb1+, total neuroepithelial cells (NE), and counting area were quantified in the forebrains of E11.5 mice using stereology. For these counts the mouse brain was divided into three areas the (GE, red), the area anterior to the GE (green), and the area posterior to the GE (purple). Independent counts were obtained in each of these areas, and all counts were combined to get number for the Entire Forebrain. Counts from Anterior and GE were also combined. Difference between the genotypes was measured with a 1-way ANOVA, followed by a Tukey's Post-Hoc test (WT n = 4, Vegf120 n = 4, Vegf188 n = 4, Vegf120/188 n = 4, *p < 0.05, '+' indicated an apparent shift in mean which was not statistically significant). Gundersen confidence estimates (CE) were obtained from each counting group, except in the GE where a Schmitz-Hof was used due to the limited number of sections with GE present within a series (CE < 0.1, m = 1).

Significant difference from the wild type was marked with an “**” ($p < 0.05$). In some instances the ANOVA did not detect a significant difference ($p > 0.1$) in any of the groups, despite the shift observed in population means. In these instances a student’s t-test was used to compare the group versus wild type, a significant difference was indicated by “+” ($p < 0.05$).

When looking at the entire forebrain, the wild type mice had the largest overall area compared to the rest of the genotypes ($p < 0.05$). The Vegf120 mice were the only group with a statistically significant decrease in Calb1-positive cells ($p < 0.05$); the other groups were unchanged versus wild type. All of the Vegf isoform mice appeared to have a decreased number of total cells; however, only the Vegf120 and Vegf188 mice had a significant decrease ($p < 0.05$). In the anterior portion, again the Vegf isoform mice had a decreased neuroepithelial area, with only the Vegf120 and Vegf188 groups being significant ($p < 0.05$). Total neuroepithelial cell numbers were significantly decreased in the anterior region of the Vegf isoform mice ($p < 0.05$). The Vegf120 mice showed a significant decrease in Calb1-positive versus wild type. While both Vegf188 and Vegf120/188 showed an increased trend in positive numbers versus wild type, the differences were not statistically significant. In the GE, both the Vegf188 mice and the Vegf120/188 mice had a significant decrease in area ($p < 0.05$) versus wild type. The Vegf120 mouse had no apparent change versus wild type. In the GE, the Vegf188 mice had a decrease in both total cell number and Calb1-positive labeled cells; however, neither shift was significantly different versus wild type.

When we combined the counts from anterior and GE portions, we found that the areas in wild type and Vegf120 showed no apparent differences while both Vegf188 and Vegf120/188 were significantly lower ($p < 0.05$). All of the Vegf isoform mice displayed significantly lower numbers of total cells versus wild type ($p < 0.05$); however, only the Vegf120 mouse showed any significant change downward relative to wild type ($p < 0.05$). The areas of the posterior section were not significantly changed among any group. The Vegf120 mice had a significant drop in the Calb1-positive cells, and both Vegf120 and Vegf188 mice showed a decrease in posterior total cells.

Consequences of altered Vegf bioavailability in early cortical lamination

At E11.5, we looked at the effects of altered Vegf bioavailability on the early neural stem cell proliferation, differentiation, and migration in parallel with the changes in extracellular matrix in the microenvironment. In order to determine the effects of these early changes we wanted to look at consequences at later developmental stages. To accomplish this, we examined the E13.5 mice in which the blood vessels are well established in the surrounding pia mater and throughout the pallial neuroepithelium. At this time point differentiation of the neural stem cells is well underway, the germinal layers of the neuroepithelium have become further stratified, forming the ventricular zone, subventricular zones, intermediate zone, subplate, cortical plate, and marginal zone (Figure 4). Tbr2-positive intermediate progenitors and Tbr1-positive post-mitotic neurons are well established and primed to begin the outward radial migration to start forming the six layers of the mammalian neocortex. Concomitantly, Calb1-positive interneuron precursors have rapidly expanded in number and are undergoing their tangential migration out of the GE along the pial surface of the pallium.

At E13.5 Laminin remains highly expressed along the pial surface basement membrane as well as in the basement membrane of the blood vessels, deposited between the endothelial cells and the perivascular cells (Figure 22, A-D).

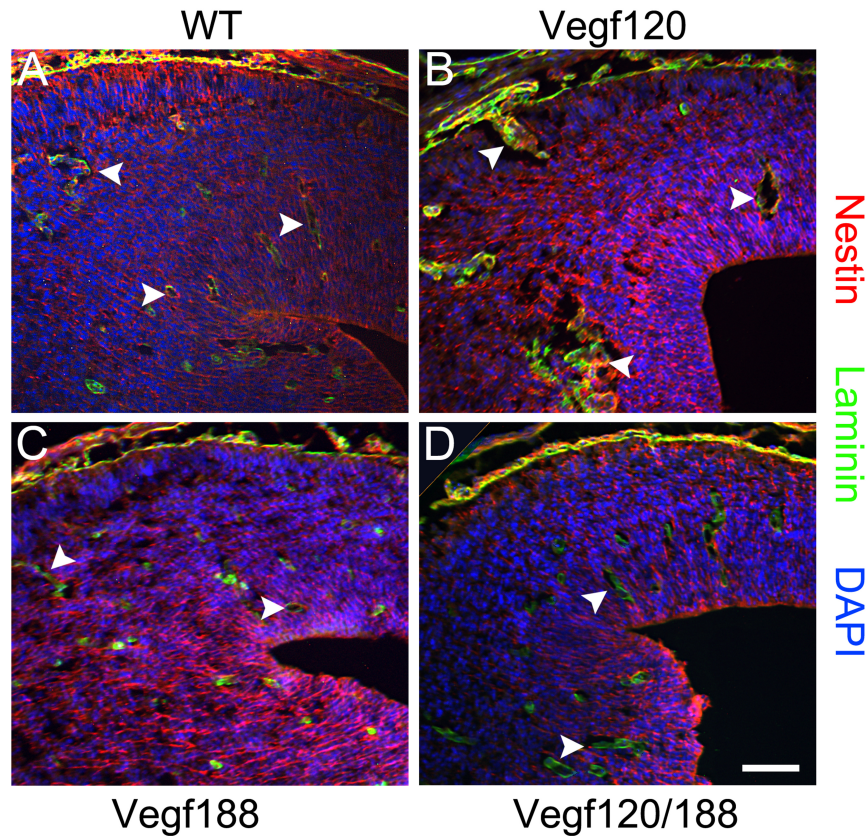


Figure 22. Vegf isoform misexpression affects radial glia morphology and periventricular blood vessels. Nestin (red), laminin (green, LN), and DAPI (blue) were immunolabeled in E13.5 mouse forebrains at the joining of the GE (bottom left) and subpallium (top right). LN immunolabeling is associated with the basement membrane at the pial surface, pial blood vessels, and periventricular blood vessels (arrowheads). The blood vessels in the Vegf120 (B) mouse are dysmorphic and have abnormally large lumens. The radial glia, labeled by nestin, appear to have thicker and more tortuous fibers in the Vegf120 and Vegf188 mice compared to their WT and Vegf120/188 counterparts. These images were shot at 10x with standard fluorescence microscopy, and the scale bar is equivalent to 50 μ m.

As vascular investment of the telencephalon is well underway (albeit incomplete), vascular abnormalities characteristic of the Vegf isoform mice have begun to manifest, particularly in the Vegf120 mice. Laminin staining of the periventricular vessels in the Vegf120 mice revealed convoluted vessels, with large lumens, and significant red blood cell hemorrhage (Figure 22, compare B to A). Nestin staining of radial glia is still present throughout the neuroepithelium in all genotypes. However, the nestin intermediate filaments in the Vegf120 and Vegf188 mice have a more intense labeling pattern and are more tortuous than those of the wild type or Vegf120/188 mice (Figure 22, A-D). Gross structural morphology of the tissue is preserved at this stage and patent blood vessels are observed throughout the telencephalon/GE as expected for this developmental stage.

At E13.5, Calb1 positive interneuron precursors are migrating tangentially along the marginal zone, and preparing to interdigitate into the proper layer of the radially differentiating neocortex. We examined the distribution of Calb1-positive cells in both the medial pallium (Figure 23A-D), and lateral pallium (Figure 23E-H). Calb1 immunolabeling was strongest in the lateral pallium of the Vegf120 and Vegf120/188 mice; however, it was still present in both the wild type and Vegf188 mice. Calb1 was not detected in the medial pallium. In parallel, we also assessed the status of developing vasculature using *G. simplicifolia* lectin B4 (Lectin) the binds to a sugar moiety on the surface of endothelial cells. Again we saw that in the Vegf120 mice there were dysmorphic vessels with abnormally large lumens.

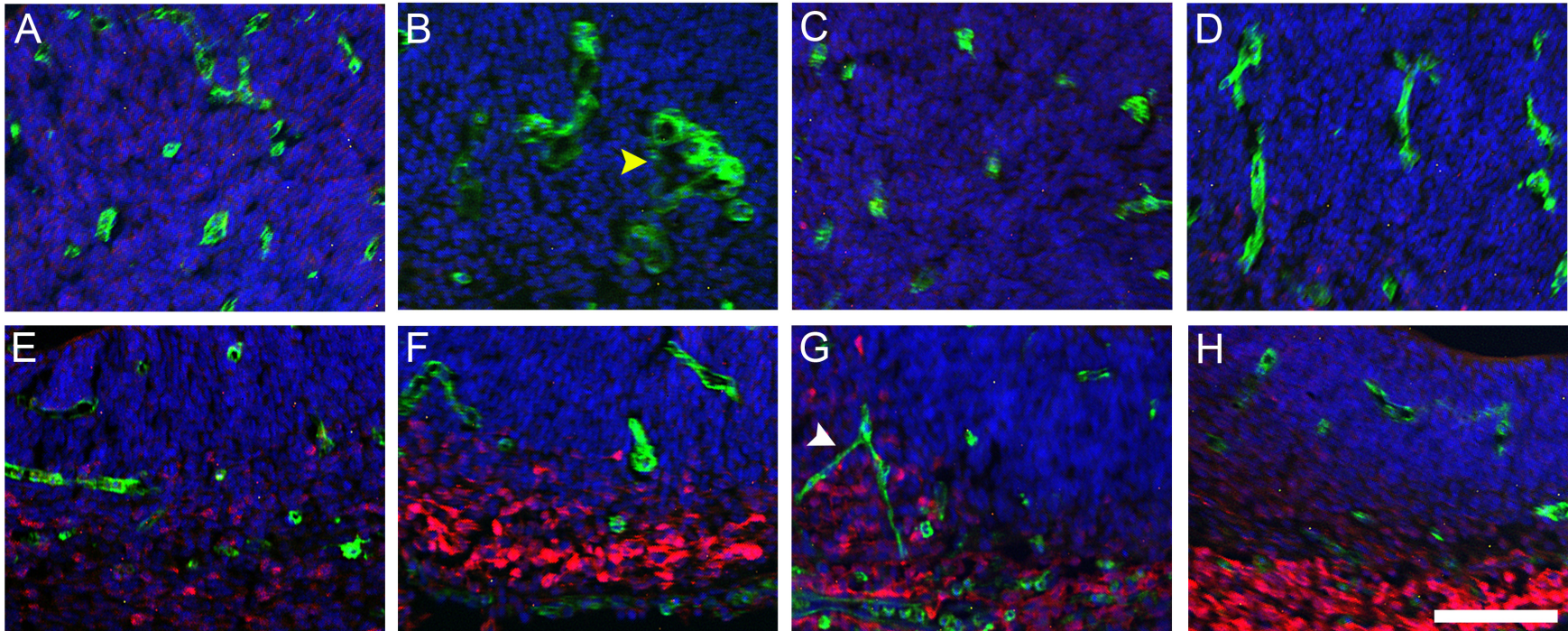


Figure 23. Vascular compromise and migration defects in the Vegf isoform mice. E13.5 mouse forebrains were labeled with Lectin (green), Calbindin (Calb1, red), and DAPI (blue) and were imaged at the middle pallium (A-D), and lateral pallium (E-H). Compared to wild type (A,E) the Vegf120 mice had highly ramified vessels with broad lumen (yellow arrow, B,F). The Vegf188 mice had long and narrow vessels (C,G, white arrowhead). The Vegf120/188 mice displayed

vessel morphology closest to that of wild type (D,H). Calb1 immunolabeling was not detected in the medial pallium (A-D), however, along the lateral pallium Calb1-positive cells were detectable in the wild type with low intensity labeling relative to the genotypes. Calb1 labeling was strongest in the Vegf120 and Vegf120/188 mice, and intermediate in the Vegf188 mice (E-H). Images were collected using standard fluorescence at 10x and the scalebar is 50 μ m.

The Vegf188 mice displayed some vessels that were narrower than their wild type counterparts, a vascular phenotype that has been previously described in the retinal [36] and hindbrain [4] vasculature in these mice. The Vegf120/188 displayed vascular patterning closest to that of the wild type reflecting the value of combined localized and diffusible Vegf isoforms during angiogenesis. Calb1-positive cells are prevalent in the GE across all of the genotype mice at E13.5; however, contrary to stereological counts at E11.5, the Vegf120 mice qualitatively had the fewest Calb1-positive cells in the GE (Figure 24, A-H). In the LGE, Calb1 was localized to both the nuclei and cytosolic processes of the interneuron precursors, although the intensity of the subcellular localization pattern differed among the Vegf isoform mice. The Vegf188 mice had a relatively high number of these Calb1-positive processes compared to wild type and the Vegf120/188, where the majority of the Calb1 labeling was restricted to the nucleus. (Figure 24, A-H).

In order to determine the effect of altered Vegf isoform profile on the specification of intermediate progenitor populations we immunolabeled the forebrains of E13.5 mice with Tbr2. At this stage in development, Tbr2 is a transcription factor specific to the intermediate progenitor population that is specified for the neuronal lineage but is still actively dividing. We speculated that altered bioavailability of Vegf would inhibit the Pax6-to-Tbr2 transition, would prevent the Tbr2 cells from migrating appropriately to the cortical plate, or would impact both developmental processes. Low magnification images of the forebrain showed that the distribution of Tbr2 was similar across all genotypes.

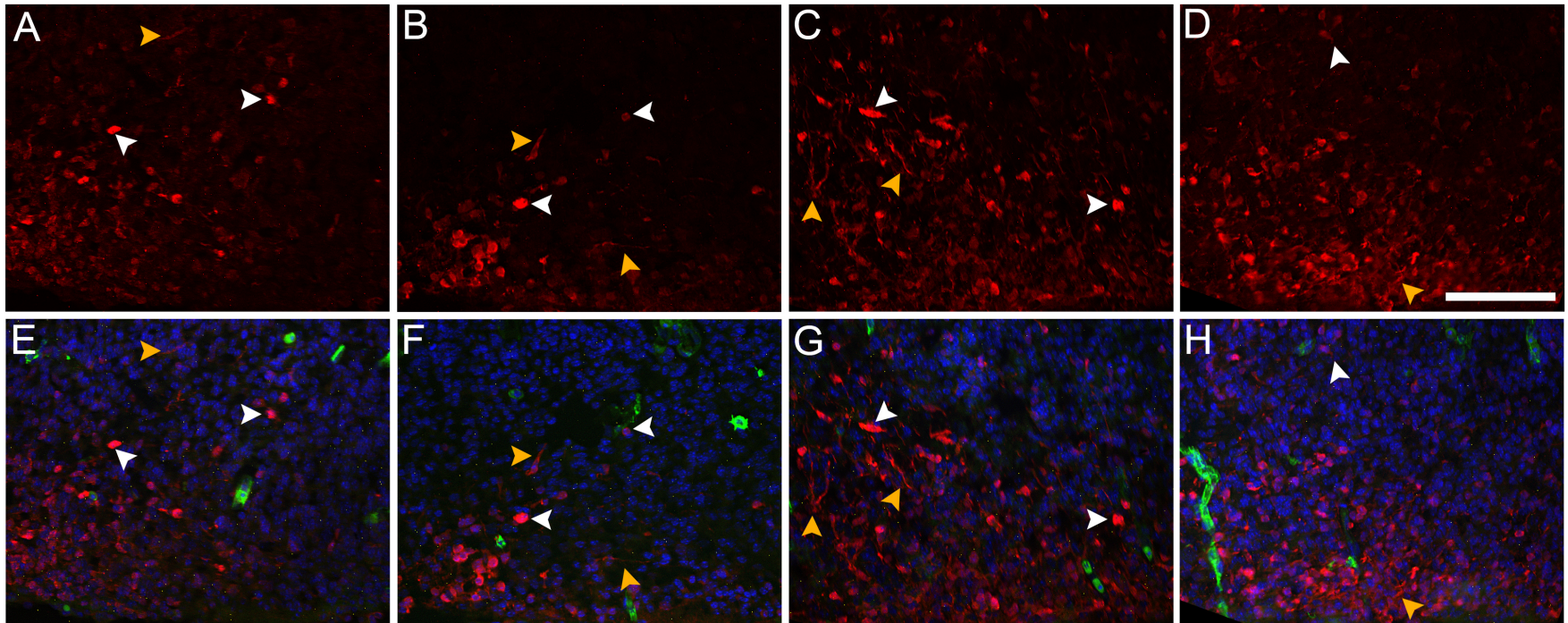


Figure 24. Vegf isoform bioavailability affects Calbindin-positive cell morphology in the LGE. E13.5 mouse forebrains were immunolabeled with Calbindin (Calb1; single channel A-D), Lectin (green), and DAPI (blue). Images were taken in the lateral GE, with the pial surface oriented towards the bottom of the image. Triple-labeled images were collected using standard immunofluorescence at 20x magnification. Vegf188 (C,G) and Vegf120/188 (D,H) had a broader swath of more intensely labeled Calb1-positive cells relative to wild type (A,E). The Vegf120 mice (B,F) had a reduced

cluster of positive cells in the GE. The Vegf188 mice also had more Calb1-positive labeling localized to the cell processes (orange arrowhead) compared to the other groups where the labeling was largely restricted to the cell soma. Representative Calb1-positive nuclei are indicated with a white arrowhead. (Scalebar = 50 μ m)

Tbr2-positive cells started at the border of the subpallium and GE and extended throughout the pallium, with population distribution stopping in the medial pallium and choroid plexus at this point in development. Tbr2-positive cells had the highest concentration along the subventricular/intermediate zone border (Figure 25, A-D). Higher magnification images of the medial pallium (Figure 25, E-H), dorsal pallium (Figure 25, I-L), lateral pallium (Figure 25, M-P), and subpallium (Figure 25, Q-T) confirmed that Tbr2-positive nuclei were present across the entire developing neocortex. In the medial pallium most of the Tbr2 cells were juxtaposed to the pial surface; however, both the wild type and Vegf188 mice had a number of Tbr2-positive cells migrating radially through the ventricular zone. In the dorsal pallium, the distribution of Tbr2-positive cells seemed equivalent across all groups, with the exception that the Vegf120 group had a wide swath of positive cells although the cells were spaced further apart. The radial distribution of Tbr2-positive cells was altered in the germinal layers of the Vegf188 mice. The Vegf188 mice had a substantial number of Tbr2-positive cells in the ventricular zone, a strong band of Tbr2-positive cells at the subventricular zone border, and a second band closer to the pial surface. This differed from the wild type and Vegf120/188 mice, in which the strongest band of Tbr2-positive cells was much closer to the pial surface. The Vegf120 mice also had bands of Tbr2-positive cells at both the subventricular zone border and near the pial surface, but the staining was much weaker in intensity than that of the other genotypes.

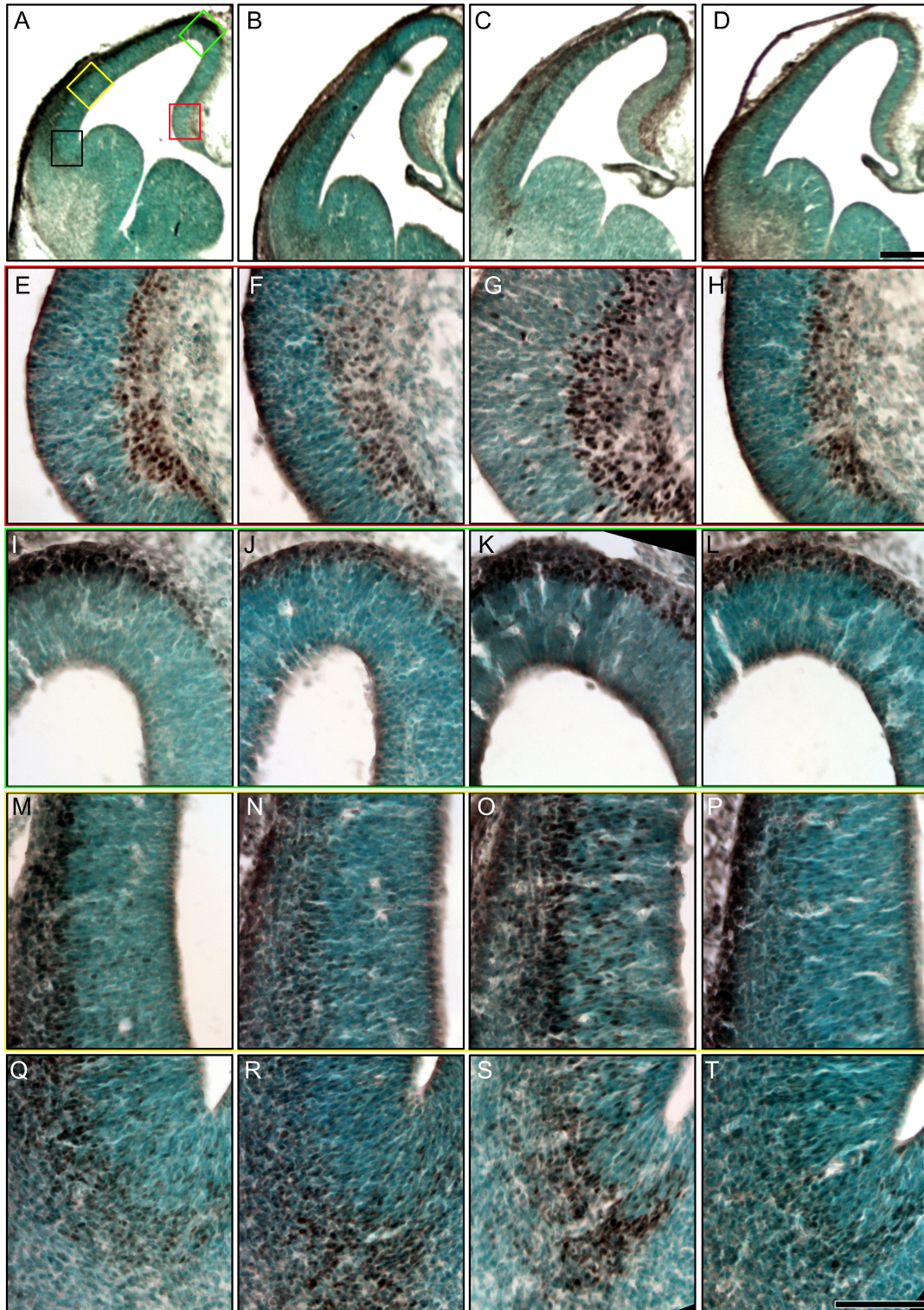


Figure 25. Radial distribution of intermediate progenitors is modulated by the available Vegf isoform profile.

Figure 25, Con't. E13.5 mouse forebrains were immunolabeled for Tbr2, developed with DAB immunohistochemistry, and nuclei counterstained with methyl-green. Low magnification images show overall distribution of Tbr2-positive intermediate progenitors in wild type (A,E,I,M,Q), Vegf120 (B,F,J,N,R), Vegf188 (C,G,K,O,S) and Vegf120/188 (D,H,L,P,T) (2x, scalebar = 125 μ m). 20x close ups were taken at the medial pallium (red box, E-H), dorsal pallium (green box, I-L), lateral pallium (yellow box, M-P), and subpallium (black box, Q-T) (scalebar = 50 μ m). The Vegf120 and Vegf188 mice qualitatively had the thickest bands of Tbr2-positive cells throughout the pallium. In general, the Vegf isoform mice appeared to have increased Tbr2-positive cells in the ventricular zones, although the Vegf120/188 pattern of Tbr2 distribution closely resembled that of wild type animals. The Vegf188 mouse had the strongest concentration of Tbr2-positive cells in ventricular and subventricular zones, especially in the medial, lateral, and subpallium (G,O,S). The wild type and Vegf120/188 mice had the strongest localization of Tbr2-positive cells near the pial zones, the intermediate zone and cortical plate.

The distribution of Tbr2-positive cells in the subpallium was roughly equivalent across all groups; however, the Vegf120 and Vegf188 mice had stronger immunolabeling compared to that of the wild type or Vegf120/188 mice.

Because of the shifted radial patterns of Tbr2-positive cells that were observed throughout the developing forebrain structures, we wanted to quantify the subsequent effects on the key post-mitotic neuron population that arises at this timepoint. Cells positive for the transcription factor, Tbr1 have left the cell cycle and are actively migrating to cortical layer destinations and differentiating along the way to acquire their final neurotransmitter phenotype [55]. We observed that Tbr1 was strongly expressed along the pial half of the neuroepithelium across both the GE and pallium (Figure 26, A-L). In the medial pallium, Tbr1 expression was most intense in the wild type and weakest in Vegf120 mice (Figure 26, E-H). In the subpallium, Tbr1 immunolabeling was roughly equivalent across all of the genotypes (Figure 26, I-L). There are angiogenesis defects that are present in the Vegf120 mice at this developmental stage. Several large vessels appear as holes in the GE of the Vegf120 mice (Figure 26B). At higher magnification, a large periventricular vessel is caught in cross section, disrupting an otherwise solid line of the Tbr1-positive cells in the Vegf120 mouse (Figure 26J, black arrowheads). Using an unbiased, stereological approach, we counted the Tbr1-positive nuclei, as well as total cell nuclei (Figure 26, M and N). We traced the neuroepithelium of the Tbr1-positive areas from the GE to the medial pallium.

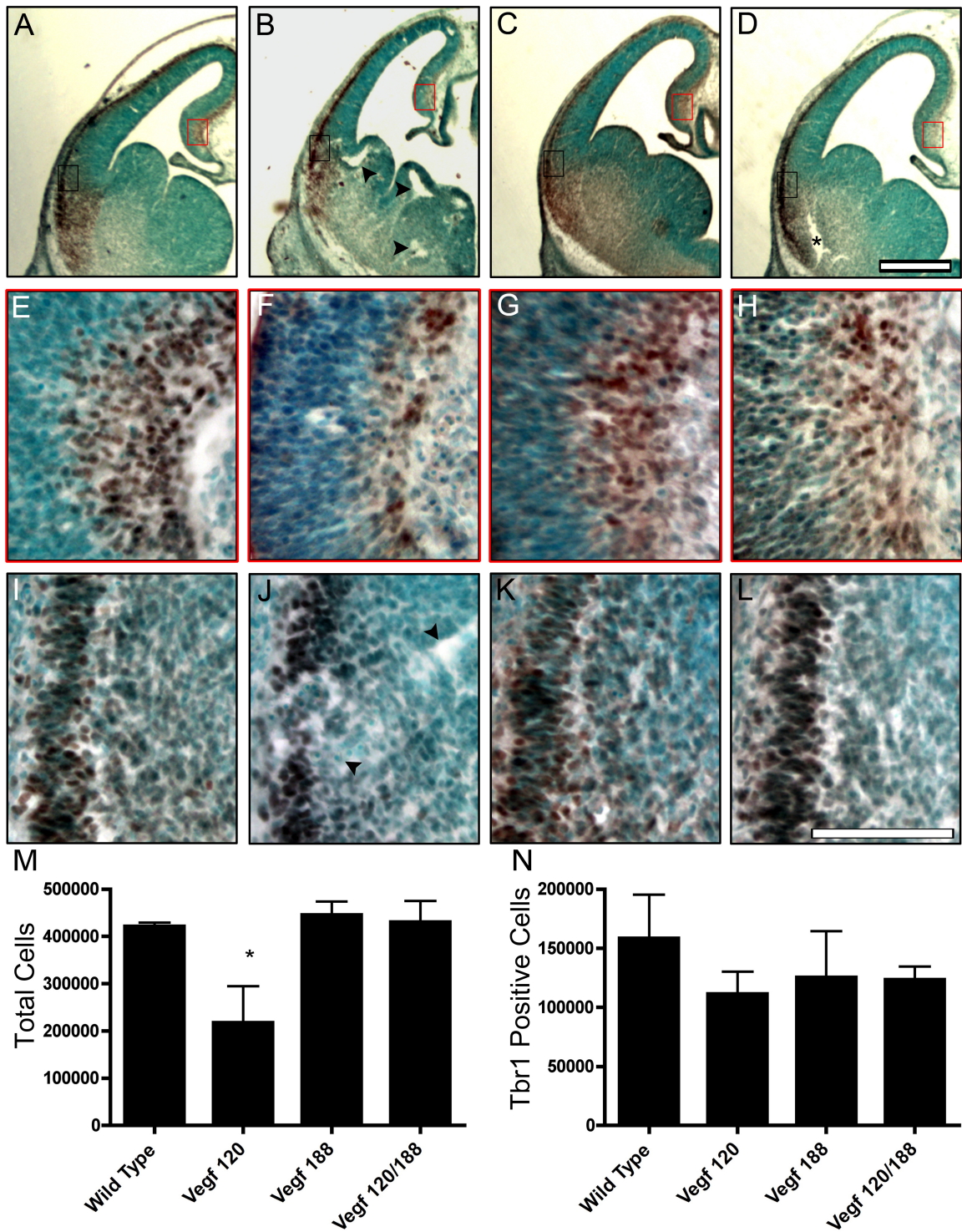


Figure 26. The available Vegf isoform profile does not affect early post-mitotic neuronal differentiation. E13.5 mouse forebrains were immunolabeled with Tbr1, developed with DAB, and counterstained with methyl green.

We surveyed Tbr1 distribution in wild type (A,E,I), Vegf120 (B,F,J), Vegf188 (C,G,K), and Vegf120/188 (D,H,L) forebrains. Low magnification showed that the dispersal of Tbr1 was the same across all genotypes. (A-D, 2x, Scalebar = 125 μ m). Tbr1 staining in the medial pallium (red box, E-H) seemed to be qualitatively lower in the Vegf120 mice compared to the other genotypes. In the subpallium Tbr1 appeared unchanged in the Vegf isoform mice (black box, I-L). At E13.5 the vasculature is well established in the neuroepithelium. Vascular defects associated with the Vegf isoform mice start to manifest, especially in the Vegf120 mice (Arrowheads, the asterisk in panel D shows a tear produced in cryosectioning, and not impaired vasculature). Unbiased quantification by stereology demonstrated that Tbr1 was not significantly different in the Vegf isoform mice compared to wild type (1-way ANOVA, N = 4 per group, p = 0.28). However, there was a significant decrease in the total number of cells in the Vegf120 isoform mice compared to the rest of the groups as determined by a 1-way ANOVA followed by Tukey's post test (P < 0.05).

We counted forebrain sections starting at the most rostral section with the presence of the GE, through the lateral and medial GEs, and stopped at the caudal GE. These counts revealed that there was no difference between the numbers of Tbr-positive nuclei in wild type or Vegf isoform mice as determined by a one-way ANOVA ($n = 4$ per genotype, $p = 0.28$). However, the Vegf120 mice did have significantly fewer total cells than the wild type, Vegf188, and Vegf120/188 mice (one-way ANOVA, Tukey's post test $p < 0.05$). All of the stereological counts had Gundersen confidence estimates less than 0.1 based on the optimal counting and unbiased sampling parameters.

Given the changes that we saw at E11.5 and E13.5 in the proliferating, differentiating, and migrating NSC populations we wanted to determine if there were any overt consequences to early cortical layering. Therefore, we conducted a histological survey at P0, an embryonic time point at which early cortical layers V and VI have been initiated but the boundaries for the upper layers are not yet clearly defined [133]. Analysis of hematoxylin-stained P0 sections revealed marked differences between the wild type and Vegf isoform mice and a representative series is shown (Figure 27). At the caudal-most end of the lateral ventricle, just prior to the emergence of the hippocampus and dentate gyrus, we observed a qualitative reduction in several of the presumptive cortical layers in the Vegf isoform mice compared to wild type. The Vegf120 mice had increased cerebrovascular hemorrhage associated with their decreased vascular integrity and early postnatal lethality as has been previously reported [4, 33, 36].

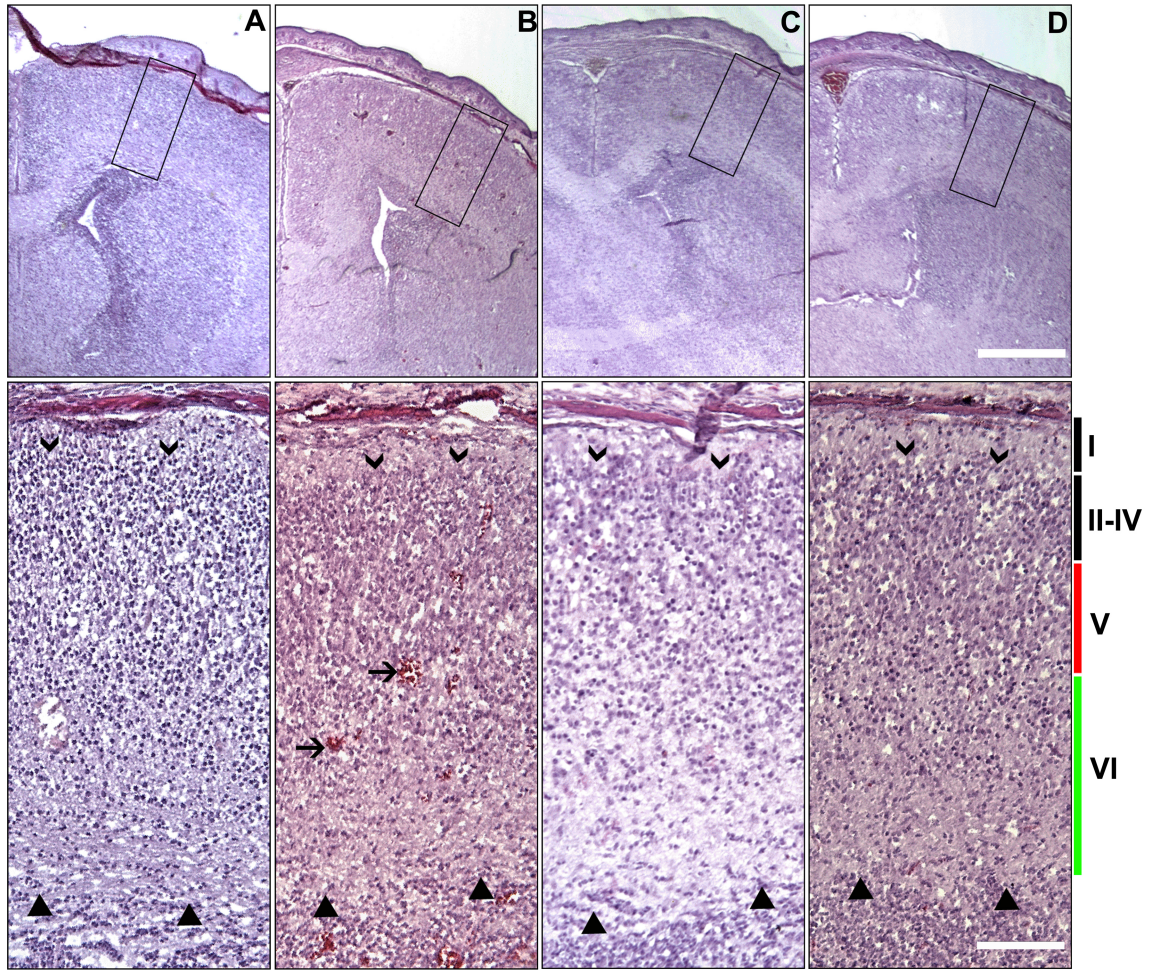


Figure 27. Vegf affects neocortical layering at postnatal day 0. Coronal sections from P0 wild type (A), Vegf120 (B), Vegf188 (C), and Vegf120/188 (D) mice were stained with hematoxylin and eosin. 2x (upper panels) and 10x (lower panels) objectives were used to image the most caudal sections of the lateral ventricle in forebrain before the emergence of the hippocampus and dentate gyrus (scale bars = 750 μ m and 150 μ m respectively). The Vegf120 mice displayed increased cerebrovascular hemorrhaging (Arrows). The beginning of layer VI is marked with triangles, and the start of the presumptive layer 1 is marked with chevrons.

In order to look more specifically at the changes in cortical layering we tracked expression of Tbr1 and Coup-TF interacting protein 2 (Ctip2), factors that have been associated with cell fate choice in upper cortical layers [134, 135]. Since the vascular plexi within the early forebrain are elaborated concomitantly with formation of the cortical layers [136, 137], we also labeled developing vasculature using Lectin (Figure 28, A-D). The Vegf188 and Vegf120/188 isoform mice showed no overt qualitative differences in blood vessel composition compared to the wild type mice. However, the Vegf120 mice displayed abnormal vessels with a distended vessel profile compared to wild type (arrows in Figure 28, B). This vascular phenotype paralleled that of the E13.5 cortical angiogenesis. Tbr1 labeling surrounding the caudal lateral ventricle was qualitatively increased in cortical layers VI and II-IV across the Vegf isoform mice relative to wild type (Figure 28, A-D). By this we refer to the considerably wider distribution of Tbr1-positive cells throughout the developing cortical layers. While positive cells are certainly present in the wild type, the pronounced distribution of the post-mitotic population is notably absent in the wild type. This is strikingly different from the Tbr1-positive distribution of cells at the earlier E13.5 timepoint prior to establishment of the cortical layers.

We further investigated Ctip2-positive cell distribution to assess the impact on upper layer differentiation. Ctip2 immunolabeling, associated with cortical layer V and also expressed in the caudate putamen, had distinct distribution patterns associated with disrupted Vegf isoform expression.

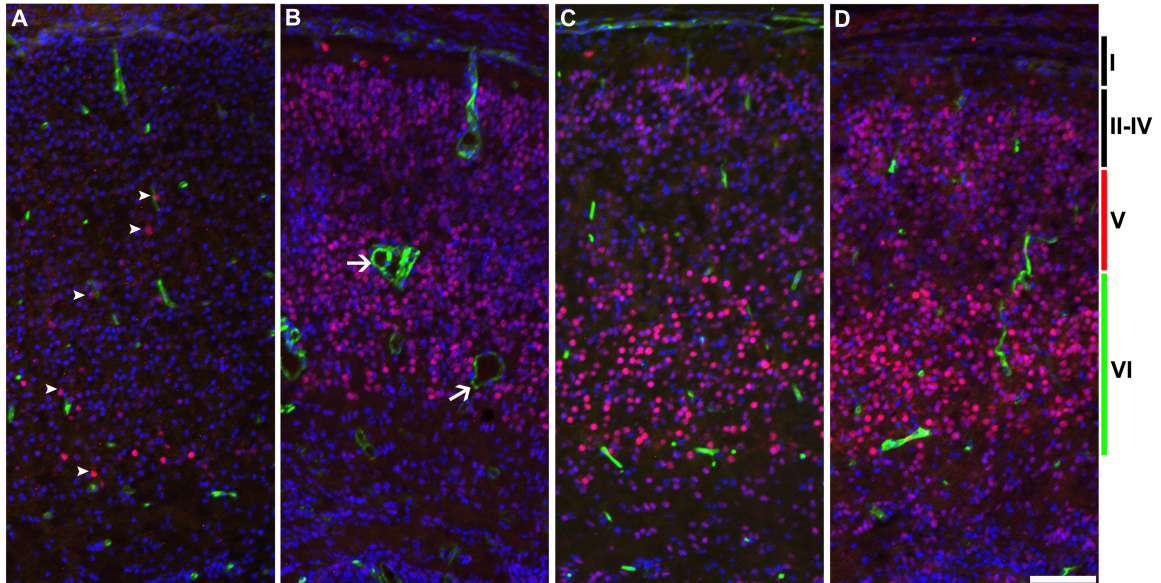


Figure 28. Vegf is required for the differentiation and stratification of Tbr1+ cells. Areas equivalent to those shown in Fig. 6 were labeled with Tbr1 (red), DAPI (blue), and Lectin (green) in wild type (A), Vegf120 (B), Vegf188 (C), and Vegf120/188 (D) P0 mice. The caudal lateral ventricle of the wild type mouse displayed low levels of Tbr1+ cells (arrow heads) in layers V and VI. The Vegf isoform mice showed substantial numbers of Tbr1+ cells scattered throughout the presumptive neocortical layers (II-VI). Lectin labeling of the vasculature showed comparatively normal vessels in the Vegf188 and Vegf120/188 mice compared wild type, but vessels of increased vessel diameter in the Vegf120 isoform mice. (Arrows, scalebar = 125 μ m)

Compared to wild type, a broader region of positive cells was present in the caudate putamen, whose cells eventually contribute to the basal ganglia and receive input from the mature cortex. A comparable band of Ctip2-positive cells was detected in all animals, but the Vegf isoform populations were shifted ventral and medial to the developing cortical layers (chevrons, Figure 29, A-D). Moreover, the distribution of Ctip2-positive nuclei of cortical layer V in the Vegf188 mice was clearly expanded relative to wild type and the other isoform mice. (Figure 29, C). A higher magnification view of the band Ctip2-positive cells reveals that in the presence of the locally-retained Vegf188 isoform, the layer V population is unable to form the distinct layering pattern normally associated with this developmental stage (Figure 30, A-D). The boundaries of the Ctip2 population are highlighted with dashed yellow lines for comparison.

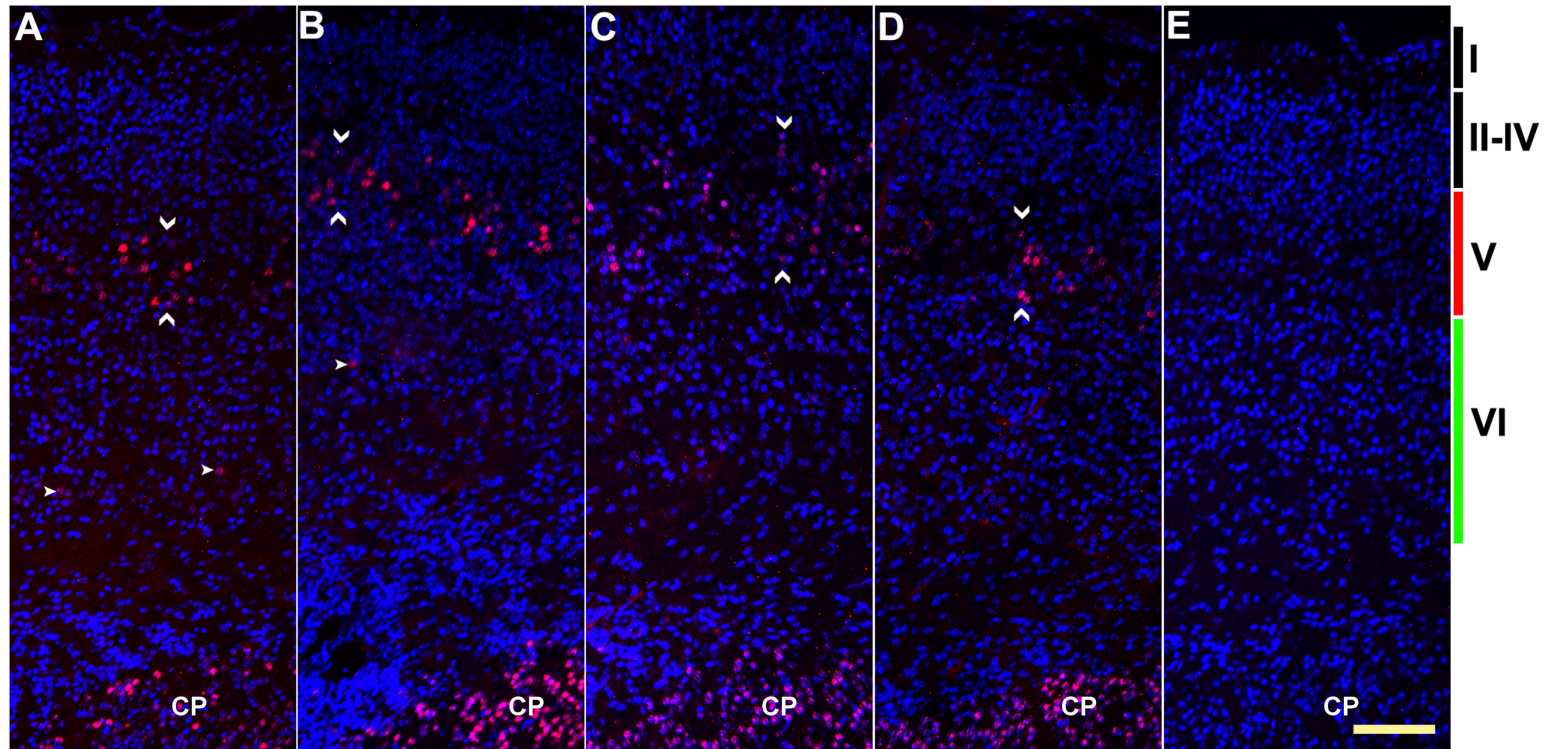


Figure 29. Vegf affects formation of neocortical layer V at P0. Layer V marker Ctip2 (red) and nuclear marker DAPI (blue) are shown at P0 in wild type (A), Vegf120 (B), Vegf188(C), and Vegf120/188 (D). The vertical region is located in the caudal-most sections of the lateral ventricles (areas equivalent to those shown in Figures 26, 27, and 29). Ctip2 was detected in layer V of all the mice with a more dorsal distribution in wider bands detected in the Vegf188 and Vegf120/188 mice (indicated by chevrons).

Several Ctip2-positive cells were detected in layer VI in the wild type and Vegf120 mice (arrowheads). Ctip2 labeling was present throughout the caudate putamen (CP) in all animals. An isotype-matched negative control is shown for comparison (E). (Scalebar = 125 μ m).

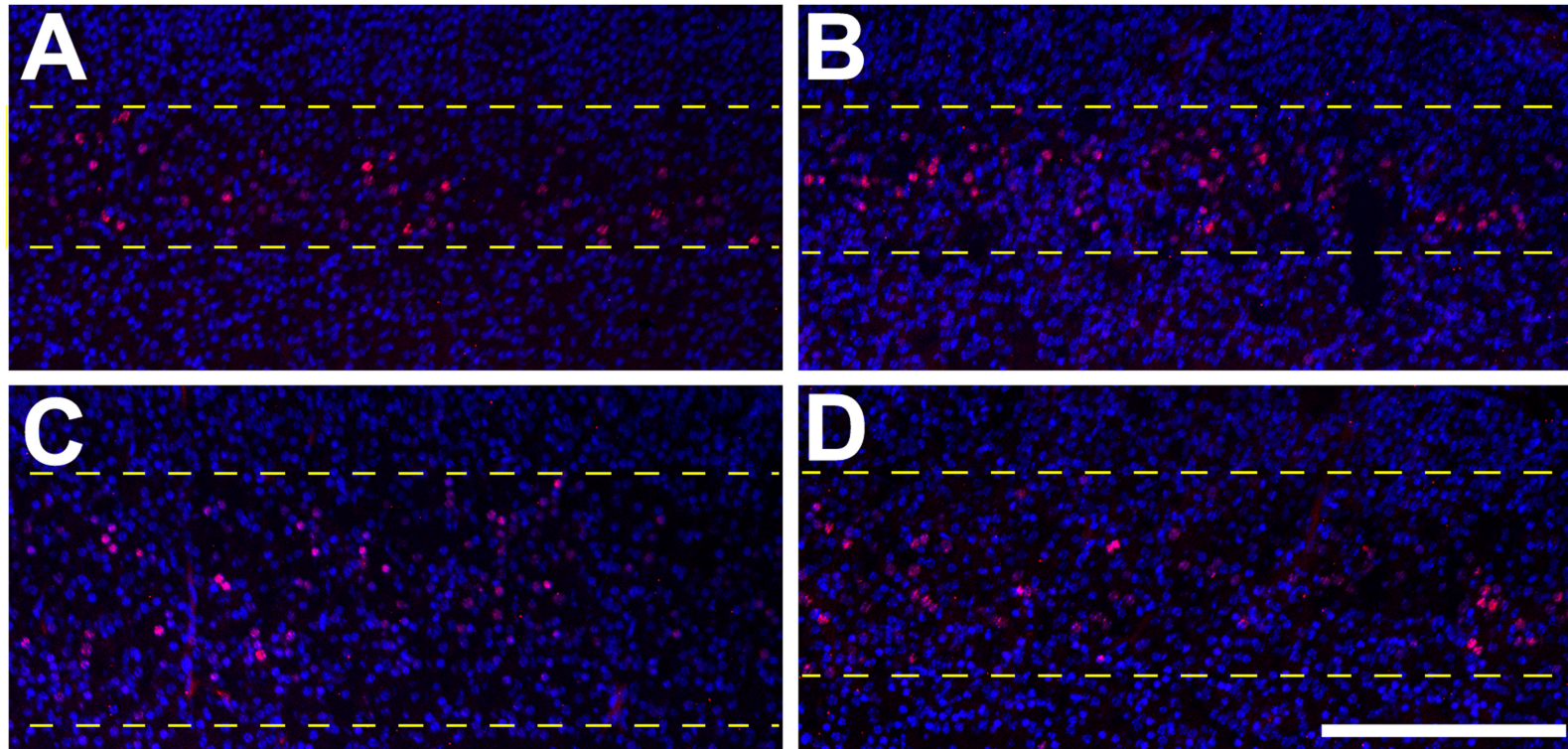


Figure 30. Vegf isoform profile affects the distribution of Ctip2+ cells of neocortical layer V. Sections equivalent to areas shown in Figure 29 were labeled for the layer V marker Ctip2 (red) and nuclear marker DAPI (blue) in wild type (A), Vegf120 (B), Vegf188(C), and Vegf120/188 (D). Ctip2 was detected in layer V of all the mice, however the positive cells occurred in a wider band in the Vegf188 mice (dashed line, Scalebar = 250 μ m).

Chapter IV

Discussion

Our results support the hypothesis that the composition of Vegf isoforms present in the microenvironment of the forebrain contributes to early cortical layering. Vegf and its receptors are expressed at the proper times and places to coordinate the establishment of the vasculature and development of NSCs in the forebrain [6]. We were particularly interested in the E9.5 developmental stage as a crux point for gene expression changes responsible for laying the groundwork for subsequent NSC differentiation and eventual neocortical layering. An advantage of this early time point is that it occurs before extensive vascularization of forebrain neuroepithelium. The blood vessels at the pial surface have not significantly invested the neuroepithelium at E9.5, which, in turn, reduces the confounding vascular variable for interpreting the gene expression results.

Using a transcriptome-wide approach, we were able to identify groups of genes whose expression was dependent upon the available isoform profile. These observed shifts in gene expression could be due to either the localization of Vegf in the ECM microenvironment, or dependent upon Vegf isoform-specific signal transduction cascades associated with differential receptor activation. The distribution of Vegf in the microenvironment is dependent upon the location of the cell producing the Vegf and the type of Vegf isoforms a given cell is making. In the case of the Vegf¹⁸⁸ mice, all of the Vegf that is produced and secreted into the microenvironment is locally retained. Therefore, only cells in close proximity

to the source can respond, unless a truncated form of Vegf188 is released by proteolytic cleavage. In the Vegf120 mice, the diffusible isoform can potentially signal at any distance from the source and reach a completely different set of cells than those in contact with the Vegf188 isoform. These scenarios would potentially affect interpretation of our transcriptome results in that different subsets of cells would be responding to Vegf signaling based on isoform localization and microenvironmental distribution. Furthermore, the Vegf isoforms have differential affinities for their receptors, and in some cases proper signaling is dependent upon ECM and ECM-interacting proteins functioning as co-receptors [138-140]. This outcome is particularly evident with the Vegf120 isoform that lacks exon 6 and 7 and has a much lower affinity for Nrps compared to the Vegf164 and Vegf188 isoforms [138]. Furthermore, VegfR2 binding is enhanced by ECM interactions, giving Vegf164 and Vegf188 isoforms differing affinities for the receptor compared to the Vegf120 isoform [11, 43, 138]. The individual Vegf isoforms have also been shown to activate different cell signaling pathways through the differential phosphorylation of tyrosines on the Vegf receptors [139,140]. Thus, shifts in gene expression patterns in the Vegf isoform mice may be attributable to a combination of several potential mechanisms. Loss of the non-diffusible Vegf isoforms may prevent ECM-mediated Vegf co-receptors from initiating normal signaling pathways, thereby altering NSC fate choice. In addition to differential Vegf isoform affinity for the Vegf receptors, the individual isoforms may initiate distinct cell signaling cascades via alternative phosphorylation of the Vegf receptors [140]. Finally, altered localization of the

non-diffusible isoforms may exclude cells, located at a distance from the source of Vegf, from receiving the Vegf signal. It is certainly feasible that developmental flexibility in terms of microenvironmental availability and receptor signaling for the Vegf isoforms may allow for a combination of mechanisms to modulate cortical development and further fine-tune the lamination process.

The expression shifts detected in the Vegf isoform mice transcriptomes provided evidence that early forebrain neuroepithelium is responsive to altered Vegf bioavailability. The neuroepithelial expression patterns are unique amongst the different Vegf isoform mice, demonstrating that each Vegf isoform has the capacity for eliciting different downstream effects on gene expression. The transcriptome expression patterns in the Vegf120 and Vegf188 mice were unique. The Vegf120/188 mice displayed a transcriptome profile that was a blend of the Vegf120 and Vegf188 expression patterns, rather than a recapitulation of wild type expression. This evidence implies that Vegf120/188 mice are not a rescue of the wild type phenotype, at the transcriptome level, but rather represent a 'loss of function' phenotype with respect to the primary Vegf164 isoform. The Vegf120/188 does rescue the Vegf120 phenotype, in that the Vegf120/188 mice are overtly healthy and viable whereas their Vegf120 counterparts are early post-natally lethal. Therefore, a single allele of Vegf188 codes for sufficient protein to allow cardiovascular development to proceed in these mice.

The microarray results provide evidence that altering Vegf bioavailability in the microenvironment can alter NSC fate decisions. Many of the differentially

expressed genes detected in the meta-array analysis and identified as enriched by DAVID with regard to GO function can be linked directly to processes involved in regulation of cell fate choice and NSC differentiation. Several genes described for their roles in neural tube patterning are changed. For example, both Shh and Bmp4 are well known for their abilities to specify cell fate based on their signaling gradients and distribution in the microenvironment. Genes directly involved in the regulation of NSC proliferation and differentiation were identified in the meta-microarray analysis (i.e Notch, Jag1, Jag2, Id4, Meis2, and Pax6). Pax6, and its enhancer Meis2, are necessary for proper differentiation and stem cell fate choice in the developing forebrain [141]. Lost or reduced expression of Pax6 at this early time point would potentially result in changes in forebrain patterning including establishment of the pallial-subpallial border [142, 143]. Pax6-positive cells shift their expression profile to become Tbr2-positive cells as they differentiate and migrate away from the ventricular zone. These cells, in turn, express other markers of differentiation as they concomitantly migrate and stratify into the six layers of the neocortex. One such example is the differentiation of Tbr1-positive cells, at E12.5-13.5, and their subsequent migration into layer VI [55].

Neurog2 is important in the differentiation of neurons and its developmental expression is regulated by Pax6 [144]. Both Neurog2 and Dlx2 contribute to NSC fate choice and interact through Notch signaling [145, 146]. Reduced Pax6 expression results in early exit from the cell cycle, which in turn results in a decrease number of upper layer neurons [147, 148]. Shifts in

expression of Pax6, Neurog2, and Dlx2 detected at E9.5 provide evidence that the early NSC populations are vulnerable to changes in the Vegf isoform profile with regard to their cell fate decisions. Any factor affecting these early stepwise NSC fate decisions would have adverse consequences on subsequent neocortical layering.

A predicted protein interaction network, generated with the Search Tool for the Retrieval of Interacting Genes (STRING 9.0; Figure 31) and using genes mined by DAVID clustering as well as several other genes of interest (Vegf, VegfR1, VegfR2, Tbr1, and Tbr2), provided an additional platform to identify potential pathways downstream of Vegf isoform mediated changes related to neocortical development. Gene links were identified that were functionally associated with epigenetic modification, cell migration, NSC specification, and fate choice. The STRING network linked Vegf and its receptors to factors essential to forebrain patterning and specification, Bmp4 and Shh [149, 150]. Id1 and Id4, effectors of Bmp4-mediated inhibition of NSC differentiation, are also networked with Vegf [151]. The STRING network demonstrated a potential role for Vegf as a bridging factor in neurovascular development by linking several factors important to both vascular patterning and neural development, such as Notch3, Hey2, and Nrp1/2. Nrp1 is well described for its role in neurovascular patterning by acting as a co-receptor for Vegf as well as semaphorins [152]. Vegf is linked to the Notch signaling pathway, which has been shown to contribute to the maintenance of the stem cell pool, as well as, to direct angiogenesis [153, 154].

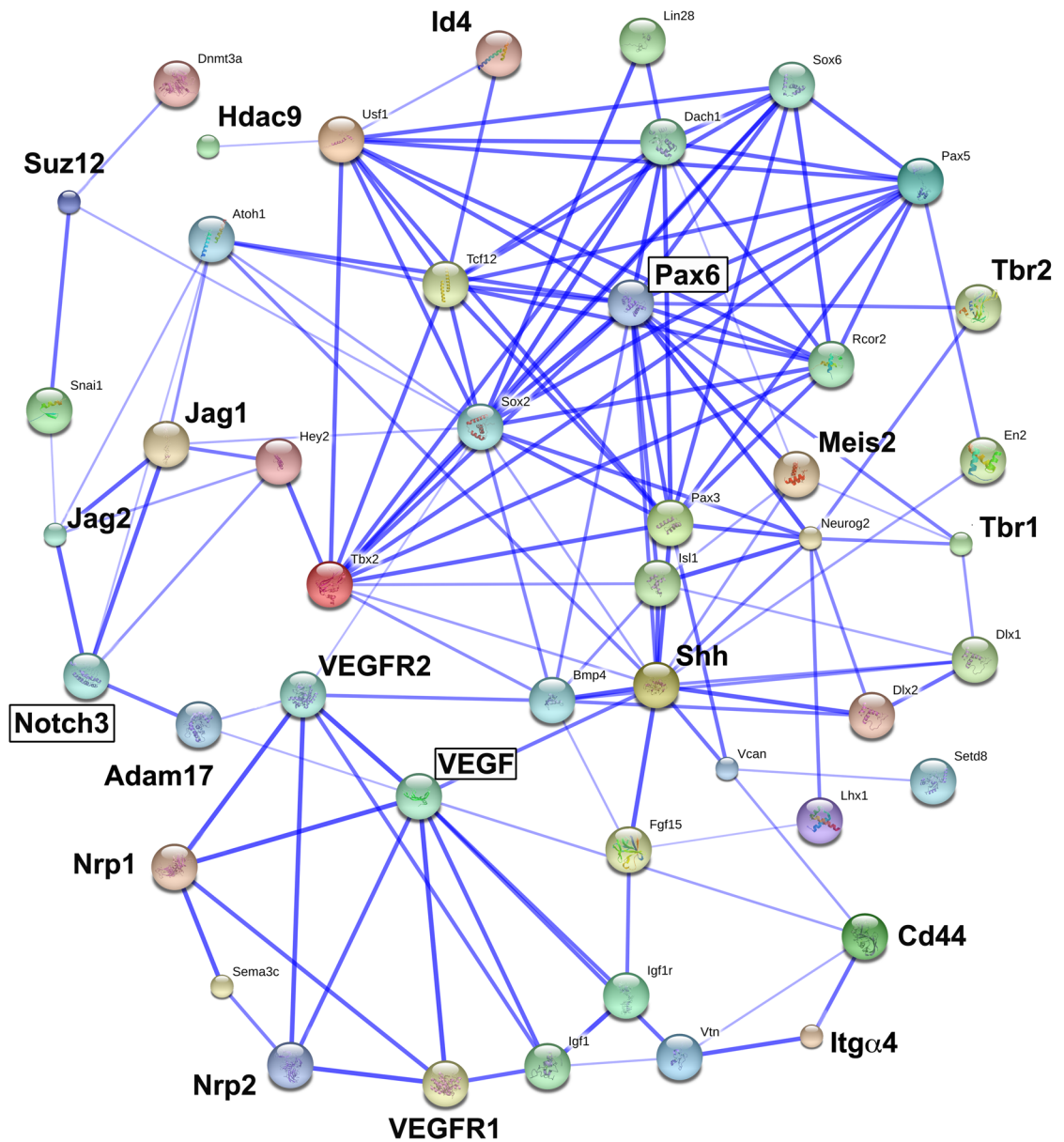


Figure 31. Predicted protein interactions network with a subset of differentially expressed genes identified in the Vegf isoform mice. We used the Search Tool for the Retrieval of Interacting Genes/Proteins (STRING) to generate evidence-based links between and among genes identified from DAVID analysis of the top enriched gene clusters. Gene acronyms were incorporated into STRING using default settings. The components in this STRING model were simplified from a network originally constructed from genes listed in Table

IV. Blue lines indicated direct evidence linking proteins with the thickness of the line reflecting confidence of interactions based upon the number of database links. The lengths of the lines, the color and size of the nodes have no significance in this schematic. To aid in network building, we incorporated five additional genes into the STRING model: Tbr1 Tbr2/Eomes, Flt1/VegfR1, Kdr/VegfR2, and the VegfA (Vegf). Genes of particular interest are indicated with larger font with Notch 3, Pax6, and Vegf genes boxed to highlight their key position within the evidence network. The STRING networks link genes shifted in the Vegf isoform mice with Vegf and its receptors, providing new directions for study involving Vegf regulation of cell fate choice. Potential effectors for modifying epigenetic regulation of gene expression, HDAC9, Suz12, Dmnt3a, and Setd8, were networked to Vegf through Notch3 or Shh. Pax6, in the center of a complex node cluster, linked to Vegf indirectly through Notch3 and Shh, as well.

STRING links were also made between Vegf and epigenetic regulators of gene expression, Hdac9, Dnmt3a, Setd8, and Suz12. These latter connections are critical for future investigations as methylation and histone modification of DNA have been implicated in cell fate regulation during the transition from NSC toward differentiated lineages [155].

Taken together, our transcriptomic data analyses lend supporting evidence linking an altered pattern of Vegf isoform expression to a shift in NSC specification and determination with consequences for early neocortex formation. The collection of genes and gene networks identified here can be used to further elucidate the mechanisms that coordinate the development of the NSC and the vasculature in the neocortex.

Relative to the E9.5 wild type gene panel, many of the genes shifted in the E11.5 wild type microarrays were also shifted in the same direction in the E9.5 Vegf isoform arrays. One interpretation of this observation is that normal Vegf isoform expression is responsible for coordinating proper timing of NSC expansion and differentiation, and that altering the Vegf isoform profile leads to precocious gene expression changes resulting in altered cortical layering. Expansion and eventual stratification of the early neuroepithelium into a six-layered neocortex is dependent upon the proper balance of NSC fate choices. We have shown that Vegf120 mice have reduced neuroepithelial volume and total cell number with unaltered Tbr2-positive populations [6] with the implication that non-diffusible Vegf isoforms are necessary to maintain NSC proliferation. When examined, the Vegf188 and Vegf120/188 mice had statistically equivalent

levels of PHH3-positive cells compared to wild type in agreement with the idea that a localized source of Vegf may be necessary for maintenance of NSC proliferation. The Vegf188 forebrain had reduced numbers of Tbr2-positive cells, the loss of which may be correlated with the reduced expression of Pax6 in the Vegf isoform mice. The Pax6-positive cells contribute directly to the genesis of Tbr2-positive intermediate progenitors, so a reduced Pax6-positive population would have significant consequences for intermediate progenitor cells and subsequent neural differentiation[148]. The reduction in Tbr2-positive cells in the Vegf188 mice may also represent a failure of Pax6-positive neural stem cells to differentiate into Tbr2-positive intermediate progenitors, or an early departure of the Tbr2-positive intermediate progenitor population down a further differentiated cell fate choice (i.e. Tbr1-positive). Interestingly, the fact that the Vegf120/188 mice resembled wild type mice with regard to numbers of PHH3- or Tbr2-positive cells may indicate that the presence of both diffusible and locally-retained Vegf isoforms may act as a functional rescue in animals lacking the Vegf164 isoform. However, the evidence for the Vegf120/188 mice as a rescue animal may not be that clear cut, given that the Vegf120/188 mice showed the largest numbers of altered genes in the microarray compared to the E9.5 wild types. In effect, the gene expression similarities of the Vegf120/188 isoform mice compared to the Vegf120 and Vegf188 mice may reflect a level of phenotypic plasticity in the Vegf120/188 mice that shift expression in an effort to develop the normal forebrain structure in the absence of Vegf164.

Changing the microenvironmental localization of Vegf, by altering the available Vegf isoform profile, should hypothetically affect Vegf's ability to serve as a migratory cue. Supporting this idea of Vegf misexpression altering migration pathways is our microarray data that identified several migration-related factors, Dlx1, Dlx2, and CXCR4, as differentially expressed in the Vegf isoform mice compared to wild type. Knock-out mice for these genes have demonstrated significant changes in interneuron migration and neocortical lamination in the developing mouse forebrain [156-158]. Stereological counts of the forebrain distribution of Calb1-positive, migratory interneurons at E11.5 demonstrated that Calb1-positive cell localization within the forebrain was dependent upon the available Vegf isoform profile. Changes in the Vegf isoform mice neocortices at P0 also give weight to this idea of Vegf orchestration of early neuron migration and final laminar localization. Hematoxylin and eosin staining of coronal P0 sections showed an altered laminar organization in the Vegf mice. Corroborating this observation, was the immunolabeling of Ctip2-positive cells and their distribution within layer V. Ctip2 positive cells are spread across a much broader area in the Vegf188 and Vegf120/188 mice, implying a role for Vegf in the establishment of layers in the neocortex by influencing the migration and final localization of post mitotic neurons.

Proper cortical development is dependent upon the proper timing of post-mitotic neuronal differentiation and their subsequent migration. Since layers of the cortex are formed from the inside out, the deeper cortical neurons of layers V and VI, are born first. Most of the neurons of these deep layers are born

between E12.5 and E14.5 [159]. Given our data, we hypothesized that alterations in Vegf isoform availability would affect the differentiation and migration of early Tbr1-positive, post-mitotic neurons. However, at E13.5 we found no changes in the distribution or quantities of Tbr1-positive cells in the forebrain, suggesting that Vegf does not have a direct effect on their ability to differentiate. However, when we looked at the distribution of Tbr1-positive cells at P0 we found that the distribution of Tbr1-positive cells in the Vegf isoform mice was vastly expanded compared to wild type. At P0, Tbr1-positive cells are mostly restricted to layer VI in wild type, with minimal expression in layers II/III. Tbr1-positive cells are generally not well established in layers II/III until P3 [160]. However, the Vegf isoform mice did have significant numbers of Tbr1-positive cells in layers II/III at P0, many more than their wild type counterparts. These data, taken together, imply that an altered Vegf isoform profile does not hinder the differentiation of these Tbr1-positive, post-mitotic neurons; however, Vegf bioavailability may affect the timing of their differentiation, migration, and final localization.

The role of Vegf in the coordination of neurovascular development is complex. Vegf and its receptors are expressed by both neuronal and vascular cell types during cortical development, and many of Vegf's downstream effectors have been shown to play a role in both angiogenesis and neurogenesis. Observing the direct effects of Vegf is often confounded by potential indirect effects caused by the impaired vasculature. However, despite these difficulties it is clear that Vegf plays an important role in the development of cortex. By

looking early on in development, we minimized indirect effects and identified Vegf isoform specific shifts in the expression of genes important to NSC differentiation independent of any vascular compromise. We were able to demonstrate that despite any of the vascular abnormalities in the Vegf isoform mice, changes in the Vegf isoform profile did not stop the proliferation, differentiation, or the migration of NSCs. The Vegf isoform mice were still able to proliferate NSCs, although reduced in the Vegf120 mice, produce both intermediate progenitors and post-mitotic neurons, and in the cases of the Vegf188 and Vegf120/188 mice, they are completely viable. Our findings imply that the Vegf isoforms serve to guide and fine tune NSC development by mediating the balance and timing of their proliferation, differentiation, migration, and final localization.

Evolution of the cortex, specifically the neocortex, is the pinnacle of mammalian development. It is a highly integrative information-processing organ, which takes sensory input and translates it into learning, memory, thought, and consciousness in general. The complex cellular histology responsible for its function is dependent on precise coordination of NSC proliferation, differentiation, and migration as well as vascular integration. Defects in any of these processes can have severe consequences for cortical development. For example, neuronal migration defects can result in developmental disorders such as lissencephaly, wherein the sulci and gyri of the brain fail to form. Furthermore, injuries to the cortex can have severe consequences in behavior, learning, and motor functions. Until recently, the dogma was that injury to the nervous system was irreparable in mammals, as it was thought there were no pluripotent cell populations in the

mature CNS capable of healing the tissue and replacing the damaged cells. However, with discovery adult neural stem cells in the subventricular zones of the cortex and subgranular zones of the dentate gyrus, healing injuries in the cortex might not be as impossible as previously thought.

In the adult, NSCs have been found in vascular niches associated with capillaries. It is thought the growth factors released from the endothelial cells of the blood vessels help maintain these adult NSC populations, and that stimulation from growth factors, like Vegf binding to VegfR2, can activate proliferation and differentiation of these adult NSCs (reviewed in [2]). Vegf is in place to serve as a mediator of NSC/endothelial cell crosstalk in the adult NSC niche, and understanding Vegf's role in mediating NSC proliferation, migration, and differentiation during development will be key to finding potential Vegf-mediated therapies in the recovery of CNS injury.

Appendix

Table I. PCR primers used to genotype Vegf isoform mice. In order to genotype wild type, Vegf isoform heterozygote and Vegf isoform homozygotes we use two sets, of primers, one set specific to the Vegf188 allele and the other specific to the Vegf120 allele. Each set contains one forward primer (common to both the wild type and Vegf allele) and two reverse primers. Of the two reverse primers one is specific to the wild type Vegf allele and the other is specific to the Vegf isoform allele. Since the Vegf188 allele was made from a single cDNA and the Vegf120 allele has exons 6 and 7 removed, the amplicon resulting from the common forward primer and the Vegf isoform specific primer is shorter than the wild type amplicon. In a reaction with the presence of the wild type allele a 400 bp band is formed, and in the presence of the Vegf isoform allele a 300 bp band is formed. In this way, wild types can be identified by the presence of a single 400 bp band, Vegf homozygotes by the presence of a single 300 bp band, and heterozygotes have both a 400 bp and a 300 bp band. In order to identify, Vegf120/188 heterozygotes both a Vegf120 and Vegf188 reactions must be run. In the Vegf120 reaction the Vegf120/188 mouse appears as a single 300 bp band, but in the Vegf188 mouse both a 300bp and 400bp band is present. The 400 bp band in the Vegf188 reaction is because the forward Vegf188 primer can bind both the Vegf188 and Vegf120 allele.

Primer	Sequence 5'-3'	120 band	188 band
Vegf120_For	CAGTCTATTGCCTCCTGACCTTCAGGGTC		
Vegf120_END_Rev	TTCAGAGCGGAGAAAGCATTGTGGTCCA	300bp	NA
Vegf120_Rev	CTTGCGTCCACACCGTCACATTAAGTCAC	400bp	NA
Vegf188_For	GATCAAACCTCACCAAAGCCAGCACATAG		
Vegf188_END_Rev	GTGGGTAGAGAAAAGAAGAGAAAACAAG	NA	300bp
Vegf188_Rev	TTGTCACATCTGCAAGTACGTTCTTAAC	400bp	400bp

Table II. Primer pairs used in qPCR analysis.

Name	Forward 5' -> 3'	Reverse 5' -> 3'	Refseq ID
Gapdh	GTGGCAAAGTGGTTGCC	GATGATGACTTTGGCTCC	NM_008084.2
Nrp1	TCAGGACCATACAGGAGATGG	TGACATCCCATTGTGCCAAC	NM_008737.2
Nrp2	AGACTACCACCCCATATCCCATGG	CTGCCCTGGTCTCACGGAT G	NM_001077403.1
Id1	AGCAAAGCGTGGCCATCTC	AGGACGTTACCTGCTC	NM_010495.2
Pax6	GCTTGGTGGTGTCTTTGTCA	TTTGCATCTGCATGGGTCT	NM_013627.3
Pax3	TTGTCCCCCACCTATAGCA	TTCCCCGTTCTCAAGCAAGA	NM_001159520.1
Cxcr7	AAGCCCTGAGGTCACTTGGTC	CAAACAAGTGCACATCCATGG	NM_001271607.1
Cxcl12	CCGCGCTCTGCATCAG	TGGCTCTCGAAGAACCGG	NM_001012477.2
Foxm1	GGAGACGTTGGGACCGAAG	CGCCRCACCACCAGCATAG	NM_008021.4
Zfx1b	AGGCATATGGTGACGCACAA	CTTGAACCTGCGGTTACCTGC	NM_015753.3
Lama4	AACTACAGGCAGCAGAGAGAGGG	AGCCGCTGTCGTCTTGTTAG	NM_010681.4
Lama5	TCCCCTACTGTGAAGCTGGC	CCAGTACCCAGGTTTACAGCG A	NM_001081171.2
Lamc3	CCCCAGAGTGCTCCAGTCTTA	GCCGTGACCATTGCATTTG	NM_011836.3
18s	GACAGCGACAGGATTGACAGATTG ATAG	GTTAGCATGCCAGAGTCTCGT TCGTT	NR_003278.3
Notch3	ACACTGGGAGTTCTCTGT	GTCTGCTGGCATGGGATA	NM_008716.2
Shh	TGTCATCGAGGAGCACAGCT	AGCTGGACTTGACCGCCATT	NM_009170.3
Suz12	AAAGGAAGGATGTAAGTTGTCCA	CGAGTAGGACTTCACCATATG G	NM_001163018.1
Fezf2	GCAAGGTGTTCAATGCTCAC	GGTGAGCTTGTGATTCTTGTA G	NM_080433.3
Hey2	GCATCCGAAGAGCAGAATCTG	GCTACTTTGATGCCATGC	NM_013904.1
Dnmt3a	CCGGTGGAAAGCAGTGACA	GGTGAGTCTTGGCATGGGTC	NM_007872.4
Vegf120	GCCAGCACATAGGAGAGATGAGC	CGGCTTGTCACATTTTCTGG	NM_001025257.3
Vegf164	GCCAGCACATAGGAGAGATGAGC	CAAGGCTCACAGTGATTTTCT GG	NM_009505.4
Vegf188	GCCAGCACATAGGAGAGATGAGC	AACAAGGCTCACAGTGAACGC T	NM_001025250.3

Table III. Differentially-expressed genes in E9.5 forebrain of Vegf isoform mice compared to wild type (WT). The 281 genes identified are presented in the heat map in Figure 1. The Fold Change value is derived by subtracting the log2 mean of the wild type signal from the Vegf isoform signal for mice expressing only Vegf120, Vegf188, or a combination of Vegf120/188. The t test p-value was determined from the batch normalized, Log2 transformed values from the array pre-filtered by a group ANOVA ($p < 0.05$) and a fold-change greater than 0.5 relative to the wild type.

Heat Map Order	Probe Set ID	Gene Title	Gene Symbol	t test Vegf120 v WT	Fold Change Vegf120	t test Vegf188 v WT	Fold Change Vegf188	t test Vegf120/188 v WT	Fold Change Vegf120/188
1	1436973_at	chaperonin subunit 8 (theta)	Cct8	0.0449	-0.4935	0.0244	-0.5402	0.0198	-0.6690
2	1430205_a_at	cell division cycle 37 homolog (S. cerevisiae)-like 1	Cdc3711	0.0258	-0.6327	0.0187	-0.4908	0.0026	-0.6023
3	1431031_at	AT rich interactive domain 4B (Rbp1 like)	Arid4b	0.0768	-0.5423	0.0931	-0.5441	0.0102	-0.9794
4	1425457_a_at	growth factor receptor bound protein 10	Grb10	0.0667	-0.5243	0.0502	-0.5453	0.0162	-0.8918
5	1415893_at	sphingosine phosphate lyase 1	Sgpl1	0.0442	-0.5629	0.0199	-0.6277	0.0038	-1.0302
6	1421582_a_at	cAMP responsive element binding protein 1	Creb1	0.0059	-0.7293	0.0201	-0.4532	0.0043	-0.8094
7	1451805_at	pleckstrin homology domain interacting protein	Phip	0.0155	-0.6308	0.2106	-0.2221	0.0205	-0.6083
8	1443229_at	ATPase family, AAA domain containing 2	Atad2	0.0168	-0.7576	0.0033	-0.6714	0.0015	-0.8735
9	1416124_at	cyclin D2	Ccnd2	0.0062	-0.6994	0.0284	-0.4201	0.0044	-0.6939
10	1420856_a_at	LanC (bacterial lantibiotic synthetase component C)-like 2 /// similar to testis-specific adriamycin sensitivity protein	Lancl2 /// LOC100045439	0.0222	-0.6942	0.0539	-0.4032	0.0302	-0.7472
11	1431096_at	integrator complex subunit 8	Ints8	0.0171	-0.6160	0.0390	-0.4099	0.0177	-0.6200
12	1416019_at	down-regulator of transcription 1	Dr1	0.0154	-0.5547	0.1050	-0.3441	0.0199	-0.6278
13	1453683_a_at	centrosomal protein 55	Cep55	0.0543	-0.6458	0.0753	-0.3713	0.0047	-0.7739

Table III,
Con't

14	1448955_s_at	Ca ²⁺ -dependent activator protein for secretion	Cadps	0.1346	-0.4617	0.1544	-0.4323	0.0401	-0.9604
15	1439127_at	expressed sequence AI314180	AI314180	0.1889	-0.2804	0.2679	-0.2407	0.0292	-0.6307
16	1439737_x_at	Mediator of RNA polymerase II transcription, subunit 6 homolog (yeast)	Med6	0.1162	-0.4537	0.2018	-0.3550	0.0113	-0.9491
17	1452489_at	vacuolar protein sorting 11 (yeast)	Vps11	0.2557	-1.7498	0.3467	-1.4185	0.0243	-4.7713
18	1424022_at	oxidative stress induced growth inhibitor 1	Osgin1	0.1944	-0.6183	0.2761	-0.5076	0.0147	-1.6527
19	1440542_at	RIKEN cDNA 7420416P09 gene	7420416P09Rik	0.2711	-2.5684	0.2397	-2.7516	0.0150	-8.1190
20	1455472_at	RIKEN cDNA A630071D13 gene	A630071D13Rik	0.0517	-0.4066	0.1760	-0.2871	0.0302	-0.5945
21	1438535_at	pleckstrin homology domain interacting protein	Phip	0.1290	-0.3772	0.0718	-0.2832	0.0080	-0.6421
22	1452772_at	tankyrase, TRF1-interacting ankyrin-related ADP-ribose polymerase 2	Tnks2	0.1314	-0.3437	0.2206	-0.2503	0.0217	-0.6322
23	1425650_at	transducin-like enhancer of split 4, homolog of Drosophila E(spl)	Tle4	0.0164	-0.3976	0.0033	-0.4774	0.0302	-0.6241
24	1429502_at	stress 70 protein chaperone, microsome-associated, human homolog	Stch	0.0230	-0.4930	0.0880	-0.3253	0.0460	-0.6231
25	1434474_at	ATP-binding cassette, sub-family A (ABC1), member 5	Abca5	0.0301	-0.6045	0.0569	-0.3678	0.0261	-0.8595
26	1450075_at	polymerase (DNA directed), eta (RAD 30 related)	Polh	0.0850	-0.5150	0.0371	-0.5955	0.0543	-0.6690
27	1447837_x_at	polymerase (DNA directed), eta (RAD 30 related)	Polh	0.0003	-0.6460	0.0002	-0.6265	0.0005	-0.6811
28	1449306_at	heat shock factor 2	Hsf2	0.1176	-0.3969	0.0457	-0.5271	0.0463	-0.5947
29	1416053_at	leucine rich repeat protein 1, neuronal	Lrrn1	0.2604	-0.2743	0.0147	-0.6594	0.0249	-0.6711
30	1458379_at	RIKEN cDNA 9330159F19 gene	9330159F19Rik	0.1207	-0.2356	0.0016	-0.6482	0.0095	-0.4544
31	1418271_at	basic helix-loop-helix domain containing, class B5	Bhlhb5	0.1917	-0.3469	0.0197	-0.6845	0.0785	-0.5750
32	1429138_at	neuronal PAS domain protein 3	Npas3	0.3388	-0.2116	0.0431	-0.5378	0.0278	-0.6281
33	1447605_at	Adult pancreas islet cells cDNA, RIKEN full-length enriched library, clone:C820020L02 product:unclassifiable, full insert sequence	---	0.2066	-0.1886	0.0049	-0.6052	0.0357	-0.4821
34	1425877_at	hyaluronoglucosaminidase 3	Hyal3	0.0648	-0.2540	0.0008	-0.5891	0.0537	-0.5387
35	1438828_at	Rap guanine nucleotide exchange factor (GEF) 6	Rapgef6	0.2408	-0.2255	0.0259	-0.6149	0.0040	-0.5439

Table III,
Con't

36	1441540_at	Nuclear receptor coactivator 7	Ncoa7	0.7409	-0.0591	0.0049	-0.8838	0.0078	-0.5794
37	1460612_at	RAN binding protein 3	Ranbp3	0.0426	-1.0599	0.0107	-1.4248	0.1214	-0.7846
38	1421138_a_at	protein kinase inhibitor beta, cAMP dependent, testis specific	Pkib	0.0823	-0.4881	0.0095	-0.9664	0.0733	-0.5450
39	1437259_at	solute carrier family 9 (sodium/hydrogen exchanger), member 2	Slc9a2	0.2954	-0.1826	0.0151	-0.5972	0.0240	-0.4606
40	1448458_at	topoisomerase (DNA) II beta	Top2b	0.0784	-0.3571	0.0055	-0.8869	0.0194	-0.7107
41	1453921_at	RIKEN cDNA 4930429F11 gene	4930429F11Rik	0.0238	-0.7223	0.0457	-0.7698	0.0304	-1.0059
42	1444749_at	Adult male hippocampus cDNA, RIKEN full-length enriched library, clone:C630010M09 product:unclassifiable, full insert sequence	---	0.6607	-0.0775	0.0169	-0.9086	0.0516	-0.4274
43	1427715_a_at	5'-nucleotidase, cytosolic IB	Nt5c1b	0.9117	-0.0192	0.0350	-0.6668	0.5181	-0.1315
44	1425574_at	Eph receptor A3	Epha3	0.5210	0.1968	0.0166	-1.1143	0.0104	-0.5875
45	1453791_at	RIKEN cDNA C130071C03 gene	C130071C03Rik	0.6690	0.2135	0.0392	-1.5736	0.0340	-0.9620
46	1423011_at	ecotropic viral integration site 1	Evi1	0.3112	0.2236	0.0450	-0.7296	0.2298	-0.2659
47	1418790_at	Fez family zinc finger 2	Fezf2	0.3110	0.3041	0.0031	-1.3764	0.0241	-0.6360
48	1441161_at	RIKEN cDNA B230216G23 gene	B230216G23Rik	0.0035	-0.6305	0.0117	-0.5347	0.0035	-0.4743
49	1450940_at	ganglioside-induced differentiation-associated-protein 1	Gdap1	0.1164	-0.5696	0.0052	-1.1448	0.0543	-0.6996
50	1446064_at	---	---	0.0617	-0.5154	0.0255	-0.9449	0.0817	-0.5161
51	1440079_at	RIKEN cDNA 3632454L22 gene	3632454L22Rik	0.1318	-0.4100	0.0226	-0.7500	0.2925	-0.3083
52	1439843_at	calcium/calmodulin-dependent protein kinase IV	Camk4	0.9278	-0.0208	0.0089	-0.8941	0.0663	-0.3315
53	1449939_s_at	delta-like 1 homolog (Drosophila)	Dll1	0.0397	0.6619	0.0807	-0.5542	0.4457	-0.2281
54	1422734_a_at	myeloblastosis oncogene	Myb	0.9507	-0.0096	0.0164	-0.6173	0.0493	-0.5480
55	1454720_at	amyloid beta (A4) precursor protein-binding, family A, member 3 /// heparan sulfate (glucosamine) 3-O-sulfotransferase 5	Apba3 /// Hs3st5	0.2044	0.2692	0.0367	-1.1111	0.0365	-0.3814
56	1427265_at	breakpoint cluster region homolog	Bcr	0.9107	-0.0219	0.0156	-0.9019	0.0824	-0.3581

Table III,
Con't

57	1448766_at	gap junction membrane channel protein beta 1	Gjb1	0.9582	-0.0243	0.0493	-4.4178	0.0146	-1.7547
58	1451443_at	nuclear factor I/X	Nfix	0.7630	0.1971	0.0147	-5.5429	0.0148	-1.9040
59	1458503_at	B-cell CLL/lymphoma 7A	Bcl7a	0.0026	0.7139	0.1593	-0.8457	0.4689	0.1512
60	1452624_at	leucine rich repeat transmembrane neuronal 1	Lrrtm1	0.3311	-0.1414	0.0117	-1.1597	0.0021	-0.5618
61	1417614_at	creatine kinase, muscle	Ckm	0.5933	0.0856	0.0415	-0.7682	0.1528	-0.2572
62	1458323_at	hypothetical protein LOC73980	LOC73980	0.0575	0.4552	0.0250	-1.0325	0.8204	-0.0542
63	1431892_a_at	phospholipase C, delta 3	Plcd3	0.8860	-0.0189	0.0238	-0.7160	0.0518	-0.3675
64	1422137_at	dual oxidase maturation factor 2	Duoxa2	0.1341	0.3593	0.0446	-0.5904	0.3393	-0.1291
65	1440327_at	expressed sequence AI195470	AI195470	0.8018	-0.0495	0.0184	-1.1394	0.0851	-0.4078
66	1436672_at	CDNA clone IMAGE:5720309	---	0.0384	0.5842	0.0251	-0.7811	0.3719	-0.2869
67	1454485_at	RIKEN cDNA 4930456G14 gene	4930456G14Rik	0.6522	0.1370	0.0424	-0.8185	0.9863	-0.0061
68	1426607_at	predicted gene, EG633640	EG633640	0.5621	0.2528	0.0050	-1.1985	0.4271	-0.2800
69	1416149_at	oligodendrocyte transcription factor 1	Olig1	0.8290	-0.0667	0.0024	-0.7563	0.0213	-0.5333
70	1417760_at	nuclear receptor subfamily 0, group B, member 1	Nr0b1	0.5810	0.1421	0.0079	-0.6796	0.7132	-0.0796
71	1422643_at	monooxygenase, DBH-like 1	Moxd1	0.8996	-0.0259	0.0038	-0.6534	0.3886	-0.1749
72	1429452_x_at	RIKEN cDNA 4933439C20 gene	4933439C20Rik	0.8380	-0.1244	0.0001	-2.0554	0.0002	-1.3444
73	1426387_x_at	RIKEN cDNA 4933439C20 gene /// phosphatidylserine decarboxylase pseudogene /// phosphatidylserine decarboxylase /// hypothetical protein LOC100044151	4933439C20Rik /// LOC100044151	0.8190	-0.0350	0.0001	-0.6442	0.0004	-0.4635
74	1434975_x_at	RIKEN cDNA 4933439C20 gene	4933439C20Rik	0.4412	-0.1594	0.0000	-1.0222	0.0001	-0.7102
75	1436944_x_at	RIKEN cDNA 4933439C20 gene /// phosphatidylserine decarboxylase pseudogene /// hypothetical protein	4933439C20Rik	0.6324	-0.1228	0.0000	-1.3420	0.0003	-1.0639

Table III,
Con't

76	1447985_s_at	ankyrin repeat and IBR domain containing 1	Ankib1	0.2947	-0.2201	0.0128	-0.8497	0.0142	-0.5659
77	1446041_at	---	---	0.7632	0.0510	0.0289	-0.6265	0.0920	-0.3322
78	1453439_at	amelotin	Amtn	0.5964	-0.0787	0.0017	-0.6018	0.1370	-0.2600
79	1454220_at	RIKEN cDNA 9330185C12 gene	933018 5C12Ri	0.8644	-0.0555	0.0084	-1.1280	0.3939	-0.3621
80	1416232_at	oligodendrocyte transcription factor 2	Olig2	0.3351	0.3620	0.0103	-1.1260	0.0995	-0.5739
81	1423260_at	inhibitor of DNA binding 4 /// similar to Id4	Id4 /// LOC100 045546	0.4654	0.3520	0.0091	-1.1087	0.1539	-0.6058
82	1435179_at	RIKEN cDNA C130071C03 gene	C13007 1C03Ri	0.9671	-0.0216	0.0034	-1.5773	0.0347	-1.1235
83	1423259_at	inhibitor of DNA binding 4 /// similar to Id4	Id4 /// LOC100 045546	0.9990	0.0006	0.0018	-1.3726	0.0356	-0.9395
84	1450928_at	similar to Id4	LOC100 045546	0.9542	-0.0262	0.0036	-1.3065	0.0186	-1.0647
85	1442734_at	---	---	0.7271	-0.0754	0.0041	-0.6530	0.0493	-0.3786
86	1437075_at	FERM domain containing 3	Frmd3	0.9710	0.0100	0.0366	-0.6470	0.1465	-0.4605
87	1421723_at	protocadherin beta 18	Pcdhb1 8	0.0234	1.0813	0.1692	-0.8376	0.9834	0.0116
88	1438612_a_at	colipase, pancreatic	Clps	0.0437	0.5656	0.0197	-0.5997	0.5789	-0.1287
89	1420680_at	cathepsin 8	Cts8	0.0382	4.9190	0.0516	-4.5050	0.9157	0.2484
90	1460275_at	G-protein coupled receptor 3	Gpr3	0.0013	0.6795	0.0712	-0.4987	0.3147	0.1800
91	1437445_at	transient receptor potential cation channel, subfamily M, member 1	Trpm1	0.0169	0.7607	0.0539	-0.5774	0.4036	-0.2107
92	1424679_at	mab-21-like 1 (C. elegans)	Mab21l 1	0.2422	0.3907	0.0439	-0.6283	0.4385	-0.2384
93	1455106_a_at	creatine kinase, brain	Ckb	0.6449	0.1137	0.0388	-0.6112	0.4281	-0.2271
94	1422706_at	transmembrane, prostate androgen induced RNA	Tmepai	0.6230	0.1124	0.0369	-0.7424	0.1953	-0.3779
95	1432516_at	RIKEN cDNA 4930447F04 gene	493044 7F04Rik	0.5306	1.2652	0.0282	-6.3059	0.2472	-3.5516
96	1451298_at	pleckstrin homology domain containing, family H (with MyTH4 domain) member 3	Plekhh3	0.9370	0.0309	0.0224	-1.0080	0.9468	0.0281

Table III,
Con't

97	1432691_at	RIKEN cDNA 9030407C09 gene	903040 7C09Ri	0.8747	0.0485	0.0250	-0.9092	0.8424	-0.0662
98	1432521_at	matrix-remodelling associated 8	Mxra8	0.5129	0.8618	0.0000	-8.5683	0.1042	-2.1666
99	1458036_at	---	---	0.1378	-0.5273	0.0115	-1.3780	0.1312	-0.5736
100	1417639_at	solute carrier family 22 (organic cation transporter), member 4	Slc22a4	0.7704	0.2695	0.0347	-5.2741	0.2894	-1.0446
101	1437648_at	phosphate cytidyltransferase 1, choline, beta isoform	Pcyt1b	0.8068	0.0578	0.0299	-1.2172	0.1336	-0.4729
102	1422160_at	histocompatibility 2, T region locus 24	H2-T24	0.9734	-0.0081	0.0058	-1.2356	0.1212	-0.4403
103	1445623_at	Transcribed locus	---	0.7884	0.1152	0.0218	-2.9506	0.0966	-0.8838
104	1420208_at	---	---	0.5652	0.1528	0.0238	-0.7087	0.8112	-0.0557
105	1458361_at	DNA cross-link repair 1C, PSO2 homolog (S. cerevisiae)	Dclre1c	0.2371	0.3243	0.0331	-0.8327	0.6618	-0.1300
106	1453144_at	RIKEN cDNA 4933439C20 gene	493343 9C20Ri	0.2929	0.4925	0.0047	-3.3092	0.0009	-1.3295
107	1453145_at	RIKEN cDNA 4933439C20 gene	493343 9C20Ri	0.2883	0.1996	0.0000	-2.0876	0.0000	-1.0494
108	1425982_a_at	Werner syndrome homolog (human) /// similar to WRN protein	LOC100 044321 /// Wrn	0.6004	0.0892	0.0163	-0.6056	0.6066	-0.1023
109	1416942_at	type 1 tumor necrosis factor receptor shedding aminopeptidase regulator	Arts1	0.5689	0.1818	0.0481	-1.5536	0.1838	-0.4745
110	1432519_at	RIKEN cDNA 1810059H22 gene	181005 9H22Ri	0.6229	0.0611	0.0295	-0.6887	0.1339	-0.2261
111	1420673_a_at	acyl-Coenzyme A oxidase 2, branched chain	Acox2	0.3434	0.1820	0.0445	-0.6438	0.9066	-0.0225
112	1453850_at	RIKEN cDNA 1500002I01 gene	150000 2I01Rik	0.8213	-0.0661	0.0132	-0.9428	0.1477	-0.4479
113	1432031_at	RIKEN cDNA 4930563E18 gene	493056 3E18Rik	0.4583	-0.0717	0.0005	-0.6240	0.0578	-0.3529
114	1419559_at	cytochrome P450, family 4, subfamily f, polypeptide 14	Cyp4f14	0.1737	0.4613	0.0158	-1.3449	0.4049	-0.5877
115	1433014_at	RIKEN cDNA 6330436F06 gene	633043 6F06Rik	0.9823	-0.0051	0.0077	-0.6888	0.1225	-0.4968
116	1437190_at	serine/threonine/tyrosine kinase 1	Styk1	0.3732	-0.1534	0.0118	-0.6180	0.2770	-0.2194
117	1441664_at	hypothetical gene supported by AK081809	LOC433 351	0.6279	-0.1598	0.0102	-2.3591	0.1170	-0.8411

Table III,
Con't

118	1445163_at	---	---	0.7233	-0.0711	0.0161	-0.6548	0.6622	-0.0941
119	1431240_at	C-type lectin domain family 2, member h	Clec2h	0.4075	0.7811	0.0480	-5.0579	0.2275	-1.1644
120	1440812_at	Transcribed locus	---	0.1183	-3.4293	0.0020	-7.1233	0.0177	-3.6981
121	1449173_at	membrane protein, palmitoylated 2 (MAGUK p55 subfamily member 2)	Mpp2	0.0035	0.6251	0.5654	0.1144	0.0350	0.3732
122	1418991_at	BCL2-antagonist/killer 1	Bak1	0.0166	0.6821	0.8789	0.0213	0.1725	0.2105
123	1424667_a_at	cut-like 1 (Drosophila)	Cutl1	0.0107	0.6098	0.1689	-0.2739	0.1144	0.2436
124	1425646_at	cDNA sequence BC016495	BC016495	0.0422	0.8934	0.4044	-0.3551	0.3264	0.4553
125	1431338_at	CASK interacting protein 1	Caskin1	0.0098	1.0064	0.7986	-0.0897	0.4379	0.2085
126	1447981_at	expressed sequence C78441	C78441	0.0074	1.4914	0.9616	-0.0268	0.3340	0.4875
127	1437531_at	transient receptor potential cation channel, subfamily M, member 1	Trpm1	0.0100	0.9264	0.1864	0.4784	0.0349	0.7617
128	1453340_at	RIKEN cDNA 1700057D03 gene	1700057D03Ri	0.0020	0.6491	0.4636	0.1713	0.1243	0.3095
129	1439148_a_at	phosphofructokinase, liver, B-type	Pfkl	0.0006	0.6696	0.5369	0.1028	0.0143	0.4853
130	1443501_at	Transcribed locus	---	0.0106	0.5993	0.6344	0.0957	0.1251	0.4411
131	1440967_at	13 days embryo heart cDNA, RIKEN full-length enriched library, clone:D330036N06 product:unclassifiable, full insert sequence /// 3 days neonate thymus cDNA, RIKEN full-length enriched library, clone:A630063I24 product:unclassifiable, full insert sequence	---	0.0064	0.6197	0.3601	0.1795	0.0740	0.4277
132	1453225_at	RIKEN cDNA A930038C07 gene	A930038C07Ri	0.0086	1.2326	0.8713	-0.0710	0.4977	0.2187
133	1458037_at	---	---	0.0119	0.7075	0.8015	0.0489	0.2824	0.2944
134	1447493_at	RIKEN cDNA A530088H08 gene	A530088H08Ri	0.0015	0.5852	0.3168	0.1274	0.0178	0.3788
135	1447564_x_at	piwi-like homolog 4 (Drosophila)	Piwi4	0.0115	0.6851	0.4800	0.1447	0.1255	0.4085
136	1427300_at	LIM homeobox protein 8	Lhx8	0.0348	1.3387	0.8521	-0.0933	0.0510	1.5549
137	1431484_at	proline rich Gla (G-carboxyglutamic acid)	Prg1	0.0044	0.5903	0.0735	-0.2422	0.3828	0.2130

Table III,
Con't

138	1423342_at	BarH-like homeobox 1	Barx1	0.0227	0.7764	0.0466	-0.6118	0.5635	0.2016
139	1459222_x_at	---	---	0.0201	0.8010	0.9260	0.0252	0.2825	0.3442
140	1423748_at	pyruvate dehydrogenase kinase, isoenzyme 1	Pdk1	0.0186	0.5892	0.9088	-0.0178	0.0897	0.2990
141	1452482_at	v-erb-b2 erythroblastic leukemia viral oncogene homolog 3 (avian)	ErbB3	0.0154	0.7707	0.2626	-0.2832	0.3675	0.2086
142	1420555_at	aristaless 3	Alx3	0.0044	0.7590	0.9928	0.0024	0.4275	0.1820
143	1457755_at	guanine nucleotide binding protein (G protein), gamma 8 subunit	Gng8	0.0008	0.6196	0.6926	0.0921	0.0713	0.3347
144	1419596_at	ectodysplasin-A /// similar to EDA-A1	Eda /// LOC100 045121	0.0017	0.6073	0.1760	0.3123	0.0002	0.5447
145	1456362_at	cytochrome P450, family 11, subfamily b, polypeptide 1	Cyp11b 1	0.0022	0.5946	0.0287	0.3871	0.0204	0.3602
146	1453847_at	RIKEN cDNA A930037O16 gene	A93003 7O16Ri k	0.0110	0.2967	0.0071	0.6151	0.0030	0.5164
147	1440665_at	---	---	0.0312	0.6876	0.0057	0.8848	0.0165	0.7267
148	1453789_at	RIKEN cDNA 4933440N22 gene	493344 0N22Ri k	0.0350	0.5725	0.0284	0.6662	0.0472	0.5884
149	1430044_at	RIKEN cDNA 4930415F15 gene	493041 5F15Rik	0.0032	0.8698	0.0186	0.6199	0.0179	0.7046
150	1457123_at	neuregulin 4	Nrg4	0.0510	1.1543	0.0481	1.1386	0.1614	0.8869
151	1446043_at	expressed sequence C81086	C81086	0.0140	0.8517	0.0706	0.5611	0.1181	0.5056
152	1421444_at	progesterone receptor	Pgr	0.0393	0.5996	0.0668	0.4603	0.1388	0.4232
153	1434364_at	mitogen-activated protein kinase kinase 14	Map3k1 4	0.0219	0.6442	0.0231	0.5480	0.0660	0.6244
154	1445731_at	---	---	0.0907	0.6358	0.0577	0.7786	0.0334	0.9889
155	1425417_x_at	killer cell lectin-like receptor, subfamily A, member 8 /// similar to killer cell lectin-like receptor subfamily A member 29 /// hypothetical protein LOC100038897	Klra8 /// LOC100 038897 /// LOC667 769	0.2177	0.4818	0.0307	1.0518	0.1281	0.6986
156	1458302_at	Transcribed locus	---	0.1222	0.3906	0.0182	0.6723	0.0918	0.4885
157	1459016_at	B6-derived CD11 +ve dendritic cells cDNA, RIKEN full-length enriched library, clone:F730301C14 product:unclassifiable, full insert	---	0.0142	0.9034	0.4735	0.2110	0.6663	0.1495

Table III,
Con't

158	1442846_at	---	---	0.0315	0.6870	0.3298	0.2496	0.5193	0.1860
159	1427615_at	integrin alpha 4	Itga4	0.0055	1.3580	0.0130	0.8352	0.0071	1.1073
160	1455989_at	gap junction membrane channel protein alpha 12	Gja12	0.0336	2.3118	0.0899	1.7956	0.2083	1.4690
161	1442970_at	FCH and double SH3 domains 2	Fchsd2	0.0191	2.9420	0.0493	2.5684	0.1107	2.0246
162	1429563_x_at	Sp110 nuclear body protein	Sp110	0.0255	0.6430	0.0679	0.5184	0.0831	0.5588
163	1451945_at	---	---	0.0055	7.9602	0.0556	6.3360	0.0311	6.6630
164	1440004_at	Transcribed locus	---	0.0011	1.1244	0.2216	0.4758	0.0794	0.5237
165	1442584_at	---	---	0.0064	0.7470	0.0468	0.5337	0.0254	0.5440
166	1417946_at	abhydrolase domain containing 3	Abhd3	0.0175	0.7575	0.0957	0.5249	0.4009	0.2525
167	1423634_at	gasdermin 1	Gsdm1	0.0438	0.6308	0.0284	0.5764	0.1811	0.3541
168	1453250_at	RIKEN cDNA 4921511C04 gene /// hypothetical protein LOC100046859	4921511C04Rik	0.0927	4.7500	0.0409	5.9604	0.4005	2.6277
169	1428909_at	RIKEN cDNA A130040M12 gene	A130040M12Rik	0.0508	4.5213	0.0479	4.6024	0.3287	2.4246
170	1458513_at	mitogen activated protein kinase 10	Mapk10	0.0350	0.6116	0.0564	0.4709	0.3731	0.2239
171	1425823_at	cDNA sequence BC026782	BC026782	0.0477	0.4553	0.0005	0.8407	0.0261	0.4256
172	1432879_at	RIKEN cDNA 6820402A03 gene	6820402A03Rik	0.0293	0.5417	0.0080	0.6988	0.1399	0.4298
173	1432877_at	RIKEN cDNA 4930544N03 gene	4930544N03Rik	0.0049	0.9883	0.0463	0.7913	0.0257	0.7969
174	1438148_at	chemokine (C-X-C motif) ligand 3	Cxcl3	0.0147	0.6316	0.0059	0.8259	0.0328	0.5988
175	1459955_at	Predicted gene, EG665317	EG665317	0.0646	1.0979	0.0234	1.1246	0.1475	0.7420
176	1446913_at	---	---	0.0551	1.4172	0.0298	1.9783	0.1822	1.0566
177	1445202_at	0 day neonate cerebellum cDNA, RIKEN full-length enriched library, clone:C230022P04 product:unclassifiable, full insert	---	0.5007	0.1505	0.0089	0.6479	0.1069	0.3673
178	1418382_at	adenomatosis polyposis coli down-regulated 1	Apcdd1	0.7450	0.0366	0.0104	0.6185	0.0055	0.4972

Table III,
Con't

179	1422236_at	RIKEN cDNA 4930560E09 gene	493056 0E09Rik	0.3321	0.4049	0.0030	1.1747	0.0723	0.6344
180	1427738_at	DNA segment, KIST 2	D0Kist2	0.0562	0.5093	0.0112	0.7811	0.0902	0.6741
181	1446487_at	---	---	0.0637	0.2908	0.0039	0.5374	0.0145	0.6222
182	1460674_at	progesterin and adipoQ receptor family member VII	Paqr7	0.3371	0.2140	0.2955	0.2440	0.0356	0.6457
183	1457152_at	---	---	0.1328	0.7797	0.1949	0.6584	0.0251	1.5879
184	1459101_at	expressed sequence C78760	C78760	0.2217	0.5384	0.8277	0.0945	0.0437	1.2300
185	1432008_at	transmembrane protein 86B	Tmem8 6b	0.0784	0.3576	0.0220	0.4844	0.0247	0.7114
186	1439762_x_at	adrenergic receptor, alpha 2c /// similar to alpha-2 adrenergic receptor	Adra2c /// LOC100 045767	0.0135	0.7380	0.0088	0.7939	0.0104	1.0096
187	1457450_at	RIKEN cDNA A830091115 gene	A83009 1115Rik	0.0326	0.6151	0.0910	0.4662	0.0119	0.8934
188	1450977_s_at	N-myc downstream regulated gene 1	Ndrq1	0.0582	0.3478	0.0127	0.5628	0.0341	0.6802
189	1421564_at	serine (or cysteine) peptidase inhibitor, clade A, member 3C	Serpina 3c	0.3222	1.7931	0.1138	2.6593	0.0146	5.6049
190	1454518_at	RIKEN cDNA 4930429L21 gene	493042 9L21Rik	0.1735	2.1009	0.4716	1.1433	0.0308	4.4145
191	1419232_a_at	apolipoprotein A-I	Apoa1	0.2595	1.5316	0.2302	1.6293	0.0402	3.6904
192	1445632_at	oxoglutarate dehydrogenase (lipoamide)	Ogdh	0.2560	0.2268	0.4302	0.1534	0.0241	0.6105
193	1427652_x_at	synaptojanin 2	Synj2	0.2075	2.0241	0.2858	1.6960	0.0169	5.3852
194	1439505_at	chloride intracellular channel 5	Clic5	0.1717	1.7416	0.1580	1.7836	0.0108	4.6125
195	1445044_at	Prostaglandin I2 (prostacyclin) synthase	Ptgis	0.2555	1.3105	0.1551	1.6678	0.0184	4.1551
196	1445813_at	WD repeat domain 27	Wdr27	0.2014	1.5557	0.1769	1.6544	0.0127	4.4101
197	1418136_at	transforming growth factor beta 1 induced transcript 1	Tgfb1i1	0.3381	0.1999	0.1732	0.3078	0.0295	0.6042
198	1421414_a_at	sema domain, transmembrane domain (TM), and cytoplasmic domain, (semaphorin) 6A	Sema6a	0.0600	0.5174	0.4010	0.2202	0.0184	0.8898
199	1430719_at	RIKEN cDNA 4833447P13 gene	483344 7P13Rik	0.6510	-0.1228	0.0328	0.6653	0.1903	0.4145
200	1444780_at	RIKEN cDNA 5330421F07 gene	533042 1F07Rik	0.2905	-0.2753	0.0066	0.6145	0.8021	0.0752
201	1440811_x_at	CD8 antigen, alpha chain	Cd8a	0.5116	-1.7008	0.0311	4.9996	0.6699	0.9744

Table III, Con't	202	1425471_x_at	---	---	0.0171	-1.0807	0.1813	0.5811	0.8877	-0.0583
	203	1447366_at	Transcribed locus	---	0.0122	-0.7230	0.9262	0.0223	0.2751	-0.3100
	204	1437913_at	B-cell leukemia/lymphoma 2 related protein A1a /// B-cell leukemia/lymphoma 2 related protein A1b /// B-cell leukemia/lymphoma 2 related protein A1c /// B-cell leukemia/lymphoma 2 related protein A1d	Bcl2a1a /// Bcl2a1b /// Bcl2a1c /// Bcl2a1d	0.0446	-0.7566	0.2172	0.4782	0.6491	0.1767
	205	1424842_a_at	Rho GTPase activating protein 24	Arhgap2 4	0.0122	-0.6607	0.9097	0.0215	0.5929	-0.1075
	206	1415996_at	thioredoxin interacting protein	Txnip	0.0051	-0.6550	0.4707	0.0768	0.0620	-0.2597
	207	1428977_at	carbohydrate (N-acetylgalactosamine 4-0) sulfotransferase 8	Chst8	0.0153	-0.6379	0.7878	-0.0412	0.3325	-0.1810
	208	1438125_at	RIKEN cDNA C230085N15 gene	C23008 5N15Ri k	0.0283	-1.0726	0.6865	0.0436	0.0005	-0.5495
	209	1441513_at	TRAF family member-associated Nf-kappa B activator	Tank	0.0186	-0.8829	0.5713	-0.1228	0.0744	-0.4744
	210	1443870_at	ATP-binding cassette, sub-family C (CFTR/MRP), member 4	Abcc4	0.0039	-0.6398	0.3866	0.1502	0.5166	-0.0988
	211	1449545_at	fibroblast growth factor 18	Fgf18	0.0308	-0.7972	0.2094	0.4399	0.3536	0.2638
	212	1434572_at	histone deacetylase 9	Hdac9	0.0056	-0.6465	0.5779	-0.1365	0.1998	-0.2911
	213	1440490_at	1 day pregnant adult female ovary cDNA, RIKEN full-length enriched library, clone:7230402P09 product:hypothetical protein, full insert sequence	---	0.0288	-0.6689	0.2462	0.2844	0.1627	-0.3421
	214	1455978_a_at	matrilin 2	Matn2	0.0340	-0.7438	0.8140	0.0509	0.2273	-0.2605
	215	1452848_at	transmembrane protein 181	Tmem1 81	0.0085	-0.6913	0.1304	-0.2766	0.3911	-0.1973
	216	1436584_at	sprouty homolog 2 (Drosophila)	Spry2	0.0117	-0.6854	0.6286	-0.1050	0.8595	-0.0482
	217	1454580_at	RIKEN cDNA 5430427N15 gene	543042 7N15Ri k	0.0032	-0.8678	0.7911	0.0532	0.1591	-0.2597
	218	1448424_at	frizzled-related protein	Frzb	0.0227	-0.7568	0.4175	0.1622	0.7124	-0.0774
	219	1460465_at	RIKEN cDNA A930038C07 gene	A93003 8C07Ri k	0.0277	-0.7047	0.3716	0.1962	0.6597	0.1111
	220	1456197_x_at	Adherens junction associated protein 1	Ajap1	0.0057	-0.7820	0.6612	0.0609	0.5643	-0.1209

Table III,
Con't

221	1450488_at	chemokine (C-C motif) ligand 24	Ccl24	0.1473	-0.3034	0.0032	0.6770	0.3860	0.1747
222	1448949_at	carbonic anhydrase 4	Car4	0.0973	-0.5683	0.0152	0.8372	0.0854	0.4857
223	1418094_s_at	carbonic anhydrase 4	Car4	0.1521	-0.4844	0.0076	0.8374	0.0852	0.4492
224	1427355_at	calcitonin/calcitonin-related polypeptide, alpha	Calca	0.0354	-0.6311	0.1552	0.3852	0.9494	-0.0144
225	1449434_at	carbonic anhydrase 3	Car3	0.0096	-0.7551	0.2441	0.2659	0.9154	0.0250
226	1437824_at	glutamate receptor, ionotropic, delta 2	Grid2	0.0000	-8.0250	0.0279	2.4672	0.1538	-1.5642
227	1449783_at	---	---	0.0032	-7.7864	0.3577	-2.2856	0.0085	-5.7836
228	1457373_at	Transcribed locus	---	0.0449	-0.8722	0.5655	0.0950	0.0055	-0.4901
229	1426568_at	solute carrier family 2 (facilitated glucose transporter), member 9	Slc2a9	0.0314	-1.3077	0.7399	0.1249	0.3326	-0.3372
230	1425470_at	---	---	0.0180	-6.4577	0.2140	2.2581	0.3291	-2.5058
231	1440716_at	RIKEN cDNA 6430604M11 gene	643060 4M11Ri k	0.0067	-0.6547	0.7408	0.0715	0.2282	-0.2667
232	1440463_at	---	---	0.0178	-0.7890	0.6798	0.0775	0.0364	-0.5302
233	1432077_at	protection of telomeres 1A	Pot1a	0.0103	-6.6941	0.0892	0.8190	0.0836	-3.8058
234	1440519_at	trans-acting transcription factor 8	Sp8	0.0025	-0.6788	0.9601	0.0076	0.0734	-0.3108
235	1420162_at	expressed sequence AA409749	AA4097 49	0.0201	-0.8820	0.4341	-0.1607	0.0006	-0.6234
236	1421749_at	---	---	0.0167	-0.6923	0.5664	0.1592	0.6044	-0.1341
237	1449534_at	synaptonemal complex protein 3	Sycp3	0.0028	-0.9412	0.1457	-0.3718	0.0143	-0.7238
238	1419926_at	Thioredoxin domain containing 10	Txndc1 0	0.0250	-0.7764	0.3548	-0.1852	0.0525	-0.3845
239	1442182_at	DnaJ (Hsp40) homolog, subfamily C, member 19	Dnajc19	0.0107	-0.7434	0.2154	-0.2541	0.0101	-0.5473
240	1420094_at	Heterogeneous nuclear ribonucleoprotein D-like	Hnrpdl	0.0065	-0.8366	0.1321	-0.2942	0.0055	-0.6404
241	1453859_at	ubiquinol-cytochrome c reductase complex chaperone, CBP3 homolog (yeast)	Uqcc	0.0346	-5.2265	0.4147	-0.5865	0.0532	-1.8841
242	1424354_at	transmembrane protein 140	Tmem1 40	0.0266	-0.8240	0.7162	0.0519	0.1099	-0.2912

Table III,
Con't

243	1453473_a_at	dynein light chain Tctex-type 1 /// similar to tctex-1 protein	Dynlt1 /// LOC100 040531 /// LOC100 040563 /// LOC100 040603 /// LOC100 040631 /// LOC100 043890	0.0041	-0.7726	0.2943	-0.1350	0.0775	-0.2678
244	1427837_at	similar to Unknown (protein for MGC:103328)	LOC100 046552	0.0387	-0.6165	0.6730	0.0787	0.6902	-0.1015
245	1459785_at	Zinc finger protein 383	Zfp383	0.0018	-1.2926	0.2695	-0.2693	0.0410	-0.5554
246	1443404_s_at	DNA segment, Chr 13, ERATO Doi 94, expressed	D13Ertd 94e	0.0262	-5.6085	0.7106	-0.4951	0.0614	-1.8316
247	1429943_at	chitobiase, di-N-acetyl-	Ctbs	0.0170	-0.9739	0.7290	-0.0605	0.0110	-0.4684
248	1435948_at	transmembrane protein 181 /// similar to G protein-coupled receptor 178	LOC100 040525 /// LOC100 040596 /// Tmem1 81	0.0293	-0.5867	0.9467	-0.0121	0.4487	-0.1532
249	1436127_at	corticotropin releasing hormone binding protein	Crhbp	0.0254	-0.6182	0.9455	-0.0104	0.0569	-0.2811
250	1436690_at	LPS-responsive beige-like anchor	Lrba	0.0188	-5.7987	0.2210	1.1627	0.2766	-1.0535
251	1441966_at	transient receptor potential cation channel, subfamily M, member 3	Trpm3	0.0134	-1.9382	0.4643	-0.3243	0.2895	-0.7373
252	1443230_at	CDNA clone IMAGE:6514950	---	0.0093	-0.8293	0.8743	-0.0326	0.1108	-0.3433
253	1458460_at	---	---	0.0024	-0.8186	0.7903	-0.0574	0.0382	-0.5550
254	1431039_at	OTU domain containing 4	Otud4	0.0083	-0.6040	0.6071	-0.0830	0.0501	-0.4205
255	1432953_at	RIKEN cDNA 4921520E09 gene	492152 0E09Rik	0.0051	-1.1486	0.5474	-0.1954	0.2932	-0.3852
256	1419681_a_at	prokineticin 2	Prok2	0.0155	-0.9286	0.8946	-0.0194	0.1534	-0.3376

Table III,
Con't

257	1457904_at	carbonic anhydrase 8	Car8	0.0353	-4.2855	0.3743	0.5202	0.0327	-1.4197
258	1416593_at	glutaredoxin	Glrx	0.0213	-0.5947	0.6153	0.0696	0.3587	-0.1452
259	1452750_at	RIKEN cDNA 5530601H04 gene	553060 1H04Ri	0.0052	-0.6939	0.9299	0.0158	0.0552	-0.5495
260	1456984_at	sex comb on midleg-like 2 (Drosophila)	Scml2	0.0086	-0.6113	0.8907	-0.0274	0.0542	-0.4555
261	1418681_at	asparagine-linked glycosylation 13 homolog (S. cerevisiae)	Alg13	0.0160	-0.6232	0.5992	-0.1207	0.1344	-0.4298
262	1431172_at	origin recognition complex, subunit 4-like (S. cerevisiae)	Orc4l	0.0049	-0.6074	0.9643	-0.0063	0.0251	-0.4625
263	1428604_at	RIKEN cDNA 2610305D13 gene	261030 5D13Ri	0.0021	-0.6384	0.2364	0.1838	0.1697	-0.3112
264	1424963_at	retinitis pigmentosa 1 homolog (human)	Rp1h	0.0053	-1.0912	0.7165	-0.0864	0.1682	-0.6638
265	1452539_a_at	CD247 antigen	Cd247	0.0010	-0.5855	0.1042	0.3750	0.7633	0.0366
266	1457646_at	homeo box A11, opposite strand transcript	Hoxa11 os	0.0097	-1.7675	0.2524	0.5410	0.2754	-0.5745
267	1451629_at	limb-bud and heart /// similar to limb-bud and heart	Lbh /// LOC100 048380	0.0097	-0.7474	0.0186	-0.5044	0.0473	-0.4575
268	1437062_s_at	phytanoyl-CoA hydroxylase interacting protein-like	Phyhipl	0.0106	-0.8595	0.0987	-0.4512	0.1150	-0.4349
269	1442905_at	Transcribed locus	---	0.0088	-0.6084	0.0475	-0.3748	0.0682	-0.3541
270	1417462_at	CAP, adenylate cyclase-associated protein 1 (yeast)	Cap1	0.0057	-0.6191	0.0212	-0.5382	0.0823	-0.4116
271	1421851_at	microtubule-associated protein 1 B	Mtap1b	0.0261	-0.6216	0.0146	-0.4531	0.0330	-0.4381
272	1438356_x_at	RIKEN cDNA 4933432K03 gene	493343 2K03Rik	0.0013	-0.7094	0.0342	-0.3222	0.0623	-0.4249
273	1454277_at	RIKEN cDNA 1700049J03 gene	170004 9J03Rik	0.0004	-0.8014	0.0165	-0.3836	0.0003	-0.8188
274	1430720_at	Y box protein 1	Ybx1	0.0018	-0.6595	0.0572	-0.2175	0.0028	-0.5614
275	1431499_at	RIKEN cDNA 4933436F18 gene	493343 6F18Rik	0.0011	-0.6086	0.7975	-0.0511	0.1075	-0.3414
276	1431611_a_at	cell adhesion molecule 1	Cadm1	0.0207	-0.7087	0.0749	-0.2813	0.0581	-0.4318
277	1425942_a_at	glycoprotein m6b	Gpm6b	0.0172	-0.7460	0.3137	-0.2250	0.1906	-0.3746
278	1440050_at	similar to Hbs1l protein	LOC100 040505/ LOC100 045696	0.0272	-0.5861	0.6385	-0.1067	0.1799	-0.3923

Table III,
Con't

279	1437568_at	matrix metalloproteinase 16	Mmp16	0.0030	-0.5974	0.3282	-0.1954	0.0121	-0.4770
280	1421895_at	eukaryotic translation initiation factor 2, subunit 3, structural gene X-linked /// similar to translation initiation factor eIF-2 gamma subunit	Eif2s3x /// LOC100 039419 /// LOC100 048746	0.0040	-0.8212	0.3153	-0.1762	0.0726	-0.6169
281	1438838_at	RIKEN cDNA B230206F22 gene	B23020 6F22Rik	0.0086	-0.6805	0.3907	-0.1808	0.0555	-0.5860

Table IV. Genes identified as differentially expressed in E9.5 Vegf isoform mice and E11.5 wild types relative to a E9.5 wild type background. A meta-analysis combining microarrays from our current study (E9.5 WT=2, E9.5 Vegf188=4, E9.5 Vegf120/188=3), Darland et al., 2011 (E9.5 WT=4, E9.5 Vegf120=4, Ref and GEO), and Hartl et al., 2008 (E9.5 WT= 6, E11.5 WT=4). Unprocessed .CEL files were downloaded from Gene Expression Omnibus (website) and combined with our arrays. The runs were PLIER normalized, Presence/Absence filtered using MAS5, and log2 transformed. To eliminate variation attributed to the different technical batches, all arrays were batch normalized using a multivariate-modeled (Genotype, Age, Batch) Empirical Bayes correction run by the R-scripts ComBat.R. Affymetrix probe set IDs from Affymetrix 430A Mouse microarray chip are provided along with the gene title and symbol, as well as the Zcut for each group and whether the gene was significantly up (1), down (-1), or not changed (0) relative to the E9.5 wild types. The genes selected for this list were all those changed in at least one of the E9.5 Vegf isoform mice. Due to the overwhelming number of total genes shifted in the forebrains of E11.5 wild type mice, we did not include in this table genes only shifted in the E11.5 group. Due to the size of this table (>200 pages) we have elected to provide this table as an electronic copy.

Table V. Covariate analysis of qPCR quantitation for key growth factor signaling genes (Shh, Notch3, CXCL12, CXCR7, Nrp1, Nrp2) and reference genes (18S rRNA and GAPDH). Statistical comparisons were done with the log2 values for each sample and the Degrees of freedom (Df), F-value, and P value for residuals (Pr) are shown based on mean and standard deviation from the mean with fold change and p-value indicated for atastistical comparisons were do

a. Shh

Factors	Df	F-Value	Pr (>F)		
Genotype	3	4.1847	0.05423		
18s	1	0.6797	0.43689		
Gapdh	1	6.2581	0.04089		
Genotype:18s	3	0.1159	0.94792		
Genotype:Gapdh	3	1.6077	0.27187		
Gapdh:18s	1	0.0011	0.975		
Genotype:18s:Gapdh	2	1.679	0.25373		
Residuals	7				
Genotype	WT	V120	V188	V120/188	
N	7	5	6	9	
Mean (ag/Total RNA)	6.7361	6.7254	3.284	4.6467	
Standard Deviation	1.1441	1.9564	0.9489	2.0856	
Tukey's Post Hoc	WT v V120	WT v V188	WT v V120/188		
p-value	0.9999	0.0816	0.2636		
Fold Change	0.0032	1.0994	0.6957		
	V120 v Vegf188	V120 v V120/188	V188 v V120/188		
p-value	0.0865	0.2785	0.5127		
Fold Change	1.0962	0.6925	-0.4037		

Table V, continued.

b. Notch3

Factors	Df	F-Value	Pr (>F)		
Genotype	3	5.3215	0.022		
18s	1	4.0225	0.0758		
Gapdh	1	11.2193	0.00853		
Genotype:18s	3	0.5704	0.6485		
Genotype:Gapdh	3	5.2256	0.0231		
Gapdh:18s	1	3.4241	0.0973		
Genotype:18s:Gapdh	3	6.3048	0.0136		
Residuals	9				
Genotype	WT	V120	V188	V120/188	
N	8	6	7	8	
Mean (ag/Total RNA)	364.468	359.1558	174.09	324.5793	
Standard Deviation	76.9364	39.9049	159.9405	94.5449	
Tukey's Post Hoc	WT v V120	WT v V188	WT v V120/188		
p-value	0.994	0.027	0.8402		
Fold Change	0.0531	1.3719	0.1943		
	V120 v Vegf188	V120 v V120/188	V188 v V120/188		
p-value	0.0228	0.7251	0.068		
Fold Change	1.3189	0.1412	-1.1776		

Table V, continued.

c. CXCL12

Factors	Df	F-Value	Pr (>F)		
Genotype	3	4.8424	0.008		
18s	1	16.9934	0.0003		
Genotype:18s	3	0.1345	0.9386		
Residuals	27				
Genotype	WT	V120	V188	V120/188	
N	8	11	7	9	
Mean (pg/Total RNA)	0.024	0.0114	0.00513	0.02	
Standard Deviation	0.013	0.0114	0.00422	0.018	
Tukey's Post Hoc	WT v V120	WT v V188	WT v V120/188		
p-value	0.0811	0.0116	0.878		
Fold Change	1.8079	2.3375	0.6472		
	V120 v Vegf188	V120 v V120/188	V188 v V120/188		
p-value	0.6368	0.3007	0.0497		
Fold Change	0.5296	-1.1607	-1.6904		

Table V, continued.

d. CXCR7

Factors	Df	F-Value	Pr (>F)
Genotype	3	6.682	0.0011
18s	1	28.4503	0.000006
Genotype:18s	3	3.8345	0.0181
Residuals	34		

Genotype	WT	V120	V188	V120/188
N	11	11	10	11
Mean (pg/Total RNA)	0.0000119	0.00000834	0.00000834	0.0000101
Standard Deviation	0.0000034	0.00000369	0.00000024	0.00000279

Tukey's Post Hoc	WT v V120	WT v V188	WT v V120/188
p-value	0.0033	0.0044	0.506
Fold Change	0.5669	0.5026	0.2251

	V120 v Vegf188	V120 v V120/188	V188 v V120/188
p-value	0.9999	0.1243	0.1412
Fold Change	-0.0643	-0.3418	-0.2775

Table V, continued.

e. Nrp1

Factors	Df	F-Value	Pr (>F)		
Genotype	3	5.5645	0.0076		
18s	1	40.8765	0.000007		
Genotype:18s	3	9.6986	0.0006		
Residuals	25				
Genotype	WT	V120	V188	V120/188	
N	6	7	5	7	
Mean (pg/Total RNA)	0.0019	0.0019	0.00054	0.005	
Standard Deviation	0.0017	0.002	0.00039	0.0071	
Tukey's Post Hoc	WT v V120	WT v V188	WT v V120/188		
p-value	0.9999	0.6671	0.0619		
Fold Change	0.5631	1.4996	-0.2198		
	V120 v Vegf188	V120 v V120/188	V188 v V120/188		
p-value	0.6834	0.0432	0.0074		
Fold Change	0.9364	-0.7829	-1.7193		

Table V, continued.

f. Nrp2

Factors	Df	F-Value	Pr (>F)
Genotype	3	4.6584	0.0102
18s	1	3.1685	0.08723
Genotype:18s	3	2.6853	0.06825
Residuals	25		

Genotype	WT	V120	V188	V120/188
N	9	7	9	9
Mean (pg/Total RNA)	0.0894	0.0557	0.0103	0.0221
Standard Deviation	0.0646	0.0905	0.0086	0.0175

Tukey's Post Hoc	WT v V120	WT v V188	WT v V120/188
p-value	0.5221	0.0098	0.048
Fold Change	1.7498	3.0489	1.9972

	V120 v Vegf188	V120 v V120/188	V188 v V120/188
p-value	0.272	0.5991	0.9345
Fold Change	1.2991	0.2473	-1.0518

Table V, continued.

g. 18S rRNA

Factors	Df	F-Value	Pr (>F)
Genotype	3	0.7431	0.5396
18s	1	1.6074	0.2202
Genotype:18s	3	0.2935	0.8296
Residuals	19		

Genotype	WT	V120	V188	V120/188
N	9	6	6	8
Mean (ag/Total RNA)	8702	11347	9964	9964
Standard Deviation	3573	2007	2303	2303

Tukey's Post Hoc	WT v V120	WT v V188	WT v V120/188
p-value	0.4931	0.9941	0.8863
Fold Change	-0.4822	0.0563	-0.2856

	V120 v Vegf188	V120 v V120/188	V188 v V120/188
p-value	0.7272	0.8685	0.9806
Fold Change	0.5385	0.1966	-0.3419

Table V, continued.

h. GAPDH

Factors	Df	F-Value	Pr (>F)
Genotype	3	1.4877	0.2498
18s	1	1.5995	0.2213
Genotype:18s	3	0.2611	0.8525
Residuals	19		

Genotype	WT	V120	V188	V120/188
N	9	6	8	8
Mean (ag/Total RNA)	1051	1272	896	1334
Standard Deviation	436	375	417	190

Tukey's Post Hoc	WT v V120	WT v V188	WT v V120/188
p-value	0.4625	0.9231	0.2384
Fold Change	-0.4028	0.2634	-0.4426

	V120 v Vegf188	V120 v V120/188	V188 v V120/188
p-value	0.8792	0.998	0.698
Fold Change	0.6662	-0.0397	-0.706

Table VI. Covariate analysis of qPCR quantitation for key transcription modulators (Suz12, Dnmt3a, Id1, Pax6, Hey 2, Fezf2, Pax3, FoxM1, and Zfhxb1) and reference genes (18S and GAPDH). Statistical comparisons were done with the log2 values for each sample and the Degrees of freedom (Df), F-value, and P value for residuals (Pr) are shown based on mean and standard deviation from the mean with fold change and p-value indicated for atatistical comparisons were do

a. Suz12

Factors	Df	F-Value	Pr (>F)
Genotype	3	1.5052	0.2784
18s	1	6.0691	0.0359
Gapdh	1	14.6298	0.0041
Genotype:18s	3	0.0849	0.9665
Genotype:Gapdh	3	4.0782	0.0439
Gapdh:18s	1	0.018	0.8963
Genotype:18s:Gapdh	2	2.5311	0.1226
Residuals	9		

Genotype	WT	V120	V188	V120/188
N	8	6	5	9
Mean (ag/Total RNA)	38.9251	45.5759	40.108	50.4278
Standard Deviation	16.9085	10.1259	16.0011	24.8914

Tukey's Post Hoc	WT v V120	WT v V188	WT v V120/188
p-value	0.7938	0.9612	0.2333
Fold Change	-0.3572	-0.0592	-0.3417
	V120 v Vegf188	V120 v V120/188	V188 v V120/188
p-value	0.9871	0.7352	0.6098
Fold Change	0.298	0.0155	-0.2825

Table VI, continued.

b. Dnmt3a

Factors	Df	F-Value	Pr (>F)		
Genotype	3	6.5292	0.0194		
18s	1	2.276	0.1751		
Gapdh	1	3.6272	0.0985		
Genotype:18s	3	0.7174	0.5724		
Genotype:Gapdh	3	1.6345	0.2615		
Gapdh:18s	1	0.0008	0.9785		
Genotype:18s:Gapdh	3	3.3742	0.0942		
Residuals	7				
Genotype	WT	V120	V188	V120/188	
N	7	5	7	7	
Mean (ag/Total RNA)	4.5659	3.8055	0.6086	3.9891	
Standard Deviation	0.9872	1.4274	0.2065	1.6956	
Tukey's Post Hoc	WT v V120	WT v V188	WT v V120/188		
p-value	0.6672	0.0131	0.7728		
Fold Change	0.1627	2.949	0.2822		
	V120 v Vegf188	V120 v V120/188	V188 v V120/188		
p-value	0.04465	0.9916	0.0285		
Fold Change	2.786	0.1195	-2.6668		

Table VI, continued.

c. Id1

Factors	Df	F-Value	Pr (>F)		
Genotype	3	11.0294	0.0048		
18s	1	4.5409	0.0706		
Gapdh	1	1.8197	0.2194		
Genotype:18s	3	0.1268	0.9412		
Genotype:Gapdh	3	1.0492	4286		
Gapdh:18s	1	2.001	0.2001		
Genotype:18s:Gapdh	2	0.0657	0.937		
Residuals					
Genotype	WT	V120	V188	V120/188	
N	8	6	8	8	
Mean (ag/Total RNA)	10.5908	13.5738	5.8083	14.8733	
Standard Deviation	3.2014	1.508	1.6885	2.7845	
Tukey's Post Hoc	WT v V120	WT v V188	WT v V120/188		
p-value	0.2859	0.1243	0.037		
Fold Change	-0.4381	0.8641	-0.5306		
	V120 v Vegf188	V120 v V120/188	V188 v V120/188		
p-value	0.0199	0.606	0.0045		
Fold Change	1.3021	-0.09258	-1.3947		

Table VI, continued.

d. Pax6

Factors	Df	F-Value	Pr (>F)
Genotype	3	4.683	0.0075
18s	1	6.5483	0.015
Genotype:18s	3	0.469	0.7058
Residuals	35		

Genotype	WT	V120	V188	V120/188
N	11	11	11	11
Mean (pg/Total RNA)	0.00019	0.00013	0.00014	0.00012
Standard Deviation	0.00004	0.00006	0.000039	0.000051

Tukey's Post Hoc	WT v V120	WT v V188	WT v V120/188
p-value	0.0207	0.0481	0.0127
Fold Change	0.6929	0.5064	0.7503

	V120 v Vegf188	V120 v V120/188	V188 v V120/188
p-value	0.9847	0.9932	0.9277
Fold Change	-0.1865	0.0574	0.2439

Table VI, continued.

e. Hey2

Factors	Df	F-Value	Pr (>F)		
Genotype	3	11.9726	0.0038		
18s	1	6.0713	0.04321		
Gapdh	1	28.1327	0.0011		
Genotype:18s	3	11.4222	0.00436		
Genotype:Gapdh	3	3.499	0.07816		
Gapdh:18s	1	0.0646	0.8067		
Genotype:18s:Gapdh	3	10.9678	0.0049		
Residuals	7				
Genotype	WT	V120	V188	V120/188	
N	8	5	7	8	
Mean (ag/Total RNA)	1.556	2.5172	2.0434	2.1275	
Standard Deviation	0.8607	1.7514	1.514	0.7691	
Tukey's Post Hoc	WT v V120	WT v V188	WT v V120/188		
p-value	0.0044	0.0126	0.0486		
Fold Change	-0.5819	-0.2952	-0.5553		
	V120 v Vegf188	V120 v V120/188	V188 v V120/188		
p-value	0.8367	0.1142	0.3837		
Fold Change	0.2868	0.0267	-0.2601		

Table VI, continued.

f. Fezf2

Factors	Df	F-Value	Pr (>F)		
Genotype	3	2.8982	0.1017		
18s	1	0.3313	0.5807		
Gapdh	1	0.6622	0.4393		
Genotype:18s	3	3.3503	0.07616		
Genotype:Gapdh	3	0.1484	0.9278		
Gapdh:18s	1	0.4203	0.5349		
Genotype:18s:Gapdh	3	0.9664	0.4545		
Residuals	8				
Genotype	WT	V120	V188	V120/188	
N	10	6	9	7	
Mean (ag/Total RNA)	2.1054	1.078	2.3214	1.8174	
Standard Deviation	0.8447	0.4201	1.9975	0.4945	
Tukey's Post Hoc	WT v V120	WT v V188	WT v V120/188		
p-value	0.1853	0.8951	0.9993		
Fold Change	1.0012	0.1256	0.1479		
	V120 v Vegf188	V120 v V120/188	V188 v V120/188		
p-value	0.1119	0.2175	0.851		
Fold Change	-0.8757	-0.8534	0.0223		

Table VI, continued.

g. Pax3

Factors	Df	F-Value	Pr (>F)		
Genotype	3	3.4357	0.081		
18s	1	0.7674	0.4101		
Gapdh	1	11.5465	0.0114		
Genotype:18s	3	0.6341	0.6162		
Genotype:Gapdh	3	0.2408	0.8653		
Gapdh:18s	1	0.1275	0.7316		
Genotype:18s:Gapdh	3	4.6572	0.043		
Residuals	7				
Genotype	WT	V120	V188	V120/188	
N	8	5	8	8	
Mean (ag/Total RNA)	2.0906	3.2895	1.742	2.2142	
Standard Deviation	0.8692	1.4534	0.7061	0.8307	
Tukey's Post Hoc	WT v V120	WT v V188	WT v V120/188		
p-value	0.1507	0.802	0.9903		
Fold Change	-0.68	0.2268	-0.099		
	V120 v Vegf188	V120 v V120/188	V188 v V120/188		
p-value	0.0748	0.2133	0.6685		
Fold Change	0.9067	0.5809	-0.3258		

Table VI, continued.

h. FoxM1

Factors	Df	F-Value	Pr (>F)
Genotype	3	5.9651	0.0099
18s	1	5.7231	0.03399
Genotype:18s	3	3.0849	0.0681
Residuals	12		

Genotype	WT	V120	V188	V120/188
N	5	4	6	5
Mean (pg/Total RNA)	0.000213	0.000072	0.0000032	0.0000043
Standard Deviation	0.000183	0.0000023	0.0000065	0.0000042

Tukey's Post Hoc	WT v V120	WT v V188	WT v V120/188
p-value	0.0787	0.0106	0.0217
Fold Change	1.0822	4.051	2.542

	V120 v Vegf188	V120 v V120/188	V188 v V120/188
p-value	0.85	0.9455	0.9939
Fold Change	2.9689	1.4599	-1.5089

Table VI, continued.

i. Zfhx1b

Factors	Df	F-Value	Pr (>F)		
Genotype	3	6.0541	0.0153		
18s	1	1.613	0.2359		
Genotype:18s	3	1.162	0.3767		
Residuals	9				

Genotype	WT	V120	V188	V120/188
N	5	4	4	4
Mean (pg/Total RNA)	68.43	25.8954	0.6308	54.5202
Standard Deviation	37.135	7.2259	0.4837	34.3632

Tukey's Post Hoc	WT v V120	WT v V188	WT v V120/188	
p-value	0.1302	0.01451	0.8476	
Fold Change	1.2821	6.8713	0.3356	

	V120 v Vegf188	V120 v V120/188	V188 v V120/188	
p-value	0.5309	0.4332	0.0618	
Fold Change	5.5892	-0.9465	-6.5357	

155

Table VII. Covariate analysis of qPCR quantitation for key extracellular matrix proteins (Lama4, Lama5, Lamc3, FN) and reference genes (18S and GAPDH). Statistical comparisons were done with the log2 values for each sample and the Degrees of freedom (Df), F-value, and P value for residuals (Pr) are shown based on mean and standard deviation from the mean with fold change and p-value indicated for a set to 0.05 (Program R, SAS).

a. Lama4

Factors	Df	F-Value	Pr (>F)
Genotype	3	6.9301	0.0224
18s	1	2.12	0.1956
Gapdh	1	1.1734	0.3203
Genotype:18s	3	3.2689	0.1011
Genotype:Gapdh	3	2.9577	0.1277
Gapdh:18s	1	0.556	0.484
Genotype:18s:Gapdh	2	9.006	0.0156
Residuals	6		

Genotype	WT	V120	V188	V120/188
N	6	4	5	10
Mean (ag/Total RNA)	1.0856	0.9452	0.4003	0.8958
Standard Deviation	0.2516	0.5338	0.1049	0.4756

Tukey's Post Hoc	WT v V120	WT v V188	WT v V120/188
p-value	0.696	0.02282	0.9999
Fold Change	0.3099	1.4438	0.6531

	V120 v Vegf188	V120 v V120/188	V188 v V120/188
p-value	0.0765	0.6335	0.01886
Fold Change	1.1338	0.3432	-0.7906

Table VII, continued.

b. Lama5

Factors	Df	F-Value	Pr (>F)		
Genotype	3	1.2288	0.3909		
18s	1	0.2838	0.6171		
Gapdh	1	0.8181	0.4072		
Genotype:18s	3	0.1388	0.9326		
Genotype:Gapdh	3	0.1289	0.8819		
Gapdh:18s	1	0.1736	0.6942		
Genotype:18s:Gapdh	2	0.5167	0.6252		
Residuals	5				
Genotype	WT	V120	V188	V120/188	
N	7	4	4	8	
Mean (ag/Total RNA)	4.228	5.6851	2.0424	4.3456	
Standard Deviation	1.2783	0.4589	0.5415	1.906	
Tukey's Post Hoc	WT v V120	WT v V188	WT v V120/188		
p-value	0.6496	0.7486	0.9698		
Fold Change	-0.5001	1.03	-0.06589		
	V120 v Vegf188	V120 v V120/188	V188 v V120/188		
p-value	0.348	0.8271	0.5818		
Fold Change	1.5301	0.4342	-1.0959		

Table VII, continued.

c. Lamc3

Factors	Df	F-Value	Pr (>F)		
Genotype	3	0.622	0.6167		
18s	1	0.5142	0.4897		
Gapdh	1	3.5498	0.0889		
Genotype:18s	3	0.6932	0.5769		
Genotype:Gapdh	3	3.1331	0.07423		
Gapdh:18s	1	0.6136	0.4516		
Genotype:18s:Gapdh	3	2.6075	0.1096		
Residuals	10				
Genotype	WT	V120	V188	V120/188	
N	10	8	10	10	
Mean (ag/Total RNA)	28.1676	29.3247	28.7057	27.9276	
Standard Deviation	0.9504	2.8385	1.2613	2.6273	
Tukey's Post Hoc	WT v V120	WT v V188	WT v V120/188		
p-value	0.5554	0.9351	0.8555		
Fold Change	-0.0534	-0.0267	0.0176		
	V120 v Vegf188	V120 v V120/188	V188 v V120/188		
p-value	0.9114	0.9386	0.9991		
Fold Change	0.02665	0.071	0.0443		

Table VII, continued.

d. FN

Factors	Df	F-Value	Pr (>F)		
Genotype	3	3.1794	0.1226		
18s	1	0.0009	0.9771		
Gapdh	1	0.145	0.719		
Genotype:18s	3	5.214	0.0535		
Genotype:Gapdh	3	0.7531	0.566		
Gapdh:18s	1	9.2813	0.0285		
Genotype:18s:Gapdh	2	2.5365	0.1705		
Residuals	9				
Genotype	WT	V120	V188	V120/188	
N	8	5	9	7	
Mean (ag/Total RNA)	6.8152	8.4892	4.5538	6.4777	
Standard Deviation	1.9687	2.6184	2.0787	2.7486	
Tukey's Post Hoc	WT v V120	WT v V188	WT v V120/188		
p-value	0.4262	0.4486	0.9916		
Fold Change	-0.3136	0.6681	0.1516		
	V120 v Vegf188	V120 v V120/188	V188 v V120/188		
p-value	0.09551	0.5416	0.3419		
Fold Change	0.9817	0.4651	-0.5165		

References

1. Holmes DI, Zachary I: **The vascular endothelial growth factor (Vegf) family: angiogenic factors in health and disease.** *Genome Biol* 2005, **6**:209.
2. Ruiz de Almodovar C, Lambrechts D, Mazzone M, Carmeliet P: **Role and therapeutic potential of Vegf in the nervous system.** *Physiol Rev* 2009, **89**:607-648.
3. Ng YS, Rohan R, Sunday ME, Demello DE, D'Amore PA: **Differential expression of Vegf isoforms in mouse during development and in the adult.** *Dev Dyn* 2001, **220**:112-121.
4. Ruhrberg C, Gerhardt H, Golding M, Watson R, Ioannidou S, Fujisawa H, Betsholtz C, Shima DT: **Spatially restricted patterning cues provided by heparin-binding Vegf-A control blood vessel branching morphogenesis.** *Genes & Development* 2002, **16**:2684-2698.
5. Ruiz de Almodovar C, Coulon C, Salin PA, Knevels E, Chounlamountri N, Poesen K, Hermans K, Lambrechts D, Van Geyte K, Dhondt J, et al: **Matrix-binding vascular endothelial growth factor (Vegf) isoforms guide granule cell migration in the cerebellum via Vegf receptor Flk1.** *The Journal of neuroscience : the official journal of the Society for Neuroscience* 2010, **30**:15052-15066.
6. Darland DC, Cain JT, Berosik MA, Saint-Geniez M, Odens PW, Schaubhut GJ, Frisch S, Stemmer-Rachamimov A, Darland T, D'Amore PA: **Vascular endothelial growth factor (Vegf) isoform regulation of early forebrain development.** *Developmental Biology* 2011, **358**:9-22.
7. Krilleke D, Ng YS, Shima DT: **The heparin-binding domain confers diverse functions of Vegf-A in development and disease: a structure-function study.** *Biochem Soc Trans* 2009, **37**:1201-1206.
8. Houck KA, Leung DW, Rowland AM, Winer J, Ferrara N: **Dual regulation of vascular endothelial growth factor bioavailability by genetic and proteolytic mechanisms.** *The Journal of biological chemistry* 1992, **267**:26031-26037.
9. Park JE, Keller GA, Ferrara N: **The vascular endothelial growth factor (Vegf) isoforms: differential deposition into the subepithelial extracellular matrix and bioactivity of extracellular matrix-bound Vegf.** *Molecular biology of the cell* 1993, **4**:1317-1326.
10. Ferrara N: **Role of vascular endothelial growth factor in the regulation of angiogenesis.** *Kidney international* 1999, **56**:794-814.

11. Chen TT, Luque A, Lee S, Anderson SM, Segura T, Iruela-Arispe ML: **Anchorage of Vegf to the extracellular matrix conveys differential signaling responses to endothelial cells.** *The Journal of Cell Biology* 2010, **188**:595-609.
12. Whitaker GB, Limberg BJ, Rosenbaum JS: **Vascular endothelial growth factor receptor-2 and neuropilin-1 form a receptor complex that is responsible for the differential signaling potency of Vegf(165) and Vegf(121).** *The Journal of biological chemistry* 2001, **276**:25520-25531.
13. Soker S, Miao HQ, Nomi M, Takashima S, Klagsbrun M: **Vegf165 mediates formation of complexes containing VegfR-2 and neuropilin-1 that enhance Vegf165-receptor binding.** *Journal of Cellular Biochemistry* 2002, **85**:357-368.
14. Soker S, Fidler H, Neufeld G, Klagsbrun M: **Characterization of novel vascular endothelial growth factor (Vegf) receptors on tumor cells that bind Vegf165 via its exon 7-encoded domain.** *The Journal of biological chemistry* 1996, **271**:5761-5767.
15. Miao HQ, Soker S, Feiner L, Alonso JL, Raper JA, Klagsbrun M: **Neuropilin-1 mediates collapsin-1/semaphorin III inhibition of endothelial cell motility: functional competition of collapsin-1 and vascular endothelial growth factor-165.** *The Journal of Cell Biology* 1999, **146**:233-242.
16. Ruhrberg C: **Growing and shaping the vascular tree: multiple roles for Vegf.** *BioEssays : news and reviews in molecular, cellular and developmental biology* 2003, **25**:1052-1060.
17. Roberts DM, Kearney JB, Johnson JH, Rosenberg MP, Kumar R, Bautch VL: **The vascular endothelial growth factor (Vegf) receptor Flt-1 (VegfR-1) modulates Flk-1 (VegfR-2) signaling during blood vessel formation.** *The American journal of pathology* 2004, **164**:1531-1535.
18. Bussolati B, Dunk C, Grohman M, Kontos CD, Mason J, Ahmed A: **Vascular endothelial growth factor receptor-1 modulates vascular endothelial growth factor-mediated angiogenesis via nitric oxide.** *The American journal of pathology* 2001, **159**:993-1008.
19. Stutfeld E, Ballmer-Hofer K: **Structure and function of Vegf receptors.** *IUBMB Life* 2009, **61**:915-922.
20. Cross MJ, Dixelius J, Matsumoto T, Claesson-Welsh L: **Vegf-receptor signal transduction.** *Trends Biochem Sci* 2003, **28**:488-494.
21. Cross MJ, Claesson-Welsh L: **FGF and Vegf function in angiogenesis: signalling pathways, biological responses and therapeutic inhibition.** *Trends Pharmacol Sci* 2001, **22**:201-207.
22. Keyt BA, Nguyen HV, Berleau LT, Duarte CM, Park J, Chen H, Ferrara N: **Identification of vascular endothelial growth factor determinants for binding KDR and FLT-1 receptors. Generation of receptor-selective Vegf variants by site-directed mutagenesis.** *The Journal of biological chemistry* 1996, **271**:5638-5646.

23. Kolodkin AL, Levensgood DV, Rowe EG, Tai YT, Giger RJ, Ginty DD: **Neuropilin is a semaphorin III receptor.** *Cell* 1997, **90**:753-762.
24. He Z, Tessier-Lavigne M: **Neuropilin is a receptor for the axonal chemorepellent Semaphorin III.** *Cell* 1997, **90**:739-751.
25. Neufeld G, Cohen T, Shraga N, Lange T, Kessler O, Herzog Y: **The neuropilins: multifunctional semaphorin and Vegf receptors that modulate axon guidance and angiogenesis.** *Trends in cardiovascular medicine* 2002, **12**:13-19.
26. Dumont DJ, Fong GH, Puri MC, Gradwohl G, Alitalo K, Breitman ML: **Vascularization of the mouse embryo: a study of flk-1, tek, tie, and vascular endothelial growth factor expression during development.** *Developmental dynamics : an official publication of the American Association of Anatomists* 1995, **203**:80-92.
27. Breier G, Albrecht U, Sterrer S, Risau W: **Expression of vascular endothelial growth factor during embryonic angiogenesis and endothelial cell differentiation.** *Development* 1992, **114**:521-532.
28. Damert A, Machein M, Breier G, Fujita MQ, Hanahan D, Risau W, Plate KH: **Up-regulation of vascular endothelial growth factor expression in a rat glioma is conferred by two distinct hypoxia-driven mechanisms.** *Cancer Research* 1997, **57**:3860-3864.
29. Senger DR, Galli SJ, Dvorak AM, Perruzzi CA, Harvey VS, Dvorak HF: **Tumor cells secrete a vascular permeability factor that promotes accumulation of ascites fluid.** *Science* 1983, **219**:983-985.
30. Plouet J, Schilling J, Gospodarowicz D: **Isolation and characterization of a newly identified endothelial cell mitogen produced by AtT-20 cells.** *The EMBO journal* 1989, **8**:3801-3806.
31. Drake CJ, Fleming PA: **Vasculogenesis in the day 6.5 to 9.5 mouse embryo.** *Blood* 2000, **95**:1671-1679.
32. Damert A, Miquerol L, Gertsenstein M, Risau W, Nagy A: **Insufficient VegfA activity in yolk sac endoderm compromises haematopoietic and endothelial differentiation.** *Development* 2002, **129**:1881-1892.
33. Carmeliet P, Ferreira V, Breier G, Pollefeyt S, Kieckens L, Gertsenstein M, Fahrig M, Vandenhoek A, Harpal K, Eberhardt C, et al: **Abnormal blood vessel development and lethality in embryos lacking a single Vegf allele.** *Nature* 1996, **380**:435-439.
34. Shalaby F, Rossant J, Yamaguchi TP, Gertsenstein M, Wu XF, Breitman ML, Schuh AC: **Failure of blood-island formation and vasculogenesis in Flk-1-deficient mice.** *Nature* 1995, **376**:62-66.
35. Carmeliet P, Lampugnani MG, Moons L, Breviario F, Compernelle V, Bono F, Balconi G, Spagnuolo R, Oosthuyse B, Dewerchin M, et al: **Targeted deficiency or cytosolic truncation of the VE-cadherin gene in mice impairs Vegf-mediated endothelial survival and angiogenesis.** *Cell* 1999, **98**:147-157.

36. Stalmans I, Ng YS, Rohan R, Fruttiger M, Bouche A, Yuce A, Fujisawa H, Hermans B, Shani M, Jansen S, et al: **Arteriolar and venular patterning in retinas of mice selectively expressing Vegf isoforms.** *The Journal of clinical investigation* 2002, **109**:327-336.
37. Ishida S, Usui T, Yamashiro K, Kaji Y, Amano S, Ogura Y, Hida T, Oguchi Y, Ambati J, Miller JW, et al: **Vegf164-mediated inflammation is required for pathological, but not physiological, ischemia-induced retinal neovascularization.** *J Exp Med* 2003, **198**:483-489.
38. James JM, Gewolb C, Bautch VL: **Neurovascular development uses Vegf-A signaling to regulate blood vessel ingression into the neural tube.** *Development* 2009, **136**:833-841.
39. Ferrara N, Houck K, Jakeman L, Leung DW: **Molecular and biological properties of the vascular endothelial growth factor family of proteins.** *Endocr Rev* 1992, **13**:18-32.
40. Rapraeger AC: **Syndecan-regulated receptor signaling.** *The Journal of Cell Biology* 2000, **149**:995-998.
41. Chang Z, Meyer K, Rapraeger AC, Friedl A: **Differential ability of heparan sulfate proteoglycans to assemble the fibroblast growth factor receptor complex in situ.** *FASEB journal : official publication of the Federation of American Societies for Experimental Biology* 2000, **14**:137-144.
42. Bullock SL, Fletcher JM, Beddington RS, Wilson VA: **Renal agenesis in mice homozygous for a gene trap mutation in the gene encoding heparan sulfate 2-sulfotransferase.** *Genes & Development* 1998, **12**:1894-1906.
43. Ferrara N, Gerber HP, LeCouter J: **The biology of Vegf and its receptors.** *Nature Medicine* 2003, **9**:669-676.
44. Miralem T, Steinberg R, Price D, Avraham H: **Vegf(165) requires extracellular matrix components to induce mitogenic effects and migratory response in breast cancer cells.** *Oncogene* 2001, **20**:5511-5524.
45. Wijelath ES, Rahman S, Namekata M, Murray J, Nishimura T, Mostafavi-Pour Z, Patel Y, Suda Y, Humphries MJ, Sobel M: **Heparin-II Domain of Fibronectin Is a Vascular Endothelial Growth Factor-Binding Domain: Enhancement of Vegf Biological Activity by a Singular Growth Factor/Matrix Protein Synergism.** *Circulation Research* 2006, **99**:853-860.
46. Carmeliet P, Tessier-Lavigne M: **Common mechanisms of nerve and blood vessel wiring.** *Nature* 2005, **436**:193-200.
47. Bautch VL, James JM: **Neurovascular development: The beginning of a beautiful friendship.** *Cell adhesion & migration* 2009, **3**:199-204.
48. Bar T: **The vascular system of the cerebral cortex.** *Adv Anat Embryol Cell Biol* 1980, **59**:I-VI,1-62.
49. Vasudevan A, Bhide PG: **Angiogenesis in the embryonic CNS: A new twist on an old tale.** *Cell Adhesion & Migration* 2008, **2**:167-169.

50. Vasudevan A, Long JE, Crandall JE, Rubenstein JL, Bhide PG: **Compartment-specific transcription factors orchestrate angiogenesis gradients in the embryonic brain.** *Nature Neuroscience* 2008, **11**:429-439.
51. James JM, Mukoyama YS: **Neuronal action on the developing blood vessel pattern.** *Seminars in Cell & Developmental Biology* 2011, **22**:1019-1027.
52. Gotz M, Barde YA: **Radial glial cells defined and major intermediates between embryonic stem cells and CNS neurons.** *Neuron* 2005, **46**:369-372.
53. Gotz M, Hartfuss E, Malatesta P: **Radial glial cells as neuronal precursors: a new perspective on the correlation of morphology and lineage restriction in the developing cerebral cortex of mice.** *Brain Res Bull* 2002, **57**:777-788.
54. Norden C, Young S, Link BA, Harris WA: **Actomyosin is the main driver of interkinetic nuclear migration in the retina.** *Cell* 2009, **138**:1195-1208.
55. Hevner RF, Shi L, Justice N, Hsueh Y, Sheng M, Smiga S, Bulfone A, Goffinet AM, Campagnoni AT, Rubenstein JL: **Tbr1 regulates differentiation of the preplate and layer 6.** *Neuron* 2001, **29**:353-366.
56. Gerhardt H, Ruhrberg C, Abramsson A, Fujisawa H, Shima D, Betsholtz C: **Neuropilin-1 is required for endothelial tip cell guidance in the developing central nervous system.** *Developmental Dynamics* 2004, **231**:503-509.
57. Virgintino D, Errede M, Robertson D, Girolamo F, Masciandaro A, Bertossi M: **Vegf expression is developmentally regulated during human brain angiogenesis.** *Histochem Cell Biol* 2003, **119**:227-232.
58. Sondell M, Lundborg G, Kanje M: **Vascular endothelial growth factor stimulates Schwann cell invasion and neovascularization of acellular nerve grafts.** *Brain Res* 1999, **846**:219-228.
59. Sondell M, Sundler F, Kanje M: **Vascular endothelial growth factor is a neurotrophic factor which stimulates axonal outgrowth through the flk-1 receptor.** *Eur J Neurosci* 2000, **12**:4243-4254.
60. Zhu Y, Jin K, Mao XO, Greenberg DA: **Vascular endothelial growth factor promotes proliferation of cortical neuron precursors by regulating E2F expression.** *FASEB J* 2003, **17**:186-193.
61. Jin K: **Vascular endothelial growth factor (Vegf) stimulates neurogenesis in vitro and in vivo.** *Proceedings of the National Academy of Sciences* 2002, **99**:11946-11950.
62. Mukoyama YS, Shin D, Britsch S, Taniguchi M, Anderson DJ: **Sensory nerves determine the pattern of arterial differentiation and blood vessel branching in the skin.** *Cell* 2002, **109**:693-705.
63. Sobeih MM, Corfas G: **Extracellular factors that regulate neuronal migration in the central nervous system.** *Int J Dev Neurosci* 2002, **20**:349-357.

64. Hynes RO: **The Extracellular Matrix: Not Just Pretty Fibrils.** *Science* 2009, **326**:1216-1219.
65. Hynes RO: **Integrins: bidirectional, allosteric signaling machines.** *Cell* 2002, **110**:673-687.
66. Hynes RO: **A reevaluation of integrins as regulators of angiogenesis.** *Nat Med* 2002, **8**:918-921.
67. Hynes RO, Lively JC, McCarty JH, Taverna D, Francis SE, Hodivala-Dilke K, Xiao Q: **The diverse roles of integrins and their ligands in angiogenesis.** *Cold Spring Harb Symp Quant Biol* 2002, **67**:143-153.
68. Niewmierzycka A, Mills J, St-Arnaud R, Dedhar S, Reichardt LF: **Integrin-linked kinase deletion from mouse cortex results in cortical lamination defects resembling cobblestone lissencephaly.** *The Journal of neuroscience : the official journal of the Society for Neuroscience* 2005, **25**:7022-7031.
69. Lathia JD, Patton B, Eckley DM, Magnus T, Mughal MR, Sasaki T, Caldwell MA, Rao MS, Mattson MP, French-Constant C: **Patterns of laminins and integrins in the embryonic ventricular zone of the CNS.** *The Journal of Comparative Neurology* 2007, **505**:630-643.
70. Englund C, Fink A, Lau C, Pham D, Daza RA, Bulfone A, Kowalczyk T, Hevner RF: **Pax6, Tbr2, and Tbr1 are expressed sequentially by radial glia, intermediate progenitor cells, and postmitotic neurons in developing neocortex.** *The Journal of Neuroscience* 2005, **25**:247-251.
71. Goetz AK: **Temporally restricted substrate interactions direct fate and specification of neural precursors derived from embryonic stem cells.** *Proceedings of the National Academy of Sciences* 2006, **103**:11063-11068.
72. Desai AR, McConnell SK: **Progressive restriction in fate potential by neural progenitors during cerebral cortical development.** *Development* 2000, **127**:2863-2872.
73. Sansom SN, Hebert JM, Thammongkol U, Smith J, Nisbet G, Surani MA, McConnell SK, Livesey FJ: **Genomic characterisation of a Fgf-regulated gradient-based neocortical protomap.** *Development* 2005, **132**:3947-3961.
74. Shen Q, Wang Y, Dimos JT, Fasano CA, Phoenix TN, Lemischka IR, Ivanova NB, Stifani S, Morrisey EE, Temple S: **The timing of cortical neurogenesis is encoded within lineages of individual progenitor cells.** *Nature Neuroscience* 2006, **9**:743-751.
75. Kowalczyk T, Pontious A, Englund C, Daza RA, Bedogni F, Hodge R, Attardo A, Bell C, Huttner WB, Hevner RF: **Intermediate neuronal progenitors (basal progenitors) produce pyramidal-projection neurons for all layers of cerebral cortex.** *Cerebral cortex* 2009, **19**:2439-2450.
76. Hevner RF: **From radial glia to pyramidal-projection neuron: transcription factor cascades in cerebral cortex development.** *Mol Neurobiol* 2006, **33**:33-50.

77. Waclaw RR, Campbell K: **Regional control of cortical lamination.** *Nature Neuroscience* 2009, **12**:1211-1212.
78. Bedogni F, Hodge RD, Elsen GE, Nelson BR, Daza RA, Beyer RP, Bammler TK, Rubenstein JL, Hevner RF: **Tbr1 regulates regional and laminar identity of postmitotic neurons in developing neocortex.** *Proceedings of the National Academy of Sciences* 2010, **107**:13129-13134.
79. Cremisi F, Philpott A, Ohnuma S: **Cell cycle and cell fate interactions in neural development.** *Current Opinion in Neurobiology* 2003, **13**:26-33.
80. Edlund T, Jessell TM: **Progression from extrinsic to intrinsic signaling in cell fate specification: a view from the nervous system.** *Cell* 1999, **96**:211-224.
81. Borello U, Pierani A: **Patterning the cerebral cortex: traveling with morphogens.** *Current Opinion in Genetics & Development* 2010, **20**:408-415.
82. Pierani A, Wassef M: **Cerebral cortex development: From progenitors patterning to neocortical size during evolution.** *Development, Growth & Differentiation* 2009, **51**:325-342.
83. Huang Z: **Molecular regulation of neuronal migration during neocortical development.** *Mol Cell Neurosci* 2009, **42**:11-22.
84. Li G, Adesnik H, Li J, Long J, Nicoll RA, Rubenstein JL, Pleasure SJ: **Regional distribution of cortical interneurons and development of inhibitory tone are regulated by Cxcl12/Cxcr4 signaling.** *The Journal of neuroscience : the official journal of the Society for Neuroscience* 2008, **28**:1085-1098.
85. Ma Q, Jones D, Borghesani PR, Segal RA, Nagasawa T, Kishimoto T, Bronson RT, Springer TA: **Impaired B-lymphopoiesis, myelopoiesis, and derailed cerebellar neuron migration in CXCR4- and SDF-1-deficient mice.** *Proceedings of the National Academy of Sciences of the United States of America* 1998, **95**:9448-9453.
86. Lu M, Grove EA, Miller RJ: **Abnormal development of the hippocampal dentate gyrus in mice lacking the CXCR4 chemokine receptor.** *Proceedings of the National Academy of Sciences of the United States of America* 2002, **99**:7090-7095.
87. Zagzag D, Lukyanov Y, Lan L, Ali MA, Esencay M, Mendez O, Yee H, Voura EB, Newcomb EW: **Hypoxia-inducible factor 1 and Vegf upregulate CXCR4 in glioblastoma: implications for angiogenesis and glioma cell invasion.** *Laboratory investigation; a journal of technical methods and pathology* 2006, **86**:1221-1232.

88. Stumm RK, Rummel J, Junker V, Culmsee C, Pfeiffer M, Krieglstein J, Holtt V, Schulz S: **A dual role for the SDF-1/CXCR4 chemokine receptor system in adult brain: isoform-selective regulation of SDF-1 expression modulates CXCR4-dependent neuronal plasticity and cerebral leukocyte recruitment after focal ischemia.** *The Journal of neuroscience : the official journal of the Society for Neuroscience* 2002, **22**:5865-5878.
89. Salcedo R, Oppenheim JJ: **Role of chemokines in angiogenesis: CXCL12/SDF-1 and CXCR4 interaction, a key regulator of endothelial cell responses.** *Microcirculation* 2003, **10**:359-370.
90. Infantino S, Moepps B, Thelen M: **Expression and Regulation of the Orphan Receptor RDC1 and Its Putative Ligand in Human Dendritic and B Cells.** *The Journal of Immunology* 2006, **176**:2197-2207.
91. Shimizu N, Soda Y, Kanbe K, Liu H-y, Mukai R, Kitamura T, Hoshino H: **A Putative G Protein-Coupled Receptor, RDC1, Is a Novel Coreceptor for Human and Simian Immunodeficiency Viruses.** *The Journal of Virology* 2000, **74**:619-626.
92. Burns JM, Summers BC, Wang Y, Melikian A, Berahovich R, Miao Z, Penfold MET, Sunshine MJ, Littman DR, Kuo CJ, et al: **A novel chemokine receptor for SDF-1 and I-TAC involved in cell survival, cell adhesion, and tumor development.** *The Journal of Experimental Medicine* 2006, **203**:2201-2213.
93. Valentin G, Haas P, Gilmour D: **The chemokine SDF1a coordinates tissue migration through the spatially restricted activation of Cxcr7 and Cxcr4b.** *Current biology : CB* 2007, **17**:1026-1031.
94. Dambly-Chaudiere C, Cubedo N, Ghysen A: **Control of cell migration in the development of the posterior lateral line: antagonistic interactions between the chemokine receptors CXCR4 and CXCR7/RDC1.** *BMC Developmental Biology* 2007, **7**:23.
95. Schutyser E, Su Y, Yu Y, Gouwy M, Zaja-Milatovic S, Van Damme J, Richmond A: **Hypoxia enhances CXCR4 expression in human microvascular endothelial cells and human melanoma cells.** *Eur Cytokine Netw* 2007, **18**:59-70.
96. Carmeliet P, Ng YS, Nuyens D, Theilmeier G, Brusselmans K, Cornelissen I, Ehler E, Kakkar VV, Stalmans I, Mattot V, et al: **Impaired myocardial angiogenesis and ischemic cardiomyopathy in mice lacking the vascular endothelial growth factor isoforms Vegf164 and Vegf188.** *Nature Medicine* 1999, **5**:495-502.
97. Rhen T, Metzger K, Schroeder A, Woodward R: **Expression of putative sex-determining genes during the thermosensitive period of gonad development in the snapping turtle, Chelydra serpentina.** *Sex Dev* 2007, **1**:255-270.
98. Therneau TM, Ballman KV: **What does PLIER really do?** *Cancer Inform* 2008, **6**:423-431.

99. Hartl D, Irmiler M, Romer I, Mader MT, Mao L, Zabel C, de Angelis MH, Beckers J, Klose J: **Transcriptome and proteome analysis of early embryonic mouse brain development.** *Proteomics* 2008, **8**:1257-1265.
100. Hubbell E, Liu WM, Mei R: **Robust estimators for expression analysis.** *Bioinformatics* 2002, **18**:1585-1592.
101. Johnson WE, Li C, Rabinovic A: **Adjusting batch effects in microarray expression data using empirical Bayes methods.** *Biostatistics* 2007, **8**:118-127.
102. Ishwaran H, Rao JS, Kogalur UB: **BAMarraytrade mark: Java software for Bayesian analysis of variance for microarray data.** *BMC Bioinformatics* 2006, **7**:59.
103. Huang da W, Sherman BT, Lempicki RA: **Systematic and integrative analysis of large gene lists using DAVID bioinformatics resources.** *Nat Protoc* 2009, **4**:44-57.
104. Huang da W, Sherman BT, Lempicki RA: **Bioinformatics enrichment tools: paths toward the comprehensive functional analysis of large gene lists.** *Nucleic Acids Res* 2009, **37**:1-13.
105. Hosack DA, Dennis G, Jr., Sherman BT, Lane HC, Lempicki RA: **Identifying biological themes within lists of genes with EASE.** *Genome Biology* 2003, **4**:R70.
106. Szklarczyk D, Franceschini A, Kuhn M, Simonovic M, Roth A, Minguéz P, Doerks T, Stark M, Müller J, Bork P, et al: **The STRING database in 2011: functional interaction networks of proteins, globally integrated and scored.** *Nucleic Acids Res* 2011, **39**:D561-568.
107. Haigh JJ, Morelli PI, Gerhardt H, Haigh K, Tsien J, Damert A, Miquerol L, Muhlner U, Klein R, Ferrara N, et al: **Cortical and retinal defects caused by dosage-dependent reductions in Vegf-A paracrine signaling.** *Developmental Biology* 2003, **262**:225-241.
108. Breier G, Risau W: **The role of vascular endothelial growth factor in blood vessel formation.** *Trends Cell Biol* 1996, **6**:454-456.
109. Millauer B, Wizigmann-Voos S, Schnurch H, Martinez R, Moller NP, Risau W, Ullrich A: **High affinity Vegf binding and developmental expression suggest Flk-1 as a major regulator of vasculogenesis and angiogenesis.** *Cell* 1993, **72**:835-846.
110. Risau W: **Mechanisms of angiogenesis.** *Nature* 1997, **386**:671-674.
111. Ishwaran H, Sunil Rao J: **Clustering gene expression profile data by selective shrinkage.** *Statistics & Probability Letters* 2008, **78**:1490-1497.
112. Hebert JM, Fishell G: **The genetics of early telencephalon patterning: some assembly required.** *Nat Rev Neurosci* 2008, **9**:678-685.
113. Lathia JD, Mattson MP, Cheng A: **Notch: from neural development to neurological disorders.** *Journal of Neurochemistry* 2008, **107**:1471-1481.

114. Sennino B, Kuhnert F, Tabruyn SP, Mancuso MR, Hu-Lowe DD, Kuo CJ, McDonald DM: **Cellular source and amount of vascular endothelial growth factor and platelet-derived growth factor in tumors determine response to angiogenesis inhibitors.** *Cancer Research* 2009, **69**:4527-4536.
115. Tanigaki K, Nogaki F, Takahashi J, Tashiro K, Kurooka H, Honjo T: **Notch1 and Notch3 instructively restrict bFGF-responsive multipotent neural progenitor cells to an astroglial fate.** *Neuron* 2001, **29**:45-55.
116. Pasini D, Bracken AP, Jensen MR, Lazzerini Denchi E, Helin K: **Suz12 is essential for mouse development and for EZH2 histone methyltransferase activity.** *The EMBO journal* 2004, **23**:4061-4071.
117. Miro X, Zhou X, Boretius S, Michaelis T, Kubisch C, Alvarez-Bolado G, Gruss P: **Haploinsufficiency of the murine polycomb gene Suz12 results in diverse malformations of the brain and neural tube.** *Dis Model Mech* 2009, **2**:412-418.
118. Watanabe D, Uchiyama K, Hanaoka K: **Transition of mouse de novo methyltransferases expression from Dnmt3b to Dnmt3a during neural progenitor cell development.** *Neuroscience* 2006, **142**:727-737.
119. Lyden D, Young AZ, Zagzag D, Yan W, Gerald W, O'Reilly R, Bader BL, Hynes RO, Zhuang Y, Manova K, Benezra R: **Id1 and Id3 are required for neurogenesis, angiogenesis and vascularization of tumour xenografts.** *Nature* 1999, **401**:670-677.
120. Fischer A, Schumacher N, Maier M, Sendtner M, Gessler M: **The Notch target genes Hey1 and Hey2 are required for embryonic vascular development.** *Genes & Development* 2004, **18**:901-911.
121. Monastirioti M, Giagtzoglou N, Koumbanakis KA, Zacharioudaki E, Deligiannaki M, Wech I, Almeida M, Preiss A, Bray S, Delidakis C: **Drosophila Hey is a target of Notch in asymmetric divisions during embryonic and larval neurogenesis.** *Development* 2010, **137**:191-201.
122. Shimizu T, Nakazawa M, Kani S, Bae YK, Kageyama R, Hibi M: **Zinc finger genes Fezf1 and Fezf2 control neuronal differentiation by repressing Hes5 expression in the forebrain.** *Development* 2010, **137**:1875-1885.
123. Ichi S, Boshnjaku V, Shen YW, Mania-Farnell B, Ahlgren S, Sapru S, Mansukhani N, McLone DG, Tomita T, Mayanil CS: **Role of Pax3 acetylation in the regulation of Hes1 and Neurog2.** *Molecular biology of the cell* 2011, **22**:503-512.
124. Sansom SN, Griffiths DS, Faedo A, Kleinjan DJ, Ruan Y, Smith J, van Heyningen V, Rubenstein JL, Livesey FJ: **The level of the transcription factor Pax6 is essential for controlling the balance between neural stem cell self-renewal and neurogenesis.** *PLoS Genetics* 2009, **5**:e1000511.

125. Dang LT, Tropepe V: **FGF dependent regulation of Zfhx1b gene expression promotes the formation of definitive neural stem cells in the mouse anterior neurectoderm.** *Neural Dev* 2010, **5**:13.
126. Wijelath ES, Rahman S, Murray J, Patel Y, Savidge G, Sobel M: **Fibronectin promotes Vegf-induced CD34 cell differentiation into endothelial cells.** *Journal of vascular surgery* 2004, **39**:655-660.
127. Caiado F, Dias S: **Endothelial progenitor cells and integrins: adhesive needs.** *Fibrogenesis Tissue Repair* 2012, **5**:4.
128. Jakobsson L, Domogatskaya A, Tryggvason K, Edgar D, Claesson-Welsh L: **Laminin deposition is dispensable for vasculogenesis but regulates blood vessel diameter independent of flow.** *FASEB journal : official publication of the Federation of American Societies for Experimental Biology* 2008, **22**:1530-1539.
129. Miner JH, Cunningham J, Sanes JR: **Roles for laminin in embryogenesis: exencephaly, syndactyly, and placentopathy in mice lacking the laminin alpha5 chain.** *The Journal of Cell Biology* 1998, **143**:1713-1723.
130. Pierce RA, Griffin GL, Mudd MS, Moxley MA, Longmore WJ, Sanes JR, Miner JH, Senior RM: **Expression of laminin alpha3, alpha4, and alpha5 chains by alveolar epithelial cells and fibroblasts.** *American Journal of Respiratory Cell and Molecular Biology* 1998, **19**:237-244.
131. Thyboll J, Kortessmaa J, Cao R, Soininen R, Wang L, Iivanainen A, Sorokin L, Risling M, Cao Y, Tryggvason K: **Deletion of the laminin alpha4 chain leads to impaired microvessel maturation.** *Molecular and Cellular Biology* 2002, **22**:1194-1202.
132. Haubst N, Georges-Labouesse E, De Arcangelis A, Mayer U, Gotz M: **Basement membrane attachment is dispensable for radial glial cell fate and for proliferation, but affects positioning of neuronal subtypes.** *Development* 2006, **133**:3245-3254.
133. Price DJ, Kennedy H, Dehay C, Zhou L, Mercier M, Jossin Y, Goffinet AM, Tissir F, Blakey D, Molnar Z: **The development of cortical connections.** *The European journal of neuroscience* 2006, **23**:910-920.
134. Fishell G, Hanashima C: **Pyramidal neurons grow up and change their mind.** *Neuron* 2008, **57**:333-338.
135. Molyneaux BJ, Arlotta P, Menezes JR, Macklis JD: **Neuronal subtype specification in the cerebral cortex.** *Nat Rev Neurosci* 2007, **8**:427-437.
136. Marin-Padilla M: **Early vascularization of the embryonic cerebral cortex: Golgi and electron microscopic studies.** *The Journal of Comparative Neurology* 1985, **241**:237-249.
137. Bar T, Budi Santoso AW: **Identification of pericytes in the central nervous system by silver staining of the basal lamina.** *Cell and Tissue Research* 1984, **236**:491-493.

138. Cebe Suarez S, Pieren M, Cariolato L, Arn S, Hoffmann U, Bogucki A, Manlius C, Wood J, Ballmer-Hofer K: **A Vegf-A splice variant defective for heparan sulfate and neuropilin-1 binding shows attenuated signaling through VegfR-2.** *Cell Mol Life Sci* 2006, **63**:2067-2077.
139. Zhang Y, Furumura M, Morita E: **Distinct signaling pathways confer different vascular responses to Vegf 121 and Vegf 165.** *Growth Factors* 2008, **26**:125-131.
140. Koch S, Tugues S, Li X, Gualandi L, Claesson-Welsh L: **Signal transduction by vascular endothelial growth factor receptors.** *Biochem J* 2011, **437**:169-183.
141. Larsen KB, Lutterodt MC, Laursen H, Graem N, Pakkenberg B, Mollgard K, Moller M: **Spatiotemporal distribution of PAX6 and MEIS2 expression and total cell numbers in the ganglionic eminence in the early developing human forebrain.** *Developmental Neuroscience* 2010, **32**:149-162.
142. Duan D, Fu Y, Paxinos G, Watson C: **Spatiotemporal expression patterns of Pax6 in the brain of embryonic, newborn, and adult mice.** *Brain Struct Funct* 2012.
143. Georgala PA, Carr CB, Price DJ: **The role of Pax6 in forebrain development.** *Dev Neurobiol* 2011, **71**:690-709.
144. Scardigli R, Baumer N, Gruss P, Guillemot F, Le Roux I: **Direct and concentration-dependent regulation of the proneural gene Neurogenin2 by Pax6.** *Development* 2003, **130**:3269-3281.
145. Ochiai W, Nakatani S, Takahara T, Kainuma M, Masaoka M, Minobe S, Namihira M, Nakashima K, Sakakibara A, Ogawa M, Miyata T: **Periventricular notch activation and asymmetric Ngn2 and Tbr2 expression in pair-generated neocortical daughter cells.** *Mol Cell Neurosci* 2009, **40**:225-233.
146. Yun K, Fischman S, Johnson J, Hrabe de Angelis M, Weinmaster G, Rubenstein JL: **Modulation of the notch signaling by Mash1 and Dlx1/2 regulates sequential specification and differentiation of progenitor cell types in the subcortical telencephalon.** *Development* 2002, **129**:5029-5040.
147. Tuoc TC, Radyushkin K, Tonchev AB, Pinon MC, Ashery-Padan R, Molnar Z, Davidoff MS, Stoykova A: **Selective cortical layering abnormalities and behavioral deficits in cortex-specific Pax6 knock-out mice.** *The Journal of neuroscience : the official journal of the Society for Neuroscience* 2009, **29**:8335-8349.
148. Quinn JC, Molinek M, Martynoga BS, Zaki PA, Faedo A, Bulfone A, Hevner RF, West JD, Price DJ: **Pax6 controls cerebral cortical cell number by regulating exit from the cell cycle and specifies cortical cell identity by a cell autonomous mechanism.** *Developmental Biology* 2007, **302**:50-65.

149. Ericson J, Muhr J, Jessell TM, Edlund T: **Sonic hedgehog: a common signal for ventral patterning along the rostrocaudal axis of the neural tube.** *The International Journal of Developmental Biology* 1995, **39**:809-816.
150. Ericson J, Muhr J, Placzek M, Lints T, Jessell TM, Edlund T: **Sonic hedgehog induces the differentiation of ventral forebrain neurons: a common signal for ventral patterning within the neural tube.** *Cell* 1995, **81**:747-756.
151. Samanta J, Kessler JA: **Interactions between ID and OLIG proteins mediate the inhibitory effects of BMP4 on oligodendroglial differentiation.** *Development* 2004, **131**:4131-4142.
152. Vieira JM, Schwarz Q, Ruhrberg C: **Selective requirements for NRP1 ligands during neurovascular patterning.** *Development* 2007, **134**:1833-1843.
153. Zhou ZD, Kumari U, Xiao ZC, Tan EK: **Notch as a molecular switch in neural stem cells.** *IUBMB Life* 2010, **62**:618-623.
154. Benedito R, Rocha SF, Woeste M, Zamykal M, Radtke F, Casanovas O, Duarte A, Pytowski B, Adams RH: **Notch-dependent VegfR3 upregulation allows angiogenesis without Vegf-VegfR2 signalling.** *Nature* 2012, **484**:110-114.
155. Feng J, Fouse S, Fan G: **Epigenetic regulation of neural gene expression and neuronal function.** *Pediatric Research* 2007, **61**:58R-63R.
156. Wang Y, Li G, Stanco A, Long JE, Crawford D, Potter GB, Pleasure SJ, Behrens T, Rubenstein JL: **CXCR4 and CXCR7 have distinct functions in regulating interneuron migration.** *Neuron* 2011, **69**:61-76.
157. Anderson SA, Eisenstat DD, Shi L, Rubenstein JL: **Interneuron migration from basal forebrain to neocortex: dependence on Dlx genes.** *Science* 1997, **278**:474-476.
158. Stumm R, Kolodziej A, Schulz S, Kohtz JD, Holtt V: **Patterns of SDF-1alpha and SDF-1gamma mRNAs, migration pathways, and phenotypes of CXCR4-expressing neurons in the developing rat telencephalon.** *The Journal of Comparative Neurology* 2007, **502**:382-399.
159. Polleux F, Dehay C, Kennedy H: **The timetable of laminar neurogenesis contributes to the specification of cortical areas in mouse isocortex.** *The Journal of Comparative Neurology* 1997, **385**:95-116.
160. McKenna WL, Betancourt J, Larkin KA, Abrams B, Guo C, Rubenstein JL, Chen B: **Tbr1 and Fezf2 regulate alternate corticofugal neuronal identities during neocortical development.** *The Journal of neuroscience : the official journal of the Society for Neuroscience* 2011, **31**:549-564.